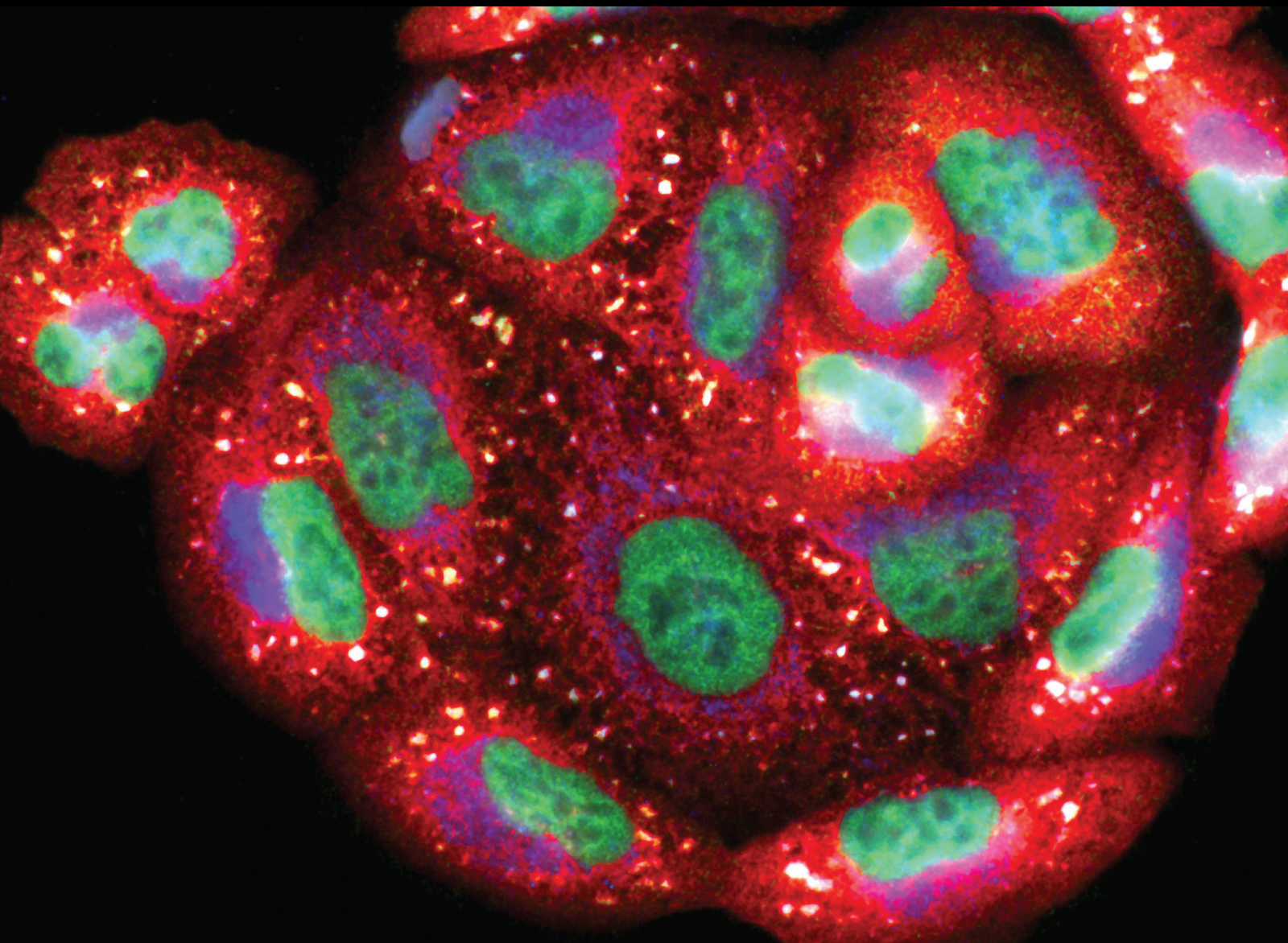


# Insights into the Molecular Mechanisms Underlying Cerebrovascular Diseases: The Role of Oxidative Stress

Lead Guest Editor: Maurizio Forte

Guest Editors: Speranza Rubattu and Stefania Crispi





---

**Insights into the Molecular Mechanisms  
Underlying Cerebrovascular Diseases: The Role  
of Oxidative Stress**

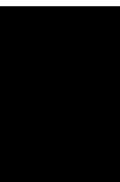
Oxidative Medicine and Cellular Longevity

---

**Insights into the Molecular Mechanisms  
Underlying Cerebrovascular Diseases:  
The Role of Oxidative Stress**

Lead Guest Editor: Maurizio Forte

Guest Editors: Speranza Rubattu and Stefania  
Crispi



---

Copyright © 2020 Hindawi Limited. All rights reserved.

This is a special issue published in "Oxidative Medicine and Cellular Longevity" All articles are open access articles distributed under the Creative Commons Attribution License, which permits unrestricted use, distribution, and reproduction in any medium, provided the original work is properly cited.

# Chief Editor

Jeannette Vasquez-Vivar, USA

## Associate Editors

Amjad Islam Aqib, Pakistan  
Angel Catalá , Argentina  
Cinzia Domenicotti , Italy  
Janusz Gebicki , Australia  
Aldrin V. Gomes , USA  
Vladimir Jakovljevic , Serbia  
Thomas Kietzmann , Finland  
Juan C. Mayo , Spain  
Ryuichi Morishita , Japan  
Claudia Penna , Italy  
Sachchida Nand Rai , India  
Paola Rizzo , Italy  
Mithun Sinha , USA  
Daniele Vergara , Italy  
Victor M. Victor , Spain

## Academic Editors

Ammar AL-Farga , Saudi Arabia  
Mohd Adnan , Saudi Arabia  
Ivanov Alexander , Russia  
Fabio Altieri , Italy  
Daniel Dias Rufino Arcanjo , Brazil  
Peter Backx, Canada  
Amira Badr , Egypt  
Damian Bailey, United Kingdom  
Rengasamy Balakrishnan , Republic of Korea  
Jiaolin Bao, China  
Ji C. Bihl , USA  
Hareram Birla, India  
Abdelhakim Bouyahya, Morocco  
Ralf Braun , Austria  
Laura Bravo , Spain  
Matt Brody , USA  
Amadou Camara , USA  
Marcio Carcho , Portugal  
Peter Celec , Slovakia  
Giselle Cerchiaro , Brazil  
Arpita Chatterjee , USA  
Shao-Yu Chen , USA  
Yujie Chen, China  
Deepak Chhangani , USA  
Ferdinando Chiaradonna , Italy

Zhao Zhong Chong, USA  
Fabio Ciccarone, Italy  
Alin Ciobica , Romania  
Ana Cipak Gasparovic , Croatia  
Giuseppe Cirillo , Italy  
Maria R. Ciriolo , Italy  
Massimo Collino , Italy  
Manuela Corte-Real , Portugal  
Manuela Curcio, Italy  
Domenico D'Arca , Italy  
Francesca Danesi , Italy  
Claudio De Lucia , USA  
Damião De Sousa , Brazil  
Enrico Desideri, Italy  
Francesca Diomede , Italy  
Raul Dominguez-Perles, Spain  
Joël R. Drevet , France  
Grégory Durand , France  
Alessandra Durazzo , Italy  
Javier Egea , Spain  
Pablo A. Evelson , Argentina  
Mohd Farhan, USA  
Ioannis G. Fatouros , Greece  
Gianna Ferretti , Italy  
Swaran J. S. Flora , India  
Maurizio Forte , Italy  
Teresa I. Fortoul, Mexico  
Anna Fracassi , USA  
Rodrigo Franco , USA  
Juan Gambini , Spain  
Gerardo García-Rivas , Mexico  
Husam Ghanim, USA  
Jayeeta Ghose , USA  
Rajeshwary Ghosh , USA  
Lucia Gimeno-Mallench, Spain  
Anna M. Giudetti , Italy  
Daniela Giustarini , Italy  
José Rodrigo Godoy, USA  
Saeid Golbidi , Canada  
Guohua Gong , China  
Tilman Grune, Germany  
Solomon Habtemariam , United Kingdom  
Eva-Maria Hanschmann , Germany  
Md Saquib Hasnain , India  
Md Hassan , India

Tim Hofer , Norway  
John D. Horowitz, Australia  
Silvana Hrelia , Italy  
Dragan Hrnčić, Serbia  
Zebo Huang , China  
Zhao Huang , China  
Tarique Hussain , Pakistan  
Stephan Immenschuh , Germany  
Norsharina Ismail, Malaysia  
Franco J. L. , Brazil  
Sedat Kacar , USA  
Andleeb Khan , Saudi Arabia  
Kum Kum Khanna, Australia  
Neelam Khaper , Canada  
Ramoji Kosuru , USA  
Demetrios Kouretas , Greece  
Andrey V. Kozlov , Austria  
Chan-Yen Kuo, Taiwan  
Gaocai Li , China  
Guoping Li , USA  
Jin-Long Li , China  
Qiangqiang Li , China  
Xin-Feng Li , China  
Jialiang Liang , China  
Adam Lightfoot, United Kingdom  
Christopher Horst Lillig , Germany  
Paloma B. Liton , USA  
Ana Lloret , Spain  
Lorenzo Loffredo , Italy  
Camilo López-Alarcón , Chile  
Daniel Lopez-Malo , Spain  
Massimo Lucarini , Italy  
Hai-Chun Ma, China  
Nageswara Madamanchi , USA  
Kenneth Maiese , USA  
Marco Malaguti , Italy  
Steven McAnulty, USA  
Antonio Desmond McCarthy , Argentina  
Sonia Medina-Escudero , Spain  
Pedro Mena , Italy  
V́ctor M. Mendoza-Núñez , Mexico  
Lidija Milkovic , Croatia  
Alexandra Miller, USA  
Sara Missaglia , Italy




Premysl Mladenka , Czech Republic  
Sandra Moreno , Italy  
Trevor A. Mori , Australia  
Fabiana Morroni , Italy  
Ange Mouithys-Mickalad, Belgium  
Iordanis Mourouzis , Greece  
Ryoji Nagai , Japan  
Amit Kumar Nayak , India  
Abderrahim Nemmar , United Arab Emirates  
Xing Niu , China  
Cristina Nocella, Italy  
Susana Novella , Spain  
Hassan Obied , Australia  
Pál Pacher, USA  
Pasquale Pagliaro , Italy  
Dilipkumar Pal , India  
Valentina Pallottini , Italy  
Swapnil Pandey , USA  
Mayur Parmar , USA  
Vassilis Paschalis , Greece  
Keshav Raj Paudel, Australia  
Ilaria Peluso , Italy  
Tiziana Persichini , Italy  
Shazib Pervaiz , Singapore  
Abdul Rehman Phull, Republic of Korea  
Vincent Pialoux , France  
Alessandro Poggi , Italy  
Zsolt Radak , Hungary  
Dario C. Ramirez , Argentina  
Erika Ramos-Tovar , Mexico  
Sid D. Ray , USA  
Muneeb Rehman , Saudi Arabia  
Hamid Reza Rezvani , France  
Alessandra Ricelli, Italy  
Francisco J. Romero , Spain  
Joan Roselló-Catafau, Spain  
Subhadeep Roy , India  
Josep V. Rubert , The Netherlands  
Sumbal Saba , Brazil  
Kunihiro Sakuma, Japan  
Gabriele Saretzki , United Kingdom  
Luciano Saso , Italy  
Nadja Schroder , Brazil

Anwen Shao , China  
Iman Sherif, Egypt  
Salah A Sheweita, Saudi Arabia  
Xiaolei Shi, China  
Manjari Singh, India  
Giulia Sita , Italy  
Ramachandran Srinivasan , India  
Adrian Sturza , Romania  
Kuo-hui Su , United Kingdom  
Eisa Tahmasbpour Marzouni , Iran  
Hailiang Tang, China  
Carla Tatone , Italy  
Shane Thomas , Australia  
Carlo Gabriele Tocchetti , Italy  
Angela Trovato Salinaro, Italy  
Rosa Tundis , Italy  
Kai Wang , China  
Min-qi Wang , China  
Natalie Ward , Australia  
Grzegorz Wegrzyn, Poland  
Philip Wenzel , Germany  
Guangzhen Wu , China  
Jianbo Xiao , Spain  
Qiongming Xu , China  
Liang-Jun Yan , USA  
Guillermo Zalba , Spain  
Jia Zhang , China  
Junmin Zhang , China  
Junli Zhao , USA  
Chen-he Zhou , China  
Yong Zhou , China  
Mario Zoratti , Italy

## Contents



---

**The Attenuation of Traumatic Brain Injury via Inhibition of Oxidative Stress and Apoptosis by Tanshinone IIA**

Yongpan Huang , Xian Long, Jiayu Tang , Xinliang Li , Xiang Zhang, Chunyan Luo, Yan Zhou, and Pan Zhang



Research Article (12 pages), Article ID 4170156, Volume 2020 (2020)

**Ezetimibe Attenuates Oxidative Stress and Neuroinflammation via the AMPK/Nrf2/TXNIP Pathway after MCAO in Rats**

Jing Yu, Wen-na Wang, Nathanael Matei, Xue Li, Jin-wei Pang, Jun Mo, Sheng-pan Chen, Ji-ping Tang, Min Yan , and John H. Zhang 

Research Article (14 pages), Article ID 4717258, Volume 2020 (2020)

**Apolipoprotein E Deficiency Aggravates Neuronal Injury by Enhancing Neuroinflammation via the JNK/c-Jun Pathway in the Early Phase of Experimental Subarachnoid Hemorrhage in Mice**

Yue Wu, Jinwei Pang, Jianhua Peng, Fang Cao, Zongduo Guo , Li Jiang, Zhipeng Teng, Zhijian Huang, Chongjie Cheng , Yong Jiang , and Xiaochuan Sun 

Research Article (15 pages), Article ID 3832648, Volume 2019 (2019)

**miR-185 and SEPT5 Genes May Contribute to Parkinson's Disease Pathophysiology**

Arman Rahimmi , Ilaria Peluso , Aref Rajabi , and Kambiz Hassanzadeh 

Research Article (8 pages), Article ID 5019815, Volume 2019 (2019)



## Research Article

# The Attenuation of Traumatic Brain Injury via Inhibition of Oxidative Stress and Apoptosis by Tanshinone IIA

Yongpan Huang <sup>1,2</sup>, Xian Long,<sup>1</sup> Jiayu Tang <sup>3</sup>, Xinliang Li <sup>2</sup>, Xiang Zhang,<sup>1</sup> Chunyan Luo,<sup>1</sup> Yan Zhou,<sup>1</sup> and Pan Zhang<sup>1</sup>

<sup>1</sup>Department of Clinic, Medicine School, Changsha Social Work College, Changsha, Hunan, China

<sup>2</sup>Department of Pharmacology, Institute of Chinese Medicine, Hunan Academy of Chinese Medicine, Changsha, China

<sup>3</sup>Department of Neurology, Brain Hospital of Hunan Province, Changsha, China

Correspondence should be addressed to Jiayu Tang; tangjiayu1978@163.com and Xinliang Li; lixinliang1024@163.com

Received 17 August 2019; Revised 31 October 2019; Accepted 28 November 2019; Published 4 May 2020

Guest Editor: Maurizio Forte

Copyright © 2020 Yongpan Huang et al. This is an open access article distributed under the Creative Commons Attribution License, which permits unrestricted use, distribution, and reproduction in any medium, provided the original work is properly cited.

Traumatic brain injury (TBI) is a major source of mortality and long-term disability worldwide. The mechanisms associated with TBI development are poorly understood, and little progress has been made in the treatment of TBI. Tanshinone IIA is an effective agent to treat a variety of disorders; however, the mechanisms of Tanshinone IIA on TBI remain unclear. The aim of the present study was to investigate the therapeutic potential of Tanshinone IIA on TBI and its underlying molecular mechanisms. Changes in microvascular permeability were examined to determine the extent of TBI with Evans blue dye. Brain edema was assessed by measuring the wet weight to dry weight ratio. The expression levels of CD11, interleukin- (IL-)  $1\beta$ , and tumor necrosis factor- (TNF-)  $\alpha$  mRNA were determined by reverse transcription-quantitative PCR. Aquaporin-4 (AQP4), glial fibrillary acidic protein (GFAP), and p47phox protein expression levels were detected by western blotting. Superoxide dismutase (SOD), catalase and glutathione peroxidase (GSH-PX) activities, and malondialdehyde (MDA) content were determined using commercial kits. Cell apoptosis was detected by western blotting and TUNEL staining. Tanshinone IIA (10 mg/kg/day, intraperitoneal administration) significantly reduced brain water content and vascular permeability at 12, 24, 48, and 72 h after TBI. Tanshinone IIA downregulated the mRNA expression levels of various factors induced by TBI, including CD11, IL- $1\beta$ , and TNF- $\alpha$ . Notably, CD11 mRNA downregulation suggested that Tanshinone IIA inhibited microglia activation. Further results showed that Tanshinone IIA treatment significantly downregulated AQP4 and GFAP expression. TBI-induced oxidative stress and apoptosis were markedly reversed by Tanshinone IIA, with an increase in SOD and GSH-PX activities and a decrease in the MDA content. Moreover, Tanshinone IIA decreased TBI-induced NADPH oxidase activation via the inhibition of p47phox. Tanshinone IIA attenuated TBI, and its mechanism of action may involve the inhibition of oxidative stress and apoptosis.

## 1. Introduction

Traumatic brain injury (TBI) is the most common cause of mortality and disability worldwide, and the damages induced by TBI can worsen the quality of life of the patients [1]. The brain damage following TBI is characterized by two phases, the initial, or primary, phase is characterized by direct cerebral tissue damage which results in glutamate release, calcium homeostasis disruption, N-methyl-D-aspartate receptor activation, permeability increase, and consecutive edema formation, which is an important self-protective

mechanism to minimize the extent of the damage immediately after TBI. Importantly, the first response phase involves diverse cellular and molecular mechanisms that are important to maintain the homeostasis of the damaged tissue [2]. These events may cause cellular structural damage, neuronal cell death, oxidative stress, brain edema, blood-brain barrier (BBB) breakdown, and inflammation [3]. Among these adverse factors, edema formation is considered to be a key to the consequences of TBI, which may deteriorate the prognosis. Accumulating evidence from clinical and experimental studies has expanded the current knowledge of the

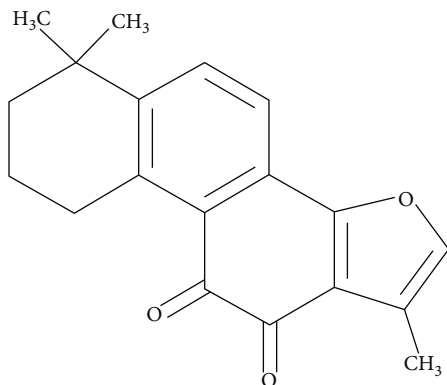


FIGURE 1: Structure of Tanshinone IIA.

pathophysiological phenomena underlying TBI and may facilitate the development of novel treatments with neuro-protective effects [4, 5].

Tanshinone IIA (Figure 1), a derivative of phenanthrenequinone derived from *Salvia miltiorrhiza* BUNGE (Danshen), possesses various pharmacological properties. A previous study showed that Tanshinone IIA is widely used in the treatment of cardiovascular and cerebrovascular diseases, inflammation, cholinesterase, collagenase, platelet aggregation, and cancer, due to its antioxidative activity [5–10]. Several previous studies showed that Tanshinone IIA has a protective effect by scavenging lipid free radicals, thus decreasing cytotoxicity *in vitro* and *in vivo* [11–14]. Further studies confirmed that Tanshinone IIA has significant protective effects against A $\beta$ -induced neurotoxicity in cultured cortical neurons and PC12 cells [15, 16]. A recent study showed that Tanshinone IIA could improve memory deficits by acting on the hippocampus in STZ-induced diabetic mice [17]. However, whether Tanshinone IIA could mitigate TBI remains unknown. Therefore, the present study is aimed at investigating the protective roles and the mechanisms of Tanshinone IIA in a rat model of TBI.

## 2. Materials and Methods

**2.1. Animal Studies and Ethics Statement.** Male Sprague-Dawley rats (weight, 220–250 g) were used in the present experiments. Animals had free access to food and water and were maintained in plastic cages at  $21 \pm 2^\circ\text{C}$  under a 12 h light/dark cycle. All the animal experiments were approved by Hunan Academy of Chinese Medicine Animal Care and Use Committee (approval no. Xiang 2019-0013). The animals were randomly assigned to the following groups: (i) Sham group ( $n = 24$ ), (ii) TBI group ( $n = 24$ ), and (iii) TBI + Tanshinone IIA (10 mg/kg/day) group ( $n = 24$ ). After TBI, rats were immediately treated with PBS or 10 mg/kg Tanshinone IIA intraperitoneally as previously described [18]. At 12, 24, 48, and 72 h following trauma, all animals were sacrificed for further analysis. In total, six animals were analyzed in each group.

**2.2. TBI Model Establishment.** A traumatic brain injury model was established as previously described [18]. The rats

were anesthetized and fixed in prone position, and the skull was cut sagittally. The injury was performed using a weight to damage the exposed area, 1.5 mm behind the coronal suture. A 2.5 mm diameter channel was drilled 2.5 mm to the right of the sagittal suture. The injury was performed in order to damage the bone window keeping the dura mater intact. The height of the falling weight was modulated to induce different degrees of contusion in the right parietal lobe. After TBI, all animals were kept and monitored until spontaneous respiration was reestablished. Sham group animals underwent anesthesia and scalp incision, but without TBI.

**2.3. Determination of Antioxidant Indices in Tissues.** The tissue levels of antioxidant indices including SOD, GSH-PX, CAT, and MDA were measured by commercial kits according to the instruction of manufacturer.

**2.4. Determination of Brain Edema.** The wet weight (WW) to dry weight (DW) ratio method was used to evaluate brain water content, as previously described [19]. The right brain hemispheres were rapidly removed from all animals post-mortem at the indicated time points after TBI. Brains were weighed (to measure the WW), dried at  $70^\circ\text{C}$  for 72 h, and weighed again (to measure the DW). The percentage of tissue water content was calculated as  $(\text{WW} - \text{DW})/\text{WW} \times 100\%$ .

**2.5. BBB Breakdown Evaluation.** Alterations in the microvascular permeability were examined to determine the extent of TBI by Evans blue dye (0.2 ml/100 g), which was injected through the femoral vein. Following anesthesia with 1% pentobarbital sodium (30–40 mg/kg), the thoracic cavity was exposed, intracardiac perfusion was performed with heparin saline, and the brain tissue was weighed, cut, and placed in dimethylformamide for 60 h at  $60^\circ\text{C}$ , centrifuged at 1,000 rpm for 5 min, and the absorbance at a wavelength of 620 nm was measured with a spectrophotometer. Data analysis was performed using Origin software (version s7.0), and the Evans blue content was calculated from the standard curve previously plotted.

**2.6. TUNEL Staining.** The formalin-fixed frontal cortex tissues were embedded in paraffin and sectioned (thickness,  $4 \mu\text{m}$ ). In total, five brain regions from each group were cut with a microtome. The sections were analyzed by TUNEL assay to detect the apoptotic rate. The TUNEL assay kit was purchased from Roche Molecular Biochemicals, and the experiment was conducted according to the manufacturer's protocol. Apoptotic cells with condensed nuclei were stained green, while normal cells were large, round, and not stained. The positive cells were analyzed under a fluorescence microscope by a blinded investigator. The extent of brain injury was evaluated by measuring the rate of TUNEL-positive cells.

**2.7. Real-Time PCR.** The gene expression level in brain tissues was determined by real-time PCR. Extracted total RNA was purified with 75% ethanol, and its concentration was determined by spectrophotometry. Then, the purified total RNA (200 ng) was retrotranscribed using a retrotranscription kit (DRR037A; Takara Bio, Inc.) and mixed to

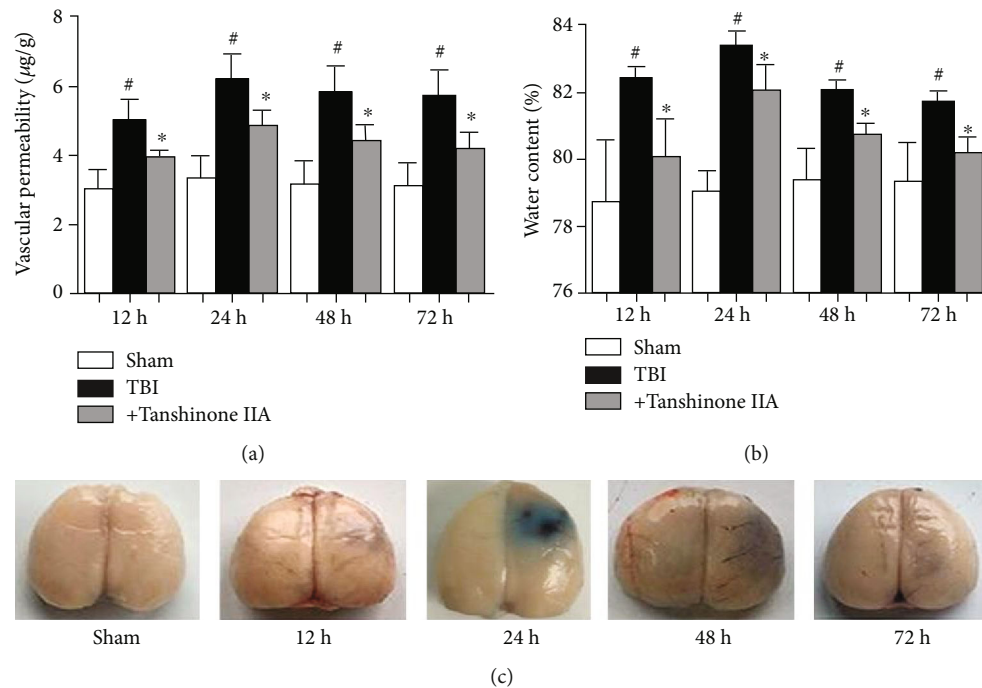


FIGURE 2: Tanshinone IIA attenuates brain tissue water content and vascular permeability. (a) Evans blue dye (0.2 ml/100 g) was injected through the femoral vein. (b) Brain tissue water content was analyzed and the percentage of tissue water content was calculated with the following formula:  $(WW - DW)/WW \times 100\%$ . (c) Evans blue staining of brain samples at 0, 12, 24, 48, and 72 h after TBI. Data are expressed as the mean  $\pm$  SEM.  $n = 6$  in each group. <sup>#</sup> $P < 0.05$  vs. Sham group; <sup>\*</sup> $P < 0.05$  vs. Tanshinone IIA group. TBI: traumatic brain injury; WW: wet weight; DW: dry weight.

obtain the first-strand cDNA template. Subsequently, the expression levels of CD68, interleukin- (IL-)1 $\beta$ , and tumor necrosis factor- (TNF-)  $\alpha$  were determined quantitatively by real-time PCR (ABI 7300) using the SYBR Premix Ex Taq kit (Takara Bio, Inc.).

**2.8. Western Blotting.** For western blotting analysis, 40  $\mu$ g protein (from each sample) was separated by SDS-PAGE (10% gel). The gel was transferred to a PVDF membrane, which was blocked with 5% milk powder and incubated with rabbit anti-aquaporin-4 (AQP4), glial fibrillary acidic protein (GFAP), and anti-p47phox at 4°C overnight. Subsequently, the membranes were washed and incubated with horseradish peroxidase-conjugated secondary antibodies, and the protein bands were developed using an ECL kit (Amersham Biosciences). The expression levels of the proteins were calculated using a Molecular Imager ChemiDoc XRS System (Bio-Rad Laboratories, Inc.). The protein expression level was normalized to  $\beta$ -actin.

**2.9. Statistical Analysis.** For statistical analysis, the SPSS software (version 21.0) was used. Data are presented as the mean  $\pm$  SEM. The data were analyzed by one-way ANOVA.  $P < 0.05$  was considered to indicate a statistically significant difference.

### 3. Results

**3.1. Effect of Tanshinone IIA on Brain Tissue Water Content and Vascular Permeability.** To test whether Tanshinone IIA

treatment exhibited neuroprotective effects after TBI, rats were sacrificed after treatment with or without Tanshinone IIA. As shown in Figure 2(c), the brain tissue water content increased significantly at 12, 24, 48, and 72 h in the TBI group, in particular, at 24 h.

The BBB is a specialized structure in the central nervous system that can block the entry of macromolecular substances from the peripheral blood into the brain parenchyma, thus maintaining cerebral homeostasis. The TBI-derived brain damage may alter the BBB permeability, promoting inflammation. Therefore, by measuring the amount of Evans blue dye in the brain, it is possible to assess the BBB breakdown and the vascular permeability in the brain tissue. The vascular permeability after TBI was examined to investigate whether Tanshinone IIA exerted its protective effect on the integrity of BBB structure and function following TBI. As shown in Figures 2(b) and 2(c), compared with the Sham group, the vascular permeability was significantly increased in the TBI group, which was reversed by Tanshinone IIA treatment.

**3.2. Effect of Tanshinone IIA on the Expression Levels of AQP4 and GFAP.** As the main water transporter in the central nervous system, AQP4 is involved in maintaining the water homeostasis in the BBB, and it is responsible for the formation of the vasogenic edema following TBI. To determine the effect of BBB impairment following TBI, the expression of AQP4 was investigated using western blotting analysis. As shown in Figure 3, TBI caused significant increases in AQP4 expression after 12, 24, 48, and 72 h. Tanshinone

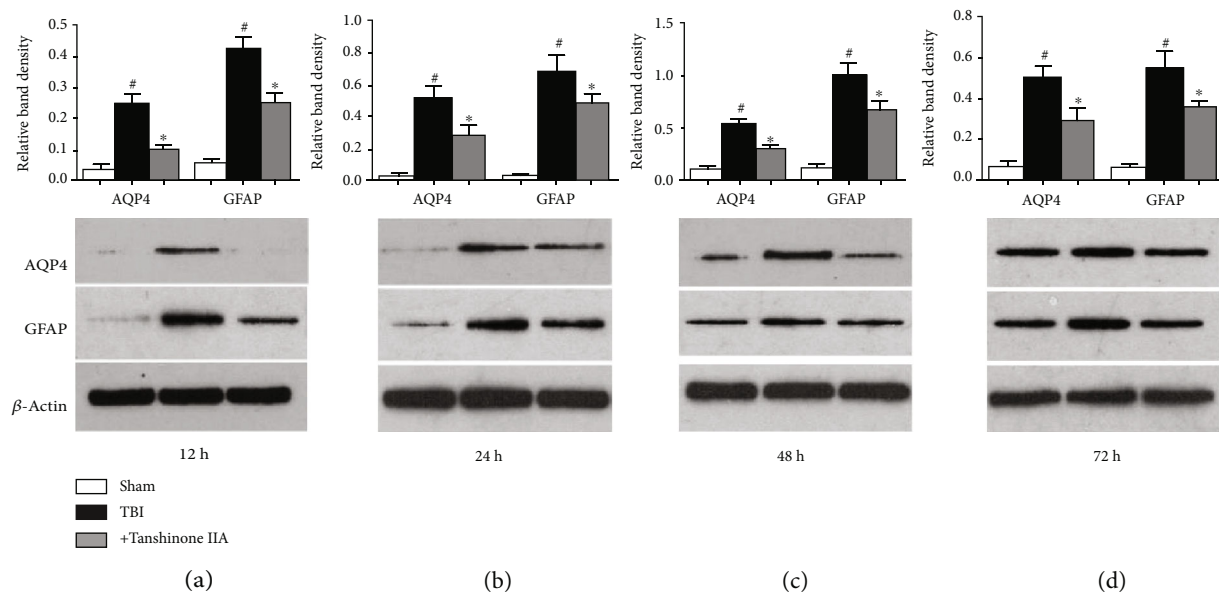


FIGURE 3: Effects of Tanshinone IIA on the expression levels of AQP4 and GFAP following TBI. (a) Western blotting analysis of AQP4 and GFAP at 12 h. (b) Western blotting analysis of AQP4 and GFAP at 24 h. (c) Western blotting analysis of AQP4 and GFAP at 48 h. (d) Western blotting analysis of AQP4 and GFAP at 72 h. Data are expressed as the mean  $\pm$  SEM.  $n = 6$  in each group. # $P < 0.05$  vs. Sham group; \* $P < 0.05$  vs. Tanshinone IIA group. TBI: traumatic brain injury; AQP4: aquaporin 4; GFAP: glial fibrillary acidic protein.

IIA treatment significantly decreased the expression level of AQP4, suggesting that Tanshinone IIA could regulate the permeability of BBB by regulating the expression levels of the proteins associated with this process. The present findings suggested that Tanshinone IIA could promote the repair of the BBB.

GFAP is only expressed in the perinuclear region and cytoplasm of mature glial cells in the central nervous system (CNS); it is involved in the formation of astrocyte cytoskeleton and has been used as surrogate marker of intracranial sequelae after TBI [20]. Therefore, the expression levels of GFAP were assessed by western blotting. As shown in Figure 3, TBI caused an increase in GFAP expression. Tanshinone IIA significantly reversed TBI-induced GFAP upregulation. The present results suggested that Tanshinone IIA alleviated TBI-induced injury.

**3.3. Effect of Tanshinone IIA on TBI-Induced Microglia Activation.** Microglia activation occurs after TBI and is considered to be an important factor underlying the damage induced by TBI. Moreover, microglia activation is associated with upregulation of IL-1 $\beta$  and TNF- $\alpha$ , thus aggravating TBI and increasing the risk of stroke. To assess microglia activation, western blotting was performed on the brain tissues at 24 h after TBI, and the expression level of the microglia activation marker CD11 was examined. As shown in Figure 4, the expression of CD11 mRNA, a marker of microglia, was increased in the brain tissue after TBI. Moreover, TNF- $\alpha$  and IL-1 $\beta$  mRNA expressions increased. However, the treatment with Tanshinone IIA downregulated the mRNA expression levels of CD11, TNF- $\alpha$ , and IL-1 $\beta$ , suggesting that Tanshinone IIA inhibited TBI-induced microglia activation.

**3.4. Effect of Tanshinone IIA on TBI-Induced Caspase-3 Activation.** Accumulating evidence demonstrated that the caspase cascade is involved in a variety of biological processes, including the initiation of apoptosis. Caspase-3 expression was analyzed to investigate whether caspase-3 was involved in TBI-induced apoptosis in the brain. As shown in Figures 5(a) and 5(b), TBI caused a significant increase in caspase-3 activation. By contrast, the caspase-3 level, upregulated by TBI, was downregulated by Tanshinone IIA treatment.

To further assess the effects of Tanshinone IIA on apoptosis, TUNEL staining was performed. As shown in Figures 5(c)–5(e), TBI increased cell apoptosis, as assessed by morphological alterations, including nuclear fragmentation and apoptotic bodies, typical of cells undergoing apoptosis. Tanshinone IIA decreased the number of apoptotic cells. The present results suggested that Tanshinone IIA exhibited protective effects on TBI by inhibiting the apoptotic pathway.

**3.5. Effect of Tanshinone IIA on TBI-Induced Oxidative Stress.** To determine the protective effect of Tanshinone IIA on TBI rats, various antioxidant factors, including superoxide dismutase (SOD), catalase (CAT), and glutathione peroxidase (GSH-PX), were examined. As shown in Figures 6(a)–6(d), compared with the Sham group, TBI caused decreases in the expression levels of SOD, CAT, and GSH-PX and an increase in MDA content. Tanshinone IIA significantly increased the activities of SOD, CAT, and GSH-PX and decreased MDA content. The present results suggested that Tanshinone IIA reduced oxidative stress.

NADPH oxidase activation is one of the main mechanisms underlying brain injury. The temporal pattern of NADPH oxidase activation and H<sub>2</sub>O<sub>2</sub> generation was

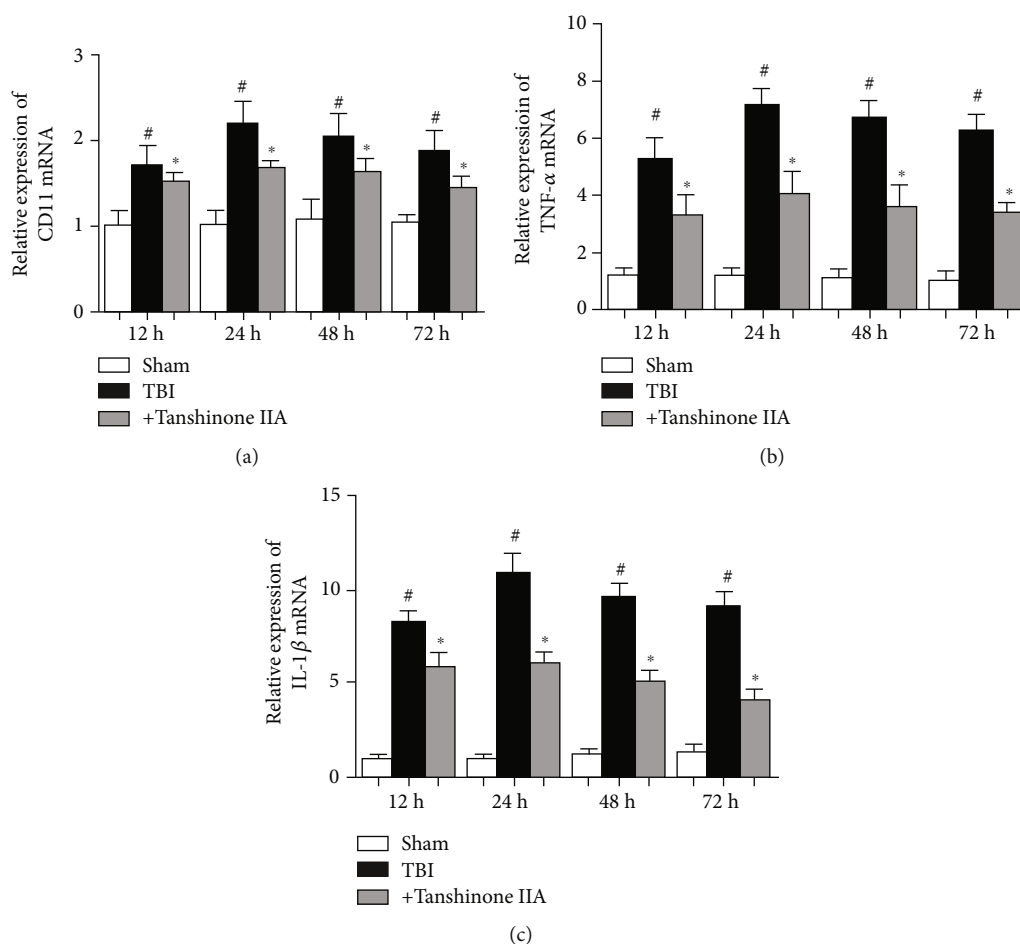


FIGURE 4: Effects of Tanshinone IIA on TBI-induced microglia activation. (a) RT-PCR analysis of the levels of CD11 expression. (b) RT-PCR analysis of the levels of TNF- $\alpha$  expression. (c) RT-PCR analysis of the levels of IL-1 $\beta$  expression. Data are expressed as the mean  $\pm$  SEM.  $n = 6$  in each group. # $P < 0.05$  vs. Sham group; \* $P < 0.05$  vs. Tanshinone IIA group. TBI: traumatic brain injury; RT: real-time.

examined in the adult rat cerebral tissue samples following TBI by controlled cortical contusion. As shown in Figures 7(a) and 7(b), mild TBI increased NADPH oxidase activity and  $H_2O_2$  levels at 24 h, but the trend increased at 48 h–72 h after TBI.

Subsequently, it was investigated whether the increase in  $H_2O_2$  generation in neurons following TBI was due to activation of NADPH oxidase. This phenomenon was examined by investigating the effect of a NADPH inhibitor, apocynin (4 mg/kg intraperitoneally administered 20 min prior to TBI), on  $H_2O_2$  generation in brain tissue following TBI. As shown in Figures 7(c)–7(g), pretreatment with apocynin markedly attenuated the generation of  $H_2O_2$  at 24 h after TBI compared with the Sham group, suggesting that NADPH oxidase served a critical role in  $H_2O_2$  production in neurons following TBI. The present findings suggested that NADPH oxidase was involved in the generation of  $H_2O_2$  following TBI.

**3.6. Effects of Tanshinone IIA on the Expression Levels of p47phox, gp91phox, and Rac1 following TBI.** A previous study reported that p47phox is the main subunit of NADPH oxidase, which is mainly expressed in the nervous system,

particularly in the microglia and the spinal cord, and is involved in ROS formation. As shown in Figures 8(a) and 8(b), p47<sup>phox</sup> subunit activation was reduced by Tanshinone IIA treatment at 24 h after TBI. However, Tanshinone IIA did not affect the translocation of Rac1 and the level of gp91phox expression. The present results suggested that Tanshinone IIA decreased NADPH oxidase activation via the inhibition of p47phox translocation.

## 4. Discussion

The present study investigated the effect of Tanshinone IIA on TBI and its underlying molecular mechanism. The present results suggested that Tanshinone IIA treatment significantly attenuated edema formation and decreased vascular permeability, inhibited inflammation, and reduced apoptosis, thus alleviating TBI-induced damage (Figure 9). Importantly, Tanshinone IIA effects were found to be associated with the inhibition of NADPH oxidase. The present results provided insight into the mechanisms underlying Tanshinone IIA function and indicated that Tanshinone may be a novel treatment to attenuate TBI.

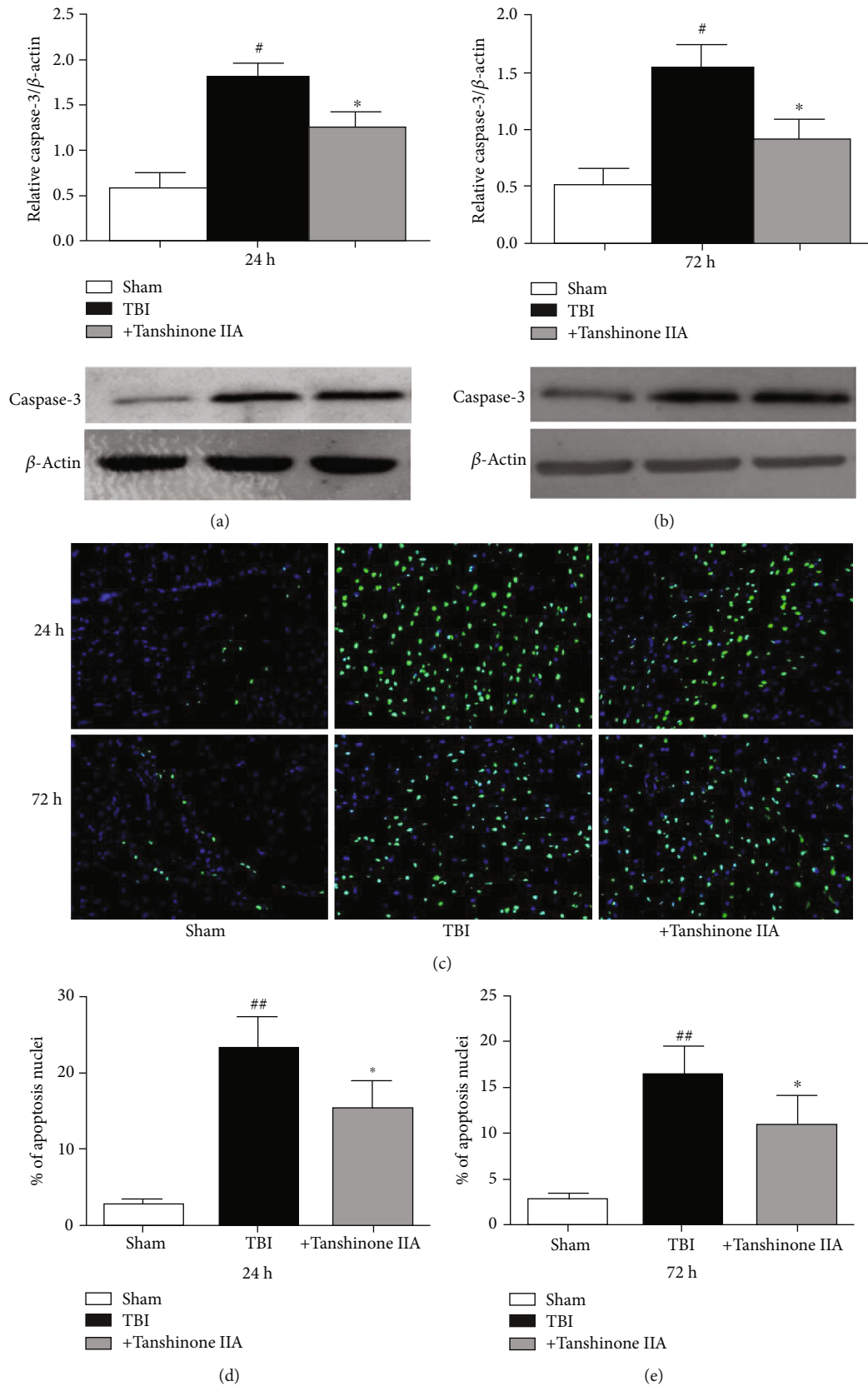


FIGURE 5: Tanshinone IIA alleviates TBI-induced apoptosis. (a, b) Western blotting analysis of Caspase-3 at 24 and 72 h. (c) TUNEL staining. Magnification,  $\times 200$ . (d, e) Apoptotic rate. Data are expressed as the mean  $\pm$  SEM.  $n = 6$  in each group.  $\#P < 0.05$  vs. Sham group;  $*P < 0.05$  vs. Tanshinone IIA group. TBI: traumatic brain injury.

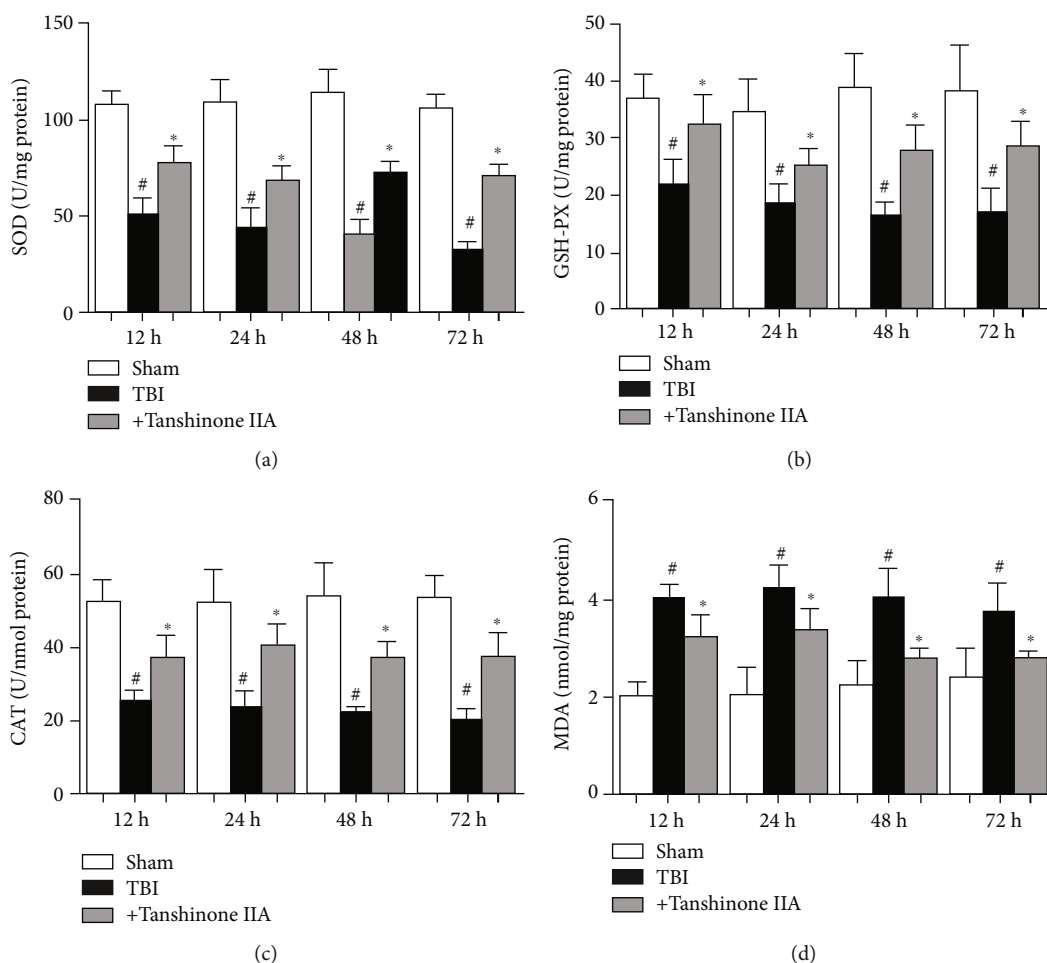


FIGURE 6: Effects of Tanshinone IIA on antioxidant levels in brain tissues. Measurement of (a) SOD, (b) GSH-PX, and (c) CAT activity. (d) MDA content. Data are expressed as the mean  $\pm$  SEM.  $n = 6$  in each group. #  $P < 0.05$  vs. Sham group; \*  $P < 0.05$  vs. Tanshinone IIA group. TBI: traumatic brain injury; SOD: superoxide dismutase; CAT: catalase; GSH-PX: glutathione peroxidase; MDA: malondialdehyde.

TBI is a leading cause of mortality and disability worldwide. The outcomes of TBI are often related to excitotoxicity, inflammation, metabolic dysfunction, oxidative stress, cellular necrosis, and apoptosis [21, 22]. In addition, its mechanisms are associated with the release of reactive oxygen species (ROS), edema formation, BBB breakdown, release of excitatory amino acids, and acute inflammatory response [23]. Edema formation and brain swelling are considered the most important symptoms of TBI. Brain tissue edema contributes to increase brain volume and intracranial pressure, impairing cerebral circulation and oxygenation, thus worsening ischemic injuries. AQP4 is the main water transporter in the brain and is involved in edema formation in TBI [24]. Previous studies showed that AQP4 regulates water homeostasis in BBB and is involved in the formation of the vasogenic edema, astrocyte migration, and neuronal excitability associated with TBI [25, 26]. Recent studies demonstrated that AQP4 deletion reduces brain edema formation after ischemia stroke in mice. AQP4 knockdown showed improved survival time compared with wide-type mice in a brain edema model. The use of AQP4-null mice provided strong evidence for AQP4 involvement in cerebral water bal-

ance. AQP4-null mice are protected from cellular (cytotoxic) brain edema produced by water intoxication, brain ischemia, or meningitis [26]. However, AQP4 deletion aggravates vasogenic (fluid leak) brain edema formed following intraparenchymal fluid infusion or brain abscess [25]. These previous studies suggested that the expression levels of AQP4 are associated with the integrity of the BBB. In the present study, Tanshinone IIA was found to exhibit protective effects on the integrity of BBB structure and function in an animal model of TBI. The present study found that AQP4 expression was significantly upregulated following TBI, and it was associated with an accumulation of Evans blue in the brain and with impaired BBB function. The TBI-induced upregulation of AQP4 was significantly attenuated in the presence of Tanshinone IIA. Moreover, previous studies demonstrated that TBI activates reactive astrogliosis, which is characterized by rapid synthesis of GFAP [27]. Additional studies demonstrated that GFAP can be used as a prognostic tool following severe TBI. Based on these previous studies, GFAP was hypothesized to be involved in the prediction of TBI severity. In the present study, TBI significantly upregulated GFAP. Moreover, the upregulation of

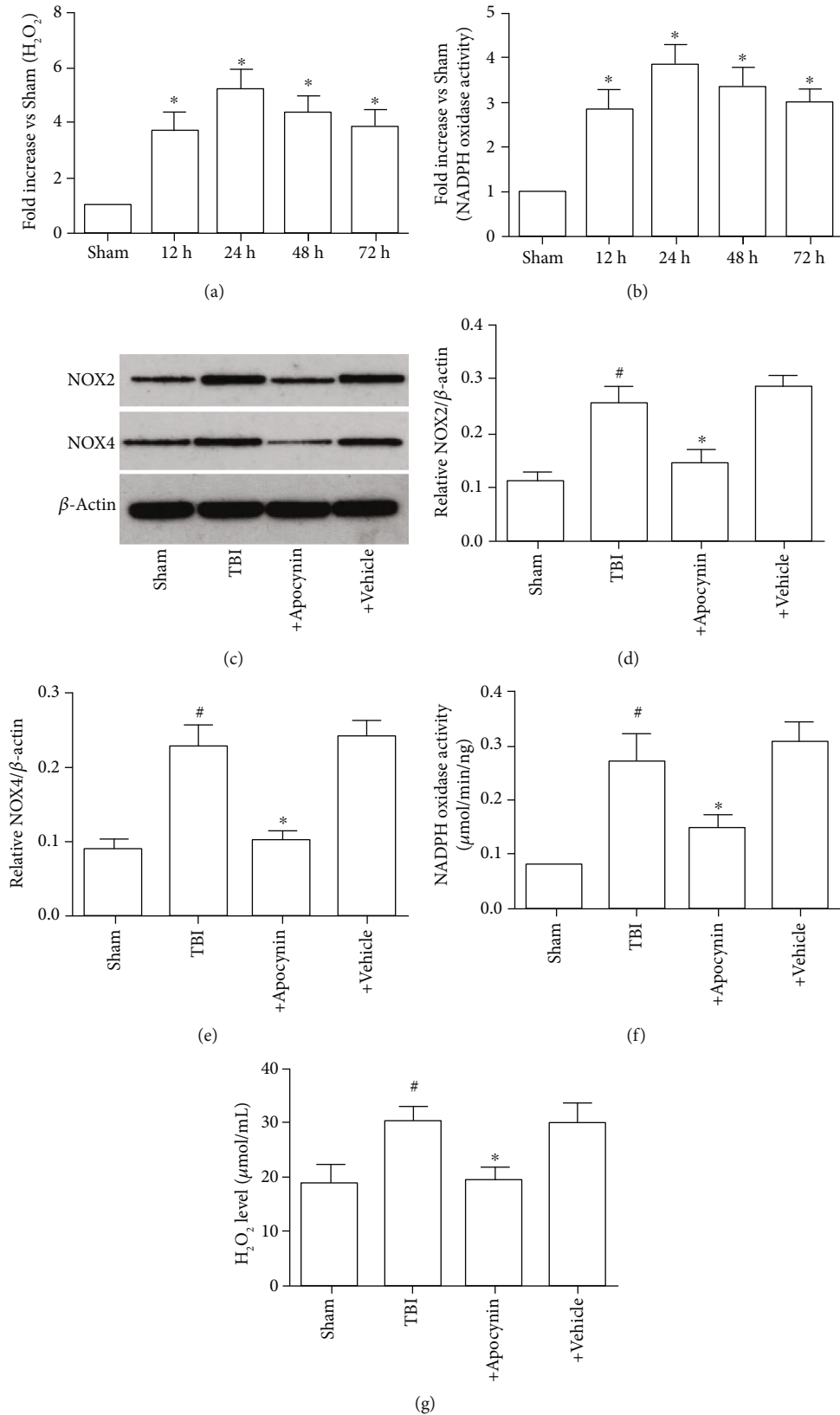


FIGURE 7: Induction of NADPH oxidase activation and  $O_2^-$  generation in the brain following TBI. (a) NADPH oxidase activity at 0, 12, 24, 48, and 72 h after TBI. (b)  $O_2^-$  production in the cerebral cortex at 0, 12, 24, 48, and 72 h after TBI. (c) Expression levels of NOX2 and NOX4. (d) Expression levels of NOX2. (e) Expression levels of NOX4. (f) NADPH oxidase activity at 24 h after TBI. (g)  $O_2^-$  production at 24 h after TBI. Data are expressed as the mean  $\pm$  SEM.  $n = 6$  in each group. # $P < 0.05$  vs. Sham group; \* $P < 0.05$  vs. Tanshinone IIA group. TBI: traumatic brain injury.



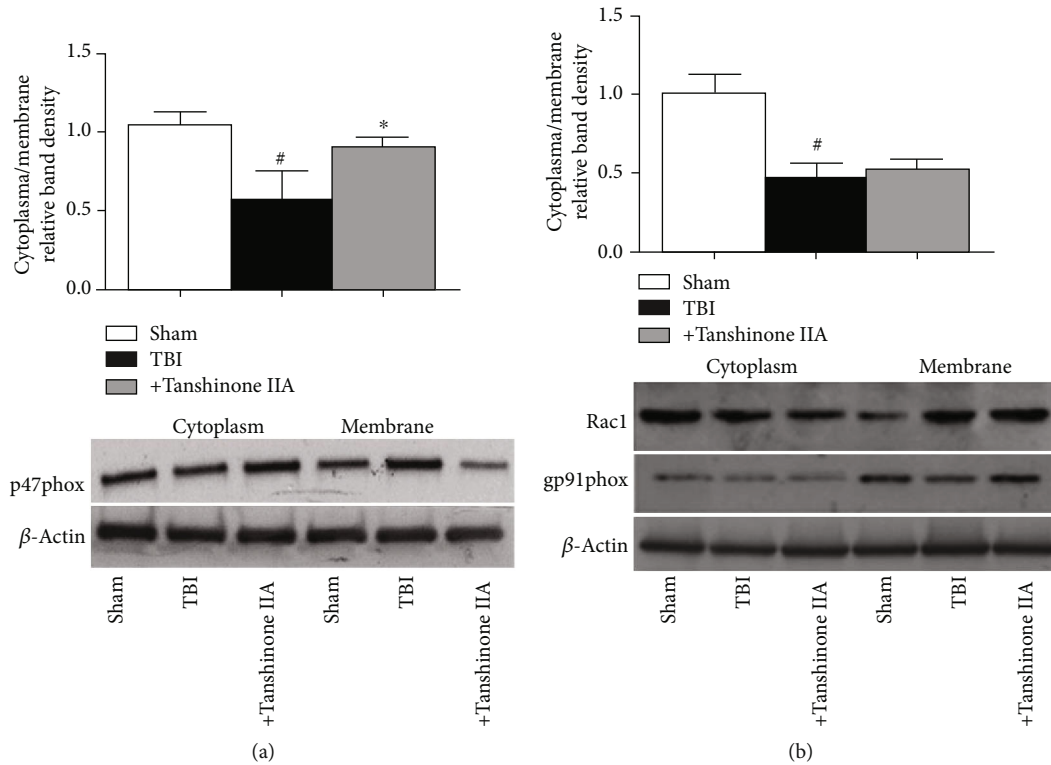


FIGURE 8: Effects of Tanshinone IIA on the expression levels of p47phox, gp91phox, and Rac1 following TBI. (a) Western blotting analysis of p47phox translocation from cytoplasm to membrane. (b) Western blotting analysis of gp91phox and Rac1 expressions.  $\beta$ -Actin was used as the loading control. Bands were analyzed by densitometric analysis. Data are expressed as the mean  $\pm$  SEM.  $n = 6$  in each group. # $P < 0.05$  vs. Sham group; \* $P < 0.05$  vs. Tanshinone IIA group. TBI: traumatic brain injury.

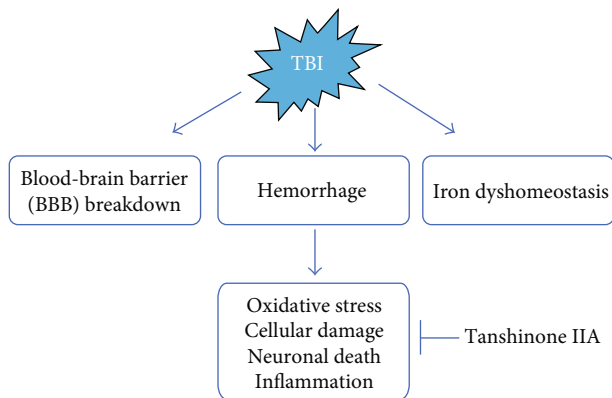


FIGURE 9: The consequence of Tanshinone IIA on TBI.

GFAP was decreased by Tanshinone IIA treatment. The present results suggested the protective effects of Tanshinone IIA on promoting the recovery of impaired BBB by decreasing the protein expression levels of factors involved in BBB breakdown following TBI.

Microglia are the most important innate immune cells in the CNS and are involved in the process of inflammation serving an important role in nervous system diseases [28, 29]. Microglia respond rapidly to changes in CNS microenvironment and pathological events, and these immune cells were shown to exhibit deleterious and beneficial roles in neuronal damage, phagocytizing necrotic cells and tissue frag-

ments, and activating or inhibiting numerous inflammatory mediators to maintain homeostasis [30]. Previous studies showed that activated microglia express high levels of CD11b, inducing the secretion of proinflammatory factors such as IL-1 $\beta$  and TNF- $\alpha$  [31]. Among the other proinflammatory factors released by activated microglia, inducible nitric oxide synthase, IL-6, and CCL2 aggravate brain damage. Microglia activation is considered as the initiator of the inflammatory response following brain damage. Several lines of studies showed that microglia activation is involved in the mediation of inflammation following TBI, contributing to neuronal damage via the release of IL-1 $\beta$ , TNF- $\alpha$ , and IL-6. Previous studies showed that activated microglia exerted neurotoxicity under certain conditions such as ischemia. These previous studies demonstrated that microglia activation increases the releases of IL-1 $\beta$ , TNF- $\alpha$ , and IL-6, further stimulating the production of matrix metalloproteinases and influencing the permeability of the BBB, inducing secondary brain edema. Therefore, these cytokines are considered to accelerate brain tissue damage following microglia activation. Inhibition of microglia activation was shown to prevent the release of inflammatory cytokines. The present study suggested that TBI induced CD11 upregulation and increased the release of IL-1 $\beta$ , TNF- $\alpha$ , and IL-6, which are neurotoxic. The present study suggested that microglia activation is significantly reduced in neurons following TBI and Tanshinone IIA treatment. These hints suggested that Tanshinone IIA could directly prevent microglia activation by decreasing apoptosis.

Accumulating evidence demonstrated that oxidative stress is considered the key contributor to secondary injury in the pathophysiology of TBI and oxidative stress is involved in the development of cerebral edema, inflammation, and secondary neuronal damage [32–34]. ROS are considered double-edged swords, since they can maintain cellular homeostasis in physiological conditions and aggravate certain pathological conditions, such as brain injury. NADPH oxidase is the main source of ROS in the brain tissue, and the activation of NADPH oxidase can deteriorate the state of TBI [35]. Overactivation of NADPH oxidase is an important mechanism underlying the increase in oxidative stress, which is associated with the occurrence and development of various diseases. NADPH oxidase is a multicomponent enzyme comprising membrane-bound cytochrome b558 (p22phox and gp91phox heterodimer) and cytosolic regulatory proteins (p67phox, p47phox, p40phox, and Rac2 GTPase). Under pathophysiological conditions, the activation of NADPH oxidase mainly relies on the phox subunits such as p47phox, which translocate to the membrane. Accumulating evidence demonstrated that the NADPH oxidase activation contributes to aggravate brain injury by mediating oxidative stress and microglia activation following TBI [36]. Additional studies showed that the inhibition of NADPH oxidase could decrease excessive ROS production following TBI, preventing programmed neuronal death and microglia activation [37]. Present results suggested that the expression level of p47phox was upregulated following TBI and the administration of Tanshinone IIA inhibited p47phox translocation. These results suggested that Tanshinone IIA reduced the TBI-associated overproduction of ROS through the inhibition of p47phox translocation.

Numerous studies demonstrated that ROS accumulation induced by TBI is a critical factor in brain damage [38]. Moreover, ROS overproduction is involved in the initiation of programmed cell death following TBI. Importantly, neuronal apoptosis may be a result of oxidative stress [37–39]. Considering the important role of oxidative stress in TBI, the investigation of ROS antioxidants or scavengers may provide novel strategies to inhibit TBI-induced cell apoptosis [32]. Tanshinone IIA is a potent antioxidant, and it is useful in the treatment of cardiovascular and cerebrovascular diseases. In particular, Tanshinone IIA can scavenge lipid free radicals, thus decreasing cytotoxicity *in vitro* and *in vivo*. In the present study, Tanshinone IIA showed antioxidative effects following TBI, including the increase in SOD, CAT, and GSH-PX activities, and decrease in MDA content, in line with previous studies. Furthermore, Tanshinone IIA treatment inhibited TBI-induced neuronal apoptosis *in vivo*. The present results suggested that the protective effects of Tanshinone IIA against TBI may involve its potent antioxidative activity.

Collectively, the present results suggested that Tanshinone IIA had neuroprotective properties including improved brain tissue edema formation, decreased the release of inflammatory mediators, and reduced oxidative damage and apoptosis via the inhibition of NADPH oxidase activation. The present results suggested that Tanshinone IIA may facilitate the development of novel therapeutic and preventive strategies for the treatment of TBI.

## Data Availability

The data used to support the findings of this study are available from the corresponding author upon request.

## Conflicts of Interest

There are no conflict of interests to declare.

## Authors' Contributions

Yongpan Huang designed and undertook experiments, and analyzed, interpreted, and presented results for group discussions. Xian Long, Chunyan Luo, Yan Zhou, Pan Zhang, and Xiang Zhang provided methods, description of results, and figures for the manuscript. Xinliang Li and Jiayu Tang provided rationale, background, framework, and feedback.

## Acknowledgments

This work was supported by Hunan National Science Funds (No. 2017JJ2343) and Hunan Provincial Administration of Traditional Chinese Medicine Research Project Fund (201894 to Jiayu Tang), Hunan Provincial Brain Hospital Key Scientific Research Project (2017A02 to Jiayu Tang), Key R&D Program of Hunan Province (2018SK1030 to Jiayu Tang), and Changsha Social Work College National Project Cultivation Project.

## References

- [1] J. Ghajar, "Traumatic brain injury," *The Lancet*, vol. 356, no. 9233, pp. 923–929, 2000.
- [2] J. J. Donkin, A. J. Nimmo, I. Cernak, P. C. Blumbergs, and R. Vink, "Substance P is associated with the development of brain edema and functional deficits after traumatic brain injury," *Journal of Cerebral Blood Flow and Metabolism*, vol. 29, no. 8, pp. 1388–1398, 2009.
- [3] J. M. Ziebell and M. C. Morganti-Kossmann, "Involvement of pro- and anti-inflammatory cytokines and chemokines in the pathophysiology of traumatic brain injury," *Neurotherapeutics*, vol. 7, no. 1, pp. 22–30, 2010.
- [4] N. Marklund, A. Bakshi, D. J. Castelbuono, V. Conte, and T. K. McIntosh, "Evaluation of pharmacological treatment strategies in traumatic brain injury," *Current Pharmaceutical Design*, vol. 12, no. 13, pp. 1645–1680, 2006.
- [5] B. Zhang, B. Wang, S. Cao, and Y. Wang, "Epigallocatechin-3-gallate (EGCG) attenuates traumatic brain injury by inhibition of edema formation and oxidative stress," *The Korean Journal of Physiology & Pharmacology*, vol. 19, no. 6, pp. 491–497, 2015.
- [6] J. Chen, Y. Bi, L. Chen, Q. Zhang, and L. Xu, "Tanshinone IIA exerts neuroprotective effects on hippocampus-dependent cognitive impairments in diabetic rats by attenuating ER stress-induced apoptosis," *Biomedicine & Pharmacotherapy*, vol. 104, pp. 530–536, 2018.
- [7] F. Maione, M. Piccolo, S. De Vita et al., "Down regulation of pro-inflammatory pathways by tanshinone IIA and cryptotanshinone in a non-genetic mouse model of Alzheimer's disease," *Pharmacological Research*, vol. 129, pp. 482–490, 2018.

- [8] F. Maione, V. Cantone, M. G. Chini, V. De Feo, N. Mascolo, and G. Bifulco, "Molecular mechanism of tanshinone IIA and cryptotanshinone in platelet anti-aggregating effects: an integrated study of pharmacology and computational analysis," *Fitoterapia*, vol. 100, pp. 174–178, 2015.
- [9] Y. Zhang, P. Jiang, M. Ye, S. H. Kim, C. Jiang, and J. Lu, "Tanshinones: sources, pharmacokinetics and anti-cancer activities," *International Journal of Molecular Sciences*, vol. 13, no. 10, pp. 13621–13666, 2012.
- [10] P. Panwar, S. Law, A. Jamroz et al., "Tanshinones that selectively block the collagenase activity of cathepsin K provide a novel class of ectosteric antiresorptive agents for bone," *British Journal of Pharmacology*, vol. 175, no. 6, pp. 902–923, 2018.
- [11] J. Fu, H. Huang, J. Liu, R. Pi, J. Chen, and P. Liu, "Tanshinone IIA protects cardiac myocytes against oxidative stress-triggered damage and apoptosis," *European Journal of Pharmacology*, vol. 568, no. 1–3, pp. 213–221, 2007.
- [12] J. Gao, G. Yang, R. Pi et al., "Tanshinone IIA protects neonatal rat cardiomyocytes from adriamycin-induced apoptosis," *Translational Research*, vol. 151, no. 2, pp. 79–87, 2008.
- [13] B. Wei, M. G. You, J. J. Ling et al., "Regulation of antioxidant system, lipids and fatty acid  $\beta$ -oxidation contributes to the cardioprotective effect of sodium tanshinone IIA sulphonate in isoproterenol-induced myocardial infarction in rats," *Atherosclerosis*, vol. 230, no. 1, pp. 148–156, 2013.
- [14] D. C. Li, X. Q. Bao, H. Sun, and D. Zhang, "Research progress in the study of protective effect of tanshinone IIA on cerebral ischemic stroke," *Yao Xue Xue Bao*, vol. 50, no. 6, pp. 635–639, 2015.
- [15] Y. H. Qian, Q. Xiao, and J. Xu, "The protective effects of tanshinone IIA on  $\beta$ -amyloid protein (1-42)-induced cytotoxicity via activation of the Bcl-xL pathway in neuron," *Brain Research Bulletin*, vol. 88, no. 4, pp. 354–358, 2012.
- [16] L. L. Shi, W. N. Yang, X. L. Chen et al., "The protective effects of tanshinone IIA on neurotoxicity induced by  $\beta$ -amyloid protein through calpain and the p35/Cdk5 pathway in primary cortical neurons," *Neurochemistry International*, vol. 61, no. 2, pp. 227–235, 2012.
- [17] C. Liu, Y. Wu, S. Zha et al., "Treatment effects of tanshinone IIA against intracerebroventricular streptozotocin induced memory deficits in mice," *Brain Research*, vol. 1631, pp. 137–146, 2016.
- [18] D. M. Feeney, M. G. Boyeson, R. T. Linn, H. M. Murray, and W. G. Dail, "Responses to cortical injury: I. methodology and local effects of contusions in the rat," *Brain Research*, vol. 211, no. 1, pp. 67–77, 1981.
- [19] R. Ge, Y. Zhu, Y. Diao, L. Tao, W. Yuan, and X. C. Xiong, "Anti-edema effect of epigallocatechin gallate on spinal cord injury in rats," *Brain Research*, vol. 1527, pp. 40–46, 2013.
- [20] J. R. Kulbe and J. W. Geddes, "Current status of fluid biomarkers in mild traumatic brain injury," *Experimental Neurology*, vol. 275, Part 3, pp. 334–352, 2016.
- [21] M. W. Ma, J. Wang, Q. Zhang et al., "NADPH oxidase in brain injury and neurodegenerative disorders," *Molecular Neurodegeneration*, vol. 12, no. 1, article 7, 2017.
- [22] D. A. Butterfield and T. T. Reed, "Lipid peroxidation and tyrosine nitration in traumatic brain injury: insights into secondary injury from redox proteomics," *Proteomics. Clinical Applications*, vol. 10, no. 12, pp. 1191–1204, 2016.
- [23] D. J. Sharp, G. Scott, and R. Leech, "Network dysfunction after traumatic brain injury," *Nature Reviews Neurology*, vol. 10, no. 3, pp. 156–166, 2014.
- [24] L. H. Wang, Z. L. Wang, W. Y. Chen, M. J. Chen, and G. Y. Xu, "The glymphatic system: concept, function and research progresses," *Sheng Li Xue Bao*, vol. 70, no. 1, pp. 52–60, 2018.
- [25] M. C. Papadopoulos and A. S. Verkman, "Aquaporin-4 and brain edema," *Pediatric Nephrology*, vol. 22, no. 6, pp. 778–784, 2007.
- [26] J. Kim, Y. H. Kim, D. Y. Park et al., "YAP/TAZ regulates sprouting angiogenesis and vascular barrier maturation," *The Journal of Clinical Investigation*, vol. 127, no. 9, pp. 3441–3461, 2017.
- [27] M. Sun, R. D. Brady, C. van der Poel et al., "A concomitant muscle injury does not worsen traumatic brain injury outcomes in mice," *Frontiers in Neurology*, vol. 9, article 1089, 2018.
- [28] J. H. Ahn, B. N. Shin, J. H. Park et al., "Pre- and post-treatment with novel antiepileptic drug oxcarbazepine exerts neuroprotective effect in the hippocampus in a gerbil model of transient global cerebral ischemia," *Brain Sciences*, vol. 9, no. 10, p. 279, 2019.
- [29] D. Boche, V. H. Perry, and J. A. Nicoll, "Review: activation patterns of microglia and their identification in the human brain," *Neuropathology and Applied Neurobiology*, vol. 39, no. 1, pp. 3–18, 2013.
- [30] Y. Tang and W. Le, "Differential roles of M1 and M2 microglia in neurodegenerative diseases," *Molecular Neurobiology*, vol. 53, no. 2, pp. 1181–1194, 2016.
- [31] W. Li, R. Deng, X. Jing, J. Chen, D. Yang, and J. Shen, "Acteoside ameliorates experimental autoimmune encephalomyelitis through inhibiting peroxynitrite-mediated mitophagy activation," *Free Radical Biology and Medicine*, vol. 146, pp. 79–91, 2019.
- [32] L. Dumitrescu, I. Popescu-Olaru, L. Cozma et al., "Oxidative stress and the microbiota-gut-brain axis," *Oxidative Medicine and Cellular Longevity*, vol. 2018, Article ID 2406594, 12 pages, 2018.
- [33] X. Chen, H. Wang, M. Zhou et al., "Valproic acid attenuates traumatic brain injury-induced inflammation *in vivo*: involvement of autophagy and the Nrf2/ARE signaling pathway," *Frontiers in Molecular Neuroscience*, vol. 11, p. 117, 2018.
- [34] G. Harish, A. Mahadevan, N. Pruthi et al., "Characterization of traumatic brain injury in human brains reveals distinct cellular and molecular changes in contusion and pericontusion," *Journal of Neurochemistry*, vol. 134, no. 1, pp. 156–172, 2015.
- [35] S. H. Lee, B. Y. Choi, A. R. Kho et al., "Inhibition of NADPH oxidase activation by apocynin rescues seizure-induced reduction of adult hippocampal neurogenesis," *International Journal of Molecular Sciences*, vol. 19, no. 10, p. 3087, 2018.
- [36] M. W. Ma, J. Wang, K. M. Dhandapani, R. Wang, and D. W. Brann, "NADPH oxidases in traumatic brain injury – promising therapeutic targets?," *Redox Biology*, vol. 16, pp. 285–293, 2018.
- [37] C. S. Piao, D. J. Loane, B. A. Stoica et al., "Combined inhibition of cell death induced by apoptosis inducing factor and caspases provides additive neuroprotection in experimental traumatic brain injury," *Neurobiology of Disease*, vol. 46, no. 3, pp. 745–758, 2012.

- [38] Y. Zhu, H. Wang, J. Fang et al., "SS-31 provides neuroprotection by reversing mitochondrial dysfunction after traumatic brain injury," *Oxidative Medicine and Cellular Longevity*, vol. 2018, Article ID 4783602, 12 pages, 2018.
- [39] Y. L. L. J. Wang, Y. T. Wang, C. Y. Xu et al., "Curcumin reduces hippocampal neuron apoptosis and JNK-3 phosphorylation in rats with A $\beta$ -induced Alzheimer's disease: protecting spatial learning and memory," *Journal of Neurorestoratology*, vol. 5, pp. 117–123, 2017.

## Research Article

# Ezetimibe Attenuates Oxidative Stress and Neuroinflammation via the AMPK/Nrf2/TXNIP Pathway after MCAO in Rats

Jing Yu,<sup>1,2</sup> Wen-na Wang,<sup>1,2</sup> Nathanael Matei,<sup>2,3</sup> Xue Li,<sup>1,2</sup> Jin-wei Pang,<sup>2</sup> Jun Mo,<sup>2</sup> Sheng-pan Chen,<sup>2</sup> Ji-ping Tang,<sup>2</sup> Min Yan <sup>1,2</sup> and John H. Zhang <sup>2,4</sup>

<sup>1</sup>Department of Anesthesiology, The Second Affiliated Hospital, Zhejiang University School of Medicine, Hangzhou, Zhejiang 310009, China

<sup>2</sup>Department of Physiology and Pharmacology, School of Medicine, Loma Linda University, Loma Linda, CA 92354, USA

<sup>3</sup>Department of Ophthalmology, University of Southern California, Los Angeles, CA 90007, USA

<sup>4</sup>Department of Neurosurgery and Anesthesiology, Loma Linda University Medical Center, Loma Linda, CA 92354, USA

Correspondence should be addressed to Min Yan; [zryanmin@zju.edu.cn](mailto:zryanmin@zju.edu.cn) and John H. Zhang; [johnzhang3910@yahoo.com](mailto:johnzhang3910@yahoo.com)

Received 16 May 2019; Revised 18 October 2019; Accepted 31 October 2019; Published 4 January 2020

Guest Editor: Maurizio Forte

Copyright © 2020 Jing Yu et al. This is an open access article distributed under the Creative Commons Attribution License, which permits unrestricted use, distribution, and reproduction in any medium, provided the original work is properly cited.

Oxidative stress and neuroinflammation play essential roles in ischemic stroke-induced brain injury. Previous studies have reported that Ezetimibe (Eze) exerts antioxidative stress and anti-inflammatory properties in hepatocytes. In the present study, we investigated the effects of Eze on oxidative stress and neuroinflammation in a rat middle cerebral artery occlusion (MCAO) model. One hundred and ninety-eight male Sprague-Dawley rats were used. Animals assigned to MCAO were given either Eze or its control. To explore the downstream signaling of Eze, the following interventions were given: AMPK inhibitor dorsomorphin and nuclear factor erythroid 2-related factor 2 (Nrf2) siRNA. Intranasal administration of Eze, 1 h post-MCAO, further increased the endogenous p-AMPK expression, reducing brain infarction, neurologic deficits, neutrophil infiltration, microglia/macrophage activation, number of dihydroethidium- (DHE-) positive cells, and malonaldehyde (MDA) levels. Specifically, treatment with Eze increased the expression of p-AMPK, Nrf2, and HO-1; Romo-1, thioredoxin-interacting protein (TXNIP), NOD-like receptor protein 3 (NLRP3), Cleaved Caspase-1, and IL-1 $\beta$  were reduced. Dorsomorphin and Nrf2 siRNA reversed the protective effects of Eze. In summary, Eze decreases oxidative stress and subsequent neuroinflammation via activation of the AMPK/Nrf2/TXNIP pathway after MCAO in rats. Therefore, Eze may be a potential therapeutic approach for ischemic stroke patients.

## 1. Introduction

Stroke accounts for 10% of all deaths worldwide [1]. The pathophysiology of stroke is composed of complex sequelae of cellular processes: oxidative stress, apoptosis, blood-brain barrier disruption, and inflammation [2–7]. Although the majority of ischemic strokes occur from embolic arterial occlusion, oxidative stress and neuroinflammation play significant roles in transient ischemic stroke and the reperfusion process [8, 9]. For example, neuroinflammatory responses to ischemic stroke are characterized by astrocyte activation and microglial resident, peripheral leukocyte infiltration, and proinflammatory mediator release. Moreover, infiltrated neutrophils and activated microglia produce free radicals

and oxidants that damage the central nervous system tissue, leading to long-term disabilities and death in stroke patients [10]. Therefore, developing a protective strategy against oxidative stress and subsequent neuroinflammation may be an effective approach for the treatment of ischemic stroke patients.

Ezetimibe (Eze) is a new lipid-lowering agent that inhibits Niemann-Pick disease type C1-like 1- (NPC1L1-) dependent cholesterol absorption [11, 12]; however, studies have shown Eze to exert pleiotropic effects independent of NPC1L1 [13–15]. For example, we have previously demonstrated that intranasal administration of Eze attenuated neuronal apoptosis through the activation of AMPK-dependent autophagy after MCAO in rats [16]. In a rat liver

ischemia/reperfusion model, Eze therapeutically exerted antioxidation effects by modulating glutathione and glutathione peroxidase [14]. In an Alzheimer mouse model, researchers reported that treatment with Eze reduced the memory dysfunctions associated with dementia [17]. Of importance, a randomized and placebo-controlled clinical study reported that treatment with Eze prevented the progression of the deleterious symptoms associated with acute stroke [18]. Lastly, in hepatocyte mouse models, studies have shown that the anti-inflammatory effects of Eze were dependent on AMPK autophagic induction and NLRP3 inflammatory inhibition [19, 20].

Mechanistically, AMPK phosphorylation promotes the activation of the master antioxidant regulator, nuclear factor erythroid 2-related factor 2 (Nrf2) [21], and reduces free radicals by increasing heme oxygenase 1 (HO-1), a downstream factor of Nrf2, which decreases proinflammatory cytokines [22]. Linking oxidative stress to inflammation in ischemic stroke, the inhibition of thioredoxin-interacting protein (TXNIP) was shown to decrease the activation of inflammasome-dependent pathways [23–25]. For example, in an acute cerebral ischemic injury model, activation of Nrf2 attenuated TXNIP and NOD-like receptor protein 3 (NLRP3) inflammasomes [26]. Taken together, Eze exerts its pleiotropic effects through activation of Nrf2 via AMPK-dependent pathways [20].

Therefore, in the current study, we assessed the hypothesis that intranasal administration of Eze may attenuate oxidative stress and neuroinflammation in a rat model of MCAO via the AMPK/Nrf2/TXNIP pathway.

## 2. Materials and Methods

**2.1. Animals.** All experiments were approved by the Institutional Animal Care and Use Committee of Loma Linda University in accordance with the NIH Guide for the Care and Use of Laboratory Animals (NIH Publications No. 8023, revised 1978) and the ARRIVE2009 Guidelines for Reporting Animal Research [27]. A total of 198 adult male Sprague-Dawley rats (260–280 g) were obtained from the Experimental Animal Center of Loma Linda University. Rats were housed in a controlled humidity and temperature room with a 12 h light/dark cycle and free access to water and food.

**2.2. MCAO Model.** The transient MCAO model was used in male Sprague-Dawley rats as previously described [28]. Briefly, anesthesia was induced intraperitoneally with a mixture of ketamine (80 mg/kg, K2573; Sigma-Aldrich, St. Louis, MO, USA) and xylazine (10 mg/kg, X1126; Sigma-Aldrich, St. Louis, MO, USA). Next, atropine was administered (0.1 mg/kg) subcutaneously. The depth of anesthesia was checked by pinch-paw reflex. The right common carotid artery (CCA), internal carotid artery (ICA), and external carotid artery (ECA) were surgically exposed. The ECA was ligated, and a 4–0 nylon suture with a silicon tip was then inserted through the ECA stump into the ICA, occluding the MCA, approximately 18 to 22 mm from the insertion point. After 2 h of MCAO, the suture was removed to begin

reperfusion. Sham rats underwent the same protocol without occlusion of the MCA.

**2.3. Experimental Design.** Animals were divided into groups for three experimental studies in a randomized fashion by generating random numbers using Excel, and experiments were performed in a blinded manner (Figure 1); the experimental groups and sample size are listed in Table 1.

**2.3.1. Experiment 1.** To determine the time course of endogenous AMPK and phosphorylated AMPK (p-AMPK) after MCAO or MCAO+Eze, 54 rats were randomly divided into 9 groups ( $n = 6$  per group): sham, MCAO 6 h, MCAO 12 h, MCAO 24 h, MCAO 72 h, MCAO+Eze 6 h, MCAO+Eze 12 h, MCAO+Eze 24 h, and MCAO+Eze 72 h. Western blot analysis was used to detect the expression of p-AMPK in the ipsilateral/right hemisphere of each group.

**2.3.2. Experiment 2.** To evaluate the neuroprotective effects of intranasal administration of Eze at 1 h after MCAO, 30 rats were randomly assigned into the following five groups ( $n = 6$  per group): (1) sham group, (2) MCAO+vehicle (10% dimethyl sulfoxide (DMSO) in phosphate-buffered saline (PBS)), (3) MCAO+Eze (250  $\mu\text{g}/\text{kg}$ ), (4) MCAO+Eze (500  $\mu\text{g}/\text{kg}$ ), and (5) MCAO+Eze (1 mg/kg). Infarction volume, modified Garcia, and beam walking scores were assessed at 24 h after MCAO ( $n = 6$  per group). After 2,3,5-triphenyltetrazolium chloride (TTC) staining, the ipsilateral/right brain samples were collected for additional western blots ( $n = 6$  per group). According to our infarction volume and neurobehavioral results, Eze at a dose of 500  $\mu\text{g}/\text{kg}$  had the highest efficacy and was used for the subsequent experiments.

To explore the effects of Eze treatment on neutrophil infiltration and microglia/macrophage activation at 24 h after MCAO, 18 rats were randomly divided into sham, MCAO +vehicle, and MCAO+Eze 500  $\mu\text{g}/\text{kg}$  groups ( $n = 6$  per group). Immunofluorescence staining of myeloperoxidase (MPO) and Iba-1 was performed, and quantitative analyses of MPO and Iba-1-positive cells were counted in the ischemic penumbra at 24 h after MCAO. The expression of MPO and Iba-1 among the three groups was measured by western blot at 24 h after MCAO.

To explore the effects of Eze treatment on oxidative stress at 24 h after MCAO, another 18 rats from sham, MCAO +vehicle, and MCAO+Eze 500  $\mu\text{g}/\text{kg}$  were used to measure malonaldehyde (MDA) levels ( $n = 6$  per group). Dihydroethidium (DHE) staining was performed, and the number of DHE-positive cells was counted in the ischemic penumbra at 24 h after MCAO (shared with the immunofluorescence-stained samples). The expression of Romo-1 among the three groups was measured by western blot at 24 h after MCAO.

**2.3.3. Experiment 3.** To explore the underlying mechanisms of Eze-mediated antioxidation and anti-inflammatory effects after MCAO, dorsomorphin, a selective AMPK inhibitor, was administered intracerebroventricularly (i.c.v.) 30 min before MCAO; Nrf2 small interfering RNA (Nrf2 siRNA) was administered i.c.v. at 48 h before MCAO, followed by administration of Eze (500  $\mu\text{g}/\text{kg}$ ) at 1 h after MCAO. Rats

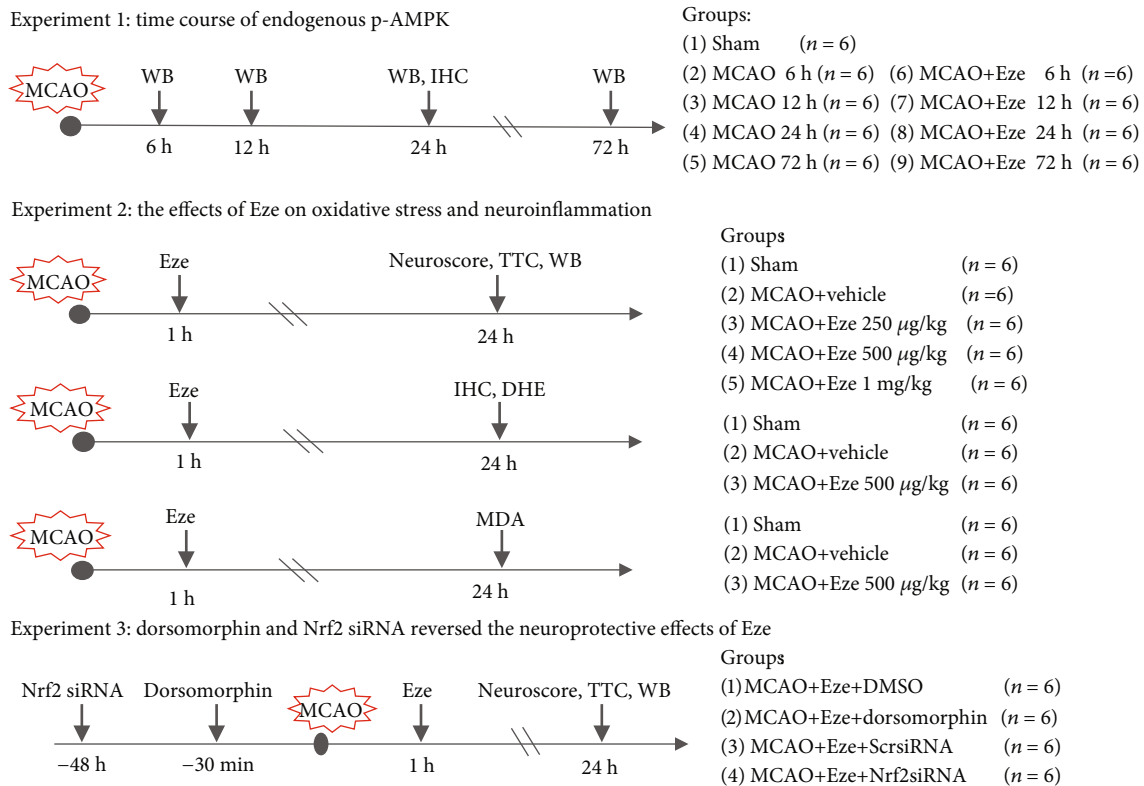


FIGURE 1: Experimental design and animal groups. DHE: dihydroethidium; DMSO: dimethyl sulfoxide; dorsomorphin: AMPK inhibitor; Eze: Ezetimibe; IHC: immunohistochemistry; MCAO: middle cerebral artery occlusion; MDA: malonaldehyde; Scr siRNA: scramble siRNA; TTC: 2,3,5-triphenyltetrazolium chloride; WB: western blot.

TABLE 1: Summary of experimental groups and mortality rate in the study. A total of 198 rats were used in the following groups: naive (24), sham (24), and MCAO (150). Each experiment utilized a predefined exclusion criterion: no infarction volume after MCAO (n = 6).

Groups	Neuroscore TTC staining	IHC DHE	MDA	WB	Mortality	Exclusion	Subtotal
<i>Experiment 1</i>							
Sham				6	0	0	6
MCAO (6 h, 12 h, 24 h, and 72 h)				8 * 6	10 (17.2%)	3	61
<i>Experiment 2</i>							
Sham	6	6	6	6	0	0	18
MCAO+vehicle	6	6	6	6	5 (21.7%)	1	24
MCAO+Eze (250 µg/kg)	6				1 (14.3%)	0	7
MCAO+Eze (500 µg/kg)	6	6	6	6	3 (14.3%)	0	21
MCAO+Eze (1 mg/kg)	6				1 (14.3%)	1	8
<i>Experiment 3</i>							
Naive+DMSO				6	0	0	6
Naive+dorsomorphin				6	0	0	6
Naive+Eze+DMSO				6	0	0	6
Naive+Eze+dorsomorphin				6	0	0	6
MCAO+Eze+DMSO	6			6	1 (14.3%)	0	7
MCAO+Eze+dorsomorphin	6			6	2 (25%)	0	8
MCAO+Eze+Scr siRNA	6			6	0	0	6
MCAO+Eze+Nrf2 siRNA	6			6	1 (14.3%)	1	8
<b>Total</b>	<b>54</b>	<b>18</b>	<b>18</b>	<b>78 (+42)</b>	<b>24 (16.7%)</b>	<b>6</b>	<b>198</b>

were randomly divided into seven groups ( $n = 6$  per group): sham, MCAO+vehicle, MCAO+Eze, MCAO+Eze+DMSO, MCAO+Eze+dorsomorphin, MCAO+Eze+scramble siRNA (Scr siRNA), and MCAO+Eze+Nrf2 siRNA. Ipsilateral brain samples were collected for TTC staining and western blots at 24 h after MCAO (sham, MCAO+vehicle, and MCAO+Eze were shared with experiment 2;  $n = 6$  per group). Infarction volume, neurobehavioral tests, and western blot analyses were performed at 24 h after MCAO.

Additionally, to evaluate the effects of AMPK inhibition via dorsomorphin, 24 rats were randomly divided into four groups: naive+DMSO, naive+dorsomorphin, naive+Eze+DMSO, and naive+Eze+dorsomorphin. The expression of phosphorylated AMPK was evaluated by western blot.

**2.4. Intranasal Administration of Eze.** Intranasal administration was performed as previously described [29]. Briefly, rats were treated 1 h after MCAO with DMSO or Eze (250  $\mu\text{g}/\text{kg}$ , 500  $\mu\text{g}/\text{kg}$ , and 1 mg/kg dissolved in 10% DMSO, purity  $\geq 98\%$ , SML-1629, Sigma-Aldrich, St. Louis, MO, USA) in a supine position under 2% isoflurane anesthesia. A total volume of 25  $\mu\text{l}$  was delivered into the bilateral nares, alternating one naris at a time, every 5 min over a period of 20 min.

**2.5. Intracerebroventricular Injection.** Intracerebroventricular (i.c.v.) administration was performed as previously described [28]. Briefly, rats were placed in a stereotaxic apparatus under 2.5% isoflurane anesthesia. A scalp incision was made along the midline, and a 1 mm burr hole was drilled into the skull. The stereotaxic i.c.v. injection site was relative to the bregma: anteroposterior 1 mm, right lateral 1.5 mm, and depth 3.5 mm. The AMPK-specific inhibitor, dorsomorphin (0.1  $\mu\text{mol}$ , purity  $\geq 98\%$ , P5499, Sigma-Aldrich, St. Louis, MO, USA), was dissolved in 20% DMSO in PBS, and 10  $\mu\text{l}$  was delivered into the ipsilateral ventricle with a Hamilton syringe (Microliter 701; Hamilton Company, USA) 30 min before MCAO [30]. The same volume of DMSO was used as a negative control. Nrf2 siRNA (SR508224; OriGene, Rockville, MD, USA) and scrambled siRNA (SR30004; OriGene) were prepared at 500 pmol in RNase free suspension buffer and administered (5  $\mu\text{l}$  of the siRNAs) 48 h before MCAO [31]. Lastly, the burr hole was sealed with bone wax, and the dissection was sutured.

**2.6. Neurobehavioral Function Assessment.** Neurobehavioral function was assessed with the modified Garcia and beam walking tests by an independent, blinded researcher at 24 h after MCAO, as previously described [32]. To understand the effect of neuronal lesions on sensorimotor areas, the modified Garcia test was used to measure hemiplegia, motor performance deficits, and abnormal postures [33]. The modified Garcia scoring system consisted of 6 tests covering spontaneous activity, symmetry in the movement of four limbs, forepaw outstretching, climbing, body proprioception, and response to vibrissae touch, with a maximum score of 18, higher scores indicating better performance. In addition, to better assess cortical motor injury, the beam walking test was used to measure dysfunction in memory, motivation, attention, somatomotor, and locomotor functions [34]. The

beam walking test was performed with a 0-5-point scale as previously described [35].

**2.7. Cerebral Infarction Volume Assessment.** Under deep anesthesia, animals were perfused with cold PBS (0.1 M, pH 7.4) as previously described [36]. Brains were removed and coronally sliced into 2 mm thick sections. Brain slices were incubated in 2% 2,3,5 triphenyltetrazolium chloride (TTC, Sigma-Aldrich, St. Louis, MO, USA) for 15 min at 37°C. The infarcted brain tissue appeared white, whereas the noninfarcted region appeared red. The infarct and total hemispheric areas of each slice were measured using ImageJ (ImageJ 1.5; NIH, Bethesda, MD, USA). The area of each slice was calculated using the following formula:  $((\text{area of contralateral} - \text{area of noninfarcted ipsilateral tissue})/2 * (\text{area of contralateral})) * 100\%$ . The area was calculated for each slice, and the average was taken to represent the percentage of infarcted area for that animal [37, 38].

**2.8. Immunofluorescence Staining.** Twenty-four hours after MCAO, under deep anesthesia, rats were perfused with ice-cold PBS and then 10% formalin. The brains were removed and fixed in formalin and then dehydrated with 30% sucrose. Next, brain samples were snap-frozen and cut into 10  $\mu\text{m}$  thick coronal sections using a cryostat (LM3050S; Leica Microsystems, Bannockburn, Germany). Immunofluorescence staining was performed as previously described [39]. Briefly, brain samples were incubated overnight at 4°C with primary antibodies including anti-Iba-1 (1:100, Abcam, ab5076) and anti-MPO (1:500, Abcam, ab65871). The sections were then incubated with the appropriate fluorescence-conjugated secondary antibodies (1:200, Jackson ImmunoResearch) for 1 h at room temperature and then visualized with a fluorescence microscope (DMI8, Leica Microsystems, Germany).

### 2.9. Measurement of Oxidative Stress

**2.9.1. MDA Assay.** Malonaldehyde (MDA), as an oxidative damage marker, was determined using the MDA assay kits (MAK805, Sigma-Aldrich, St. Louis, MO, USA) as per the manufacturer's protocols.

**2.9.2. DHE Staining.** Dihydroethidium (DHE) staining was performed as previously described [40]. Briefly, 10  $\mu\text{m}$  thick frozen brain sections were incubated with 2  $\mu\text{mol}/\text{l}$  fluorescent dye DHE (D1168, Thermo Fisher Scientific, Waltham, MA, USA) at 37°C for 30 min in a humidified chamber and protected from light. The DHE-positive cells were observed under a fluorescence microscope (DMI8, Leica Microsystems, Germany), and the positive cells were counted by using ImageJ software (ImageJ 1.5; NIH, Bethesda, MD, USA).

**2.10. Western Blot Analysis.** After TTC staining at 24 h after MCAO, brain slices were separated into the contralateral and ipsilateral hemispheres, flash frozen in liquid nitrogen, and then stored at  $-80^\circ\text{C}$  freezer. Western blot was performed as previously described [41]. Nuclear proteins were extracted from tissue homogenates using a nuclear extraction kit (ab113474, Abcam, Cambridge, MA, USA) according to



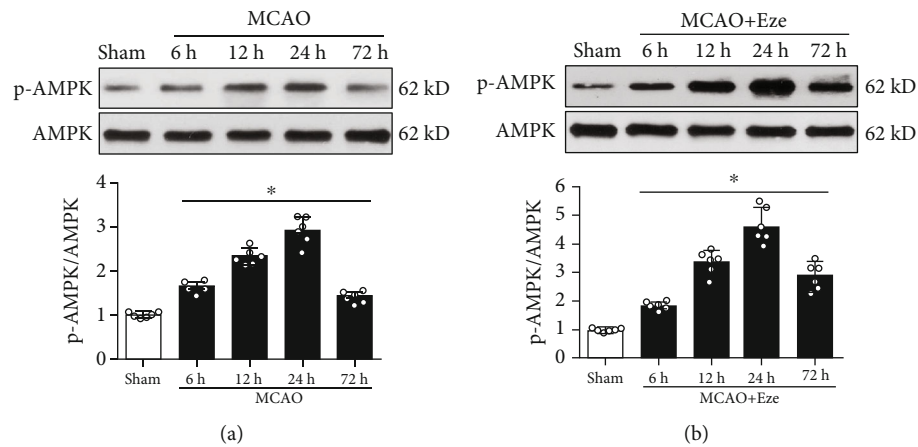


FIGURE 2: Expression of endogenous p-AMPK after MCAO. (a) Representative western blot bands and quantitative analysis of p-AMPK expression in the ipsilateral hemisphere after MCAO. (b) Representative western blot band and quantitative analysis of p-AMPK expression after treatment with Ezetimibe. The dose of Ezetimibe was 500 µg/kg. \* $p < 0.05$  vs. sham.  $n = 6$  per group.

the manufacturer's protocol. Equal amounts of protein samples from the ipsilateral hemispheres were separated by 10% SDS-PAGE and transferred onto nitrocellulose membranes. After blocking with 5% nonfat milk at 20–25°C for 1 h, samples were incubated overnight at 4°C with primary antibodies against AMPK (1:1000, CST, 5832), phosphorylated AMPK (p-AMPK, 1:1000, CST, 2535), Nrf2 (1:1000, Abcam, ab31163), HO-1 (1:1000, Abcam, ab13248), TXNIP (1:500, Proteintech, 18243-1-AP), NLRP3 (1:500, Abcam, ab214185), Caspase-1 (1:500, NOVUS, NBPI-45433), Interleukin- (IL-) 1 $\beta$  (1:500, Abcam, ab9787), Romo-1 (1:200, AVIVA Systems Biology, ARP58431\_P050), Iba-1 (1:1000, Abcam, ab5076), MPO (1:500, Abcam, ab65871); Lamin B1 (1:1000, Proteintech, 12987-1-AP), and  $\beta$ -actin (1:4000, Santa Cruz Biotechnology, sc-47778). Appropriate secondary antibodies (1:4000, Santa Cruz Biotechnology) were selected for the incubated membrane the following day for 1 h at room temperature. Immunoblots were then visualized with an ECL Plus chemiluminescence reagent kit (RPN3243; Amersham Bioscience, Bensenville, IL, USA) and quantified with optical methods using the ImageJ software (ImageJ 1.5; NIH, Bethesda, MD, USA). The results were normalized using  $\beta$ -actin or Lamin B1 as an internal control.

**2.11. Statistical Analysis.** All data were expressed as the mean and standard deviation (mean  $\pm$  SD). Statistical analysis was performed with GraphPad Prism 6 software (La Jolla, CA, USA). Before analysis, the Shapiro-Wilk test was used to test normality. For parametric data, one-way ANOVA with post hoc Tukey test was used to test for differences among groups.  $p < 0.05$  was considered statistically significant.

### 3. Results

**3.1. Mortality and Exclusion.** Of the 198 total animals used, 144 were subjected to MCAO, and the overall mortality was 16.7% (24/144). No significant difference was observed in mortality between the MCAO groups ( $p > 0.05$ ). No rats died in the sham and naive groups. Six animals were excluded

from this study due to no infarction volume after MCAO (Table 1).

**3.2. Time-Course of Endogenous p-AMPK after MCAO.** The expression of endogenous p-AMPK in the ipsilateral/right cerebral hemispheres after MCAO was assessed by western blot. As shown in Figure 2(a), the expression of p-AMPK increased at 6 h, reaching its peak at 24 h, and decreased by 72 h after MCAO compared to the sham group ( $p < 0.05$ ). After Eze treatment, the endogenous p-AMPK expression further increased at 6, 12, 24, and 72 h after MCAO compared to the sham group ( $p < 0.05$ , Figure 2(b)).

**3.3. Eze Treatment Reduced Brain Infarction and Ameliorated Neurobehavioral Deficiency at 24 h after MCAO.** In the vehicle group, infarction volume was significantly increased, while Garcia scores were significantly decreased compared to the sham group ( $p < 0.05$ , Figure 3). Intranasally administered Eze 500 µg/kg and Eze 1 mg/kg significantly reduced the infarction volume and improved neurological outcomes at 24 h after MCAO compared to the vehicle group ( $p < 0.05$ , Figures 3(a)–3(c)). With no additional therapeutic effects observed with Eze 1 mg/kg treatments, we used Eze 500 µg/kg for the subsequent studies. There were no significant differences in beam walking scores between the MCAO groups (Figure 3(d)).

**3.4. Eze Treatment Inhibited Neutrophil Infiltration and Microglia/Macrophage Activation at 24 h after MCAO.** MPO levels were used to assess neutrophil infiltration [8]. Iba-1 levels were used to evaluate microglia/macrophage activation in the brain tissue [42]. Immunofluorescence staining and western blot were used to evaluate whether the anti-inflammatory effects of Eze were caused by a reduction of neutrophil infiltration or microglia/macrophage activation in the ischemic penumbra at 24 h after MCAO. The immunofluorescence staining results showed that Eze treatment significantly decreased the number of MPO and Iba-1-positive cells in the ischemic penumbra compared to the

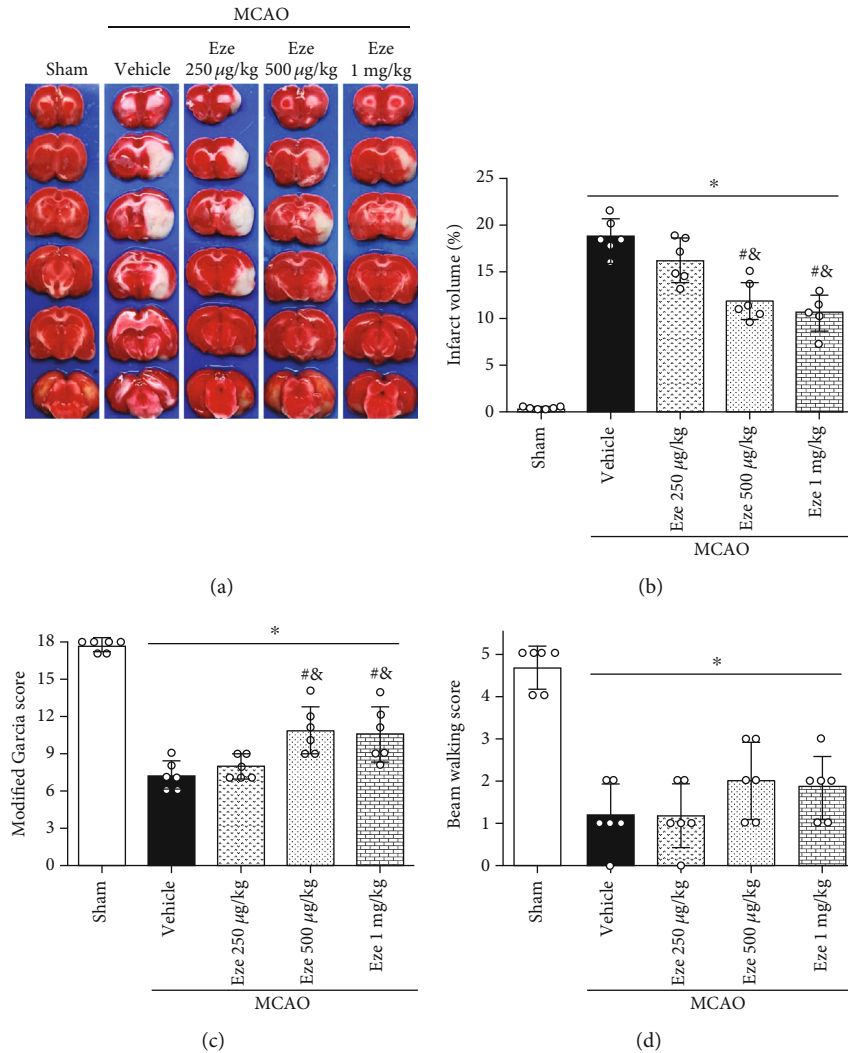


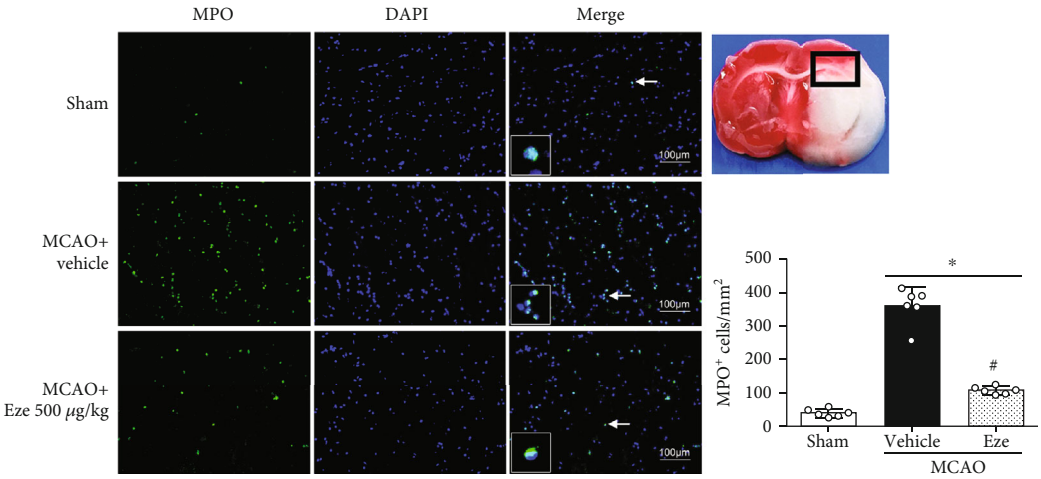
FIGURE 3: Eze reduced brain infarction and improved neurological outcomes at 24 h after MCAO. (a–c) Intranasal administration of Eze reduced infarction volume and improved the Garcia score at 24 h after MCAO. (d) There were no differences in beam walking scores between the MCAO groups. \* $p < 0.05$  vs. sham, # $p < 0.05$  vs. vehicle, and & $p < 0.05$  vs. Eze 250  $\mu$ g/kg.  $n = 6$  per group. Eze: Ezetimibe.

vehicle group ( $p < 0.05$ , Figures 4(a) and 4(c)). Paralleling these findings, western blot results reported a decrease in expression of MPO and Iba-1 in the ipsilateral hemisphere after Eze treatment compared to the vehicle group ( $p < 0.05$ , Figures 4(b) and 4(d)).

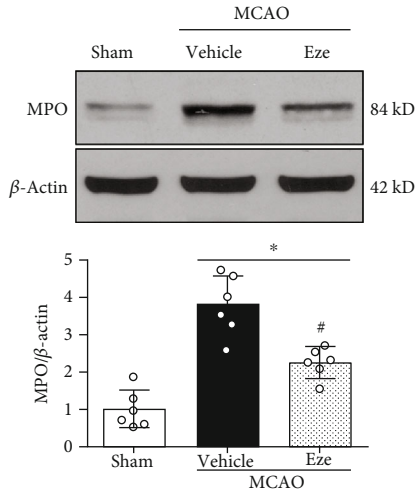
**3.5. Eze Treatment Reduced Oxidative Stress Injury at 24 h after MCAO.** Oxidative stress levels of the ipsilateral hemisphere after MCAO were measured by MDA levels, DHE staining, and Romo-1 expression. At 24 h after MCAO, DHE-positive cells and MDA levels were higher in the vehicle group compared to the sham group ( $p < 0.05$ , Figures 5(a)–5(c)); however, after intranasal administration of Eze, DHE-positive cells and MDA levels were significantly reduced compared to the vehicle group ( $p < 0.05$ , Figures 5(a)–5(c)). In the vehicle group, Romo-1, a marker of oxidative stress [43], was increased compared to that in the sham group ( $p < 0.05$ , Figure 5(d)), while treatment with Eze significantly reduced the expression of Romo-1 at 24 h

after MCAO ( $p < 0.05$ , Figure 5(d)). Nrf2 is a transcription factor involved in the endogenous antioxidant stress system [26]. Our results showed no significant difference in total-Nrf2; however, the nuclear-Nrf2 expression increased in the vehicle group compared to the sham group (Figures 5(e) and 5(f)). Treatment with Eze significantly increased total-Nrf2 expression and further increased the expression of nuclear-Nrf2 at 24 h after MCAO compared to the vehicle group ( $p < 0.05$ , Figures 5(e) and 5(f)).

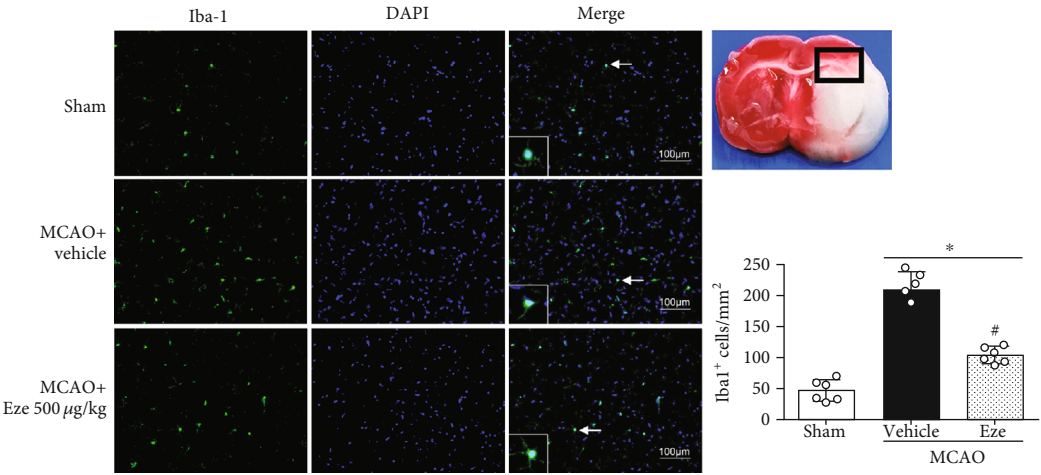
**3.6. Dorsomorphin and Nrf2 siRNA Abolished the Neuroprotective Effects of Eze at 24 h after MCAO.** Treatment with Eze reduced infarction volume and increased Garcia scores at 24 h after MCAO; however, this effect was reversed with the administration of both dorsomorphin ( $p < 0.05$ , Figures 6(a)–6(c)) and Nrf2 siRNA ( $p < 0.05$ , Figures 6(a)–6(c)). No significant differences were observed in beam walking scores between MCAO groups (Figure 6(d)).



(a)



(b)



(c)

FIGURE 4: Continued.

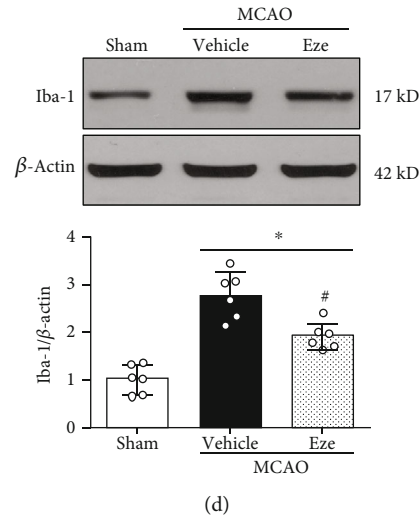


FIGURE 4: Eze inhibited microglia/macrophage activation and neutrophil infiltration at 24 h after MCAO. (a, c) Immunofluorescence revealed that treatment with Eze reduced the number of MPO-positive cells and Iba-1-positive cells in the ischemic penumbra region. (b, d) Representative western blot bands and quantitative analyses of MPO and Iba-1 protein levels at 24 h after MCAO. \* $p < 0.05$  vs. sham; # $p < 0.05$  vs. vehicle.  $n = 6$  per group. Eze: Ezetimibe. Scale bar = 100  $\mu$ m.

**3.7. Eze Treatment Attenuated Oxidative Stress and Neuroinflammation via Activation of the AMPK/Nrf2/TXNIP Pathway after MCAO in Rats.** In the naive rat, the endogenous p-AMPK expression was significantly increased in the ipsilateral cortex after Eze treatment. Inhibition of AMPK with dorsomorphin significantly decreased the expression of p-AMPK in both naive and Eze-treated animals ( $p < 0.05$ , Figure S1).

In the vehicle group at 24 h, the expression of p-AMPK, HO-1, TXNIP, NLRP3, Cleaved Caspase-1, and IL-1 $\beta$  increased compared to that in the sham group ( $p < 0.05$ , Figures 7(a) and 7(b) and 7(d)–7(h)). Intranasal administration of Eze increased the protein expression of total-Nrf2 and further increased p-AMPK and HO-1, while TXNIP, NLRP3, Cleaved Caspase-1, and IL-1 $\beta$  were reduced compared to that in the vehicle group ( $p < 0.05$ , Figures 7(a)–7(h)). However, inhibition of AMPK with dorsomorphin significantly decreased the protein expression of p-AMPK, Nrf2, and HO-1, while TXNIP, NLRP3, Cleaved Caspase-1, and IL-1 $\beta$  were increased compared to that in the MCAO+Eze+DMSO group at 24 h after MCAO ( $p < 0.05$ , Figures 7(a)–7(h)). Consistently, knockdown of endogenous Nrf2 with Nrf2 siRNA significantly decreased the protein expression of Nrf2 and HO-1, while TXNIP, NLRP3, Cleaved Caspase-1, and IL-1 $\beta$  were increased compared to that in the MCAO +Eze+Scr siRNA group at 24 h after MCAO ( $p < 0.05$ , Figures 7(a) and 7(c)–7(h)).

## 4. Discussion

In the present study, we demonstrated that Eze attenuated oxidative stress and neuroinflammation after MCAO. We made the following novel observations: (1) Eze further increased the endogenous p-AMPK expression after MCAO; (2) intranasal administration of Eze significantly reduced the infarction volume and improved neurological outcomes

after MCAO; (3) Eze treatment inhibited neutrophil infiltration, microglia/macrophage activation, and oxidative stress-associated injuries in the ischemic penumbra regions after MCAO; (4) the antioxidative stress and anti-inflammatory effects of Eze were facilitated through the increased expression of p-AMPK, Nrf2, and HO-1, while Romo-1, TXNIP, NLRP3, Cleaved Caspase-1, and IL-1 $\beta$  were reduced following MCAO; and (5) pretreatment with dorsomorphin and Nrf2 siRNA reversed the beneficial effects of Eze on brain infarction, neurobehavioral function, and inflammatory protein expression. Taken together, our findings suggest that Eze attenuated oxidative stress and neuroinflammatory sequelae of MCAO via activation of the AMPK/Nrf2/TXNIP signaling pathway (Figure 8).

Accumulating scientific evidence suggests that neuroinflammation and oxidative stress are the main pathological processes responsible for the impairment of neurological function in MCAO [26, 29, 44, 45]. Clinically, Eze, a NPC1L1 inhibitor, is mainly used as a treatment for hypercholesterolemia; however, in addition to its lipid-lowering activity, several studies have reported that Eze may attenuate ischemic-related oxidative stress and inflammation [14, 19]. For example, in a rat liver ischemia/reperfusion model, Eze was reported to attenuate oxidative radicals, modulate NO production, and increase eNOS activity [13]. Independent of cholesterol regulation, other studies have shown that treatment with Eze improved renal injury outcomes in nondiabetic chronic kidney disease patients with dyslipidemia, which may be explained by the asymmetric dimethylarginine-lowering and antioxidative effects of Eze [46]. In a clinical study evaluating the neurological deterioration after embolic stroke resulting from atrial fibrillation in older patients, Lappegard et al. demonstrated that anti-inflammatory therapy with Eze may ameliorate the deterioration of neurocognitive function and loss of volume in cerebral areas [47]. Consistent with these findings, we demonstrated that

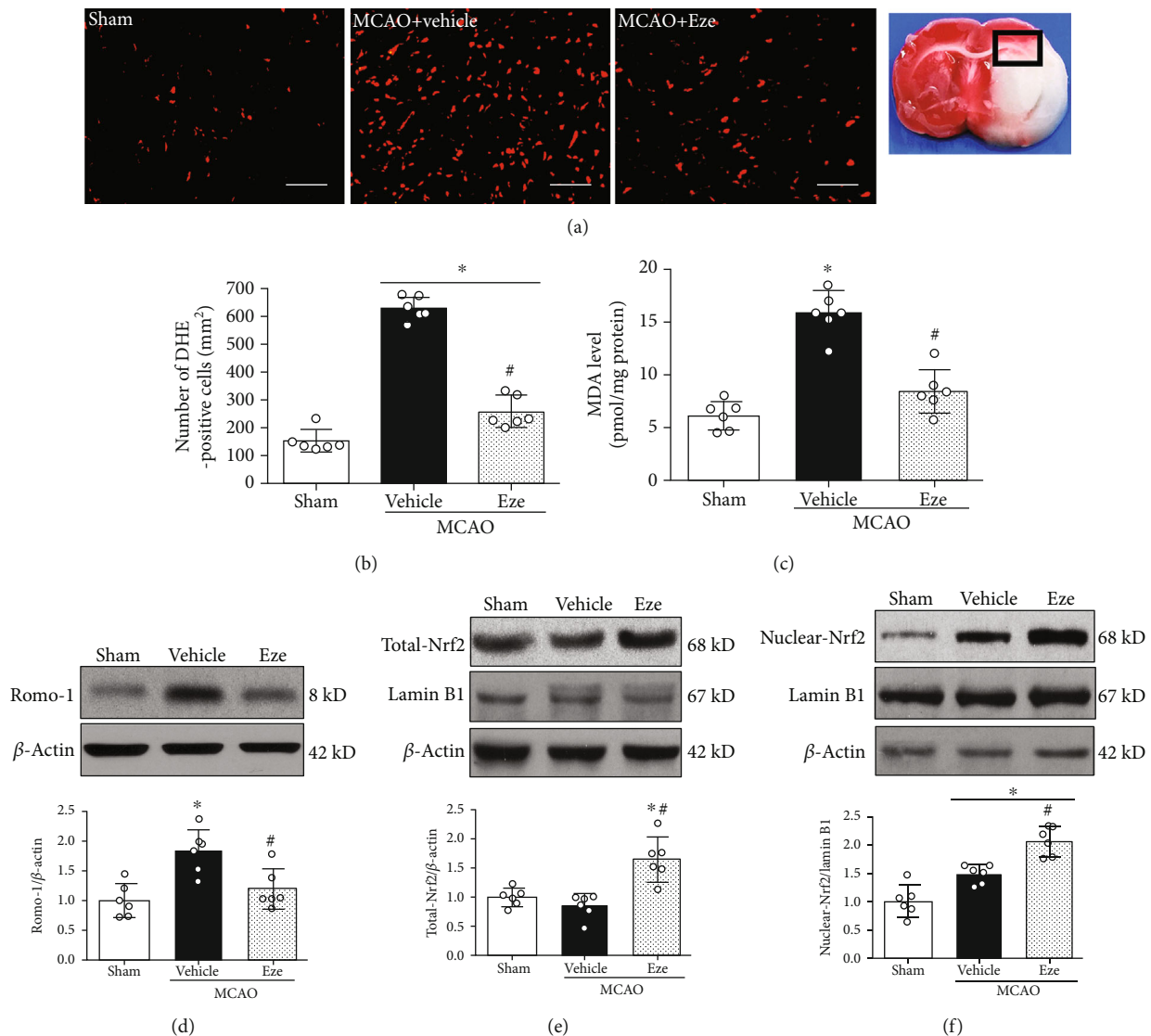


FIGURE 5: Eze reduced oxidative stress injury at 24 h after MCAO. (a) Representative microphotograph of DHE staining in the ischemic penumbra region. (b) Quantitative analysis of DHE-positive cells in the ischemic penumbra region. (c) The MDA level in the ischemic penumbra region. (d) Representative western blot band and quantitative analysis of Romo-1 expression. (e, f) Representative western blot bands and quantitative analyses of total-Nrf2 and nuclear-Nrf2 expression. \* $p < 0.05$  vs. sham; # $p < 0.05$  vs. vehicle.  $n = 6$  per group. DHE: dihydroethidium; Eze: Ezetimibe; MDA: malonaldehyde. Scale bar = 100  $\mu$ m.

treatment with Eze reduced brain infarction, neutrophil infiltration, microglia/macrophage activation, MDA levels, and DHE-positive cell numbers. Specifically, Eze treatment reduced the protein expression of Romo-1 (oxidative stress marker) and IL-1 $\beta$  (inflammatory marker). Congruently, neurological outcomes were improved after Eze administration at 24 h after MCAO.

Given that studies have reported Eze treatment to increase AMPK phosphorylation, novel and unique mechanistic endpoints are being investigated around AMPK regulation [16, 19, 20]. According to literature, Eze increases the oxygen consumption rate (OCR) and decreases the amount of ATP [48], which causes an elevation of ADP/ATP ratio that subsequently activates AMPK [20]. Therefore, Eze maintains cellular energy by regulating ATP consumption and

generation via phosphorylation of AMPK [19]. Confirming this mechanistic link, our results showed that the endogenous p-AMPK expression was acutely increased after MCAO, and it was further increased after Eze treatment. To confirm that Eze regulates AMPK, a specific inhibitor of AMPK was administered with Eze. This intervention reversed the neuroprotective effects of Eze, increasing the infarction volume and neurobehavioral deficits; reducing the expression of p-AMPK, Nrf-2, and HO-1; and upregulating the expression of TXNIP, NLRP3, Cleaved Caspase-1, and IL-1 $\beta$ . This mechanistic study confirms a link between Eze and AMPK.

Nrf2 has traditionally been involved in upregulating antioxidant systems to reduce oxidative stress in the brain [49]. Under oxidative stress conditions, Nrf2 dissociates from Kelch-like ECH-associated protein 1 (Keap1) and translocates

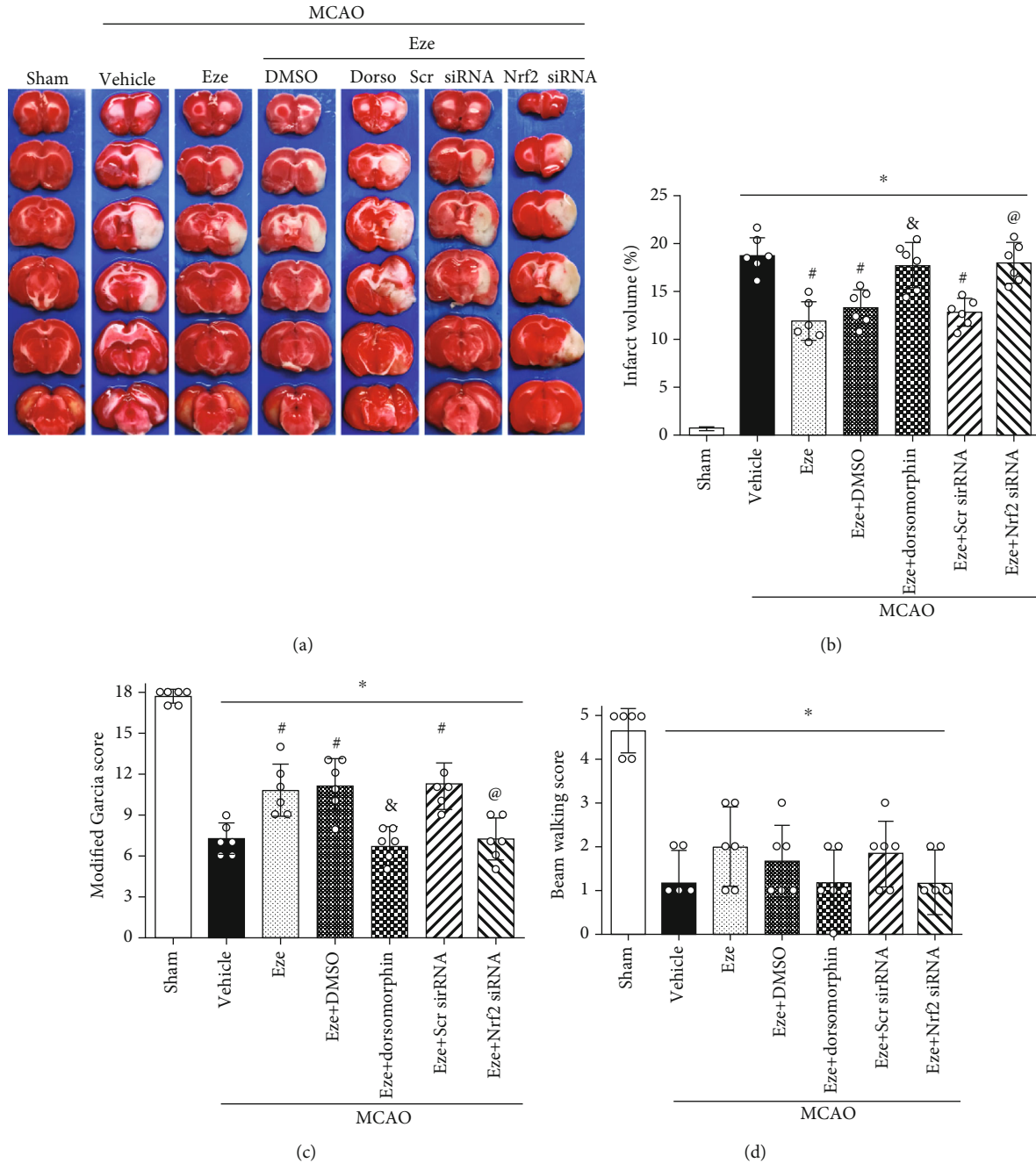


FIGURE 6: Dorsomorphin and Nrf2 siRNA reversed the neuroprotective effects of Eze after MCAO. (a) Representative image of TTC-staining brain slices, (b) quantified infarction volumes, (c) modified Garcia scores, and (d) beam walking scores at 24 h after MCAO. \* $p < 0.05$  vs. sham, # $p < 0.05$  vs. vehicle, & $p < 0.05$  vs. Eze+DMSO, and @ $p < 0.05$  vs. Eze+Scr siRNA.  $n = 6$  per group. Dorso: dorsomorphin; Eze: Ezetimibe; Scr siRNA: scramble siRNA.

into the nucleus to bind to antioxidant response elements (ARE), which activates downstream antioxidant defense enzymes, such as HO-1 [50]. NLRP3 is an inflammasome protein complex located in the cell that binds to pro-Caspase-1 to cause neuronal apoptosis and inflammation in ischemic injuries [51]. Activation of AMPK and downstream inhibition of both NLRP3 inflammasomes and IL-1 $\beta$  mediates the anti-inflammatory effects of Eze [19]. Therefore, inhibition of NLRP3 inflammasomes via the AMPK pathway

is neuroprotective in ischemic stroke [45]. Of importance, TXNIP, a redox-regulated protein, can bind to and activate the NLRP3 inflammasome in response to the oxidative stress associated with stroke [23], and when TXNIP is inhibited, Nrf2 acts as a negative regulator of the NLRP3 inflammasome [26]. Our results showed that Eze significantly enhanced the phosphorylation of AMPK; increased the expression of Nrf2 and HO-1; and subsequently decreased the expression of TXNIP, NLRP3, Cleaved Caspase-1, and IL-1 $\beta$ . Similarly,

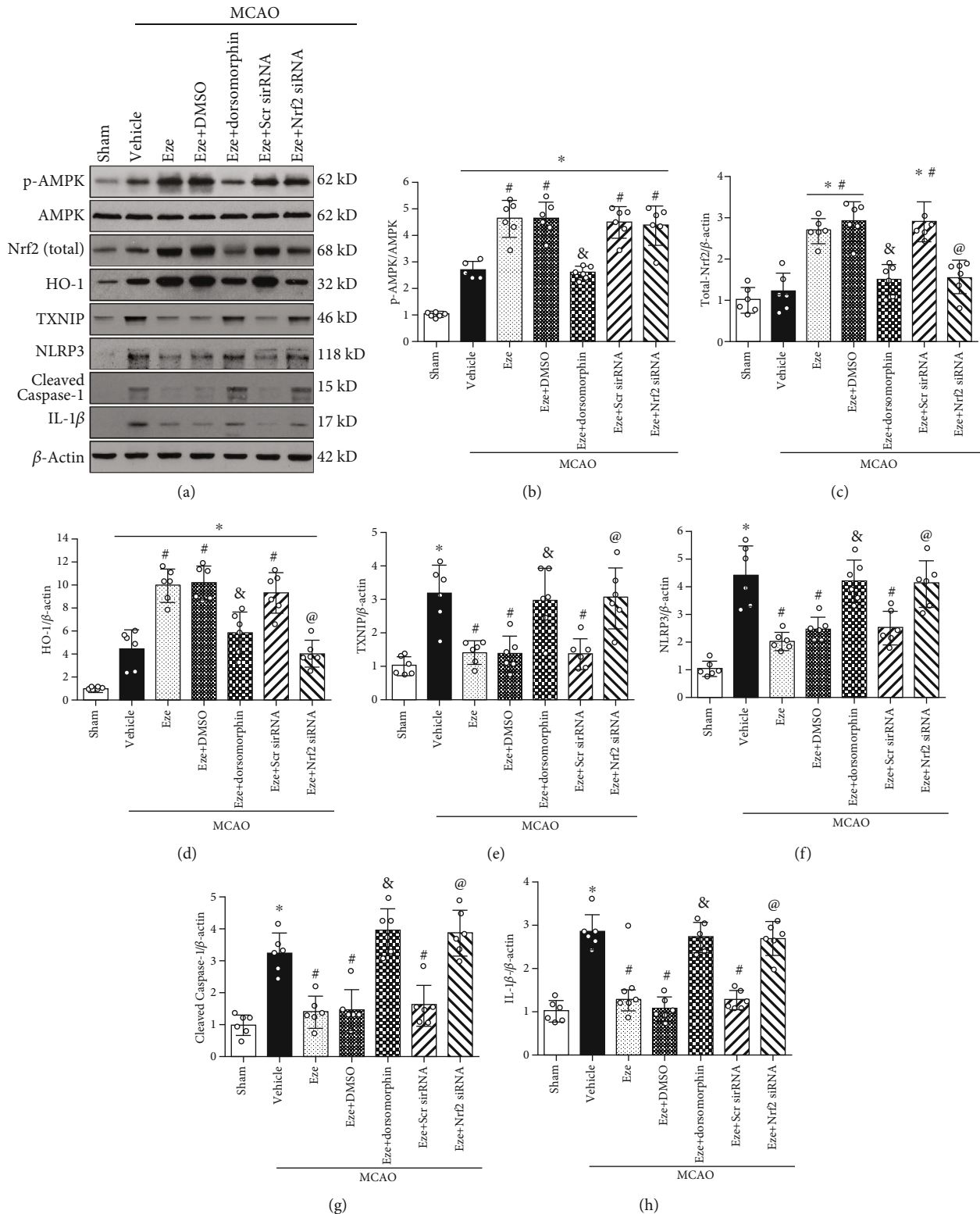


FIGURE 7: Eze attenuated oxidative stress and neuroinflammation via the AMPK/Nrf2/TXNIP pathway after MCAO. (a) Representative western blot bands. (b–h) Quantitative analyses of p-AMPK, Nrf2, HO-1, TXNIP, NLRP3, Cleaved Caspase-1, and IL-1β in the ipsilateral hemisphere at 24 h after MCAO. \* $p < 0.05$  vs. sham, # $p < 0.05$  vs. vehicle, & $p < 0.05$  vs. Eze+DMSO, and @ $p < 0.05$  vs. Eze+Scr siRNA.  $n = 6$  per group. Eze: Ezetimibe; Scr siRNA: scramble siRNA.

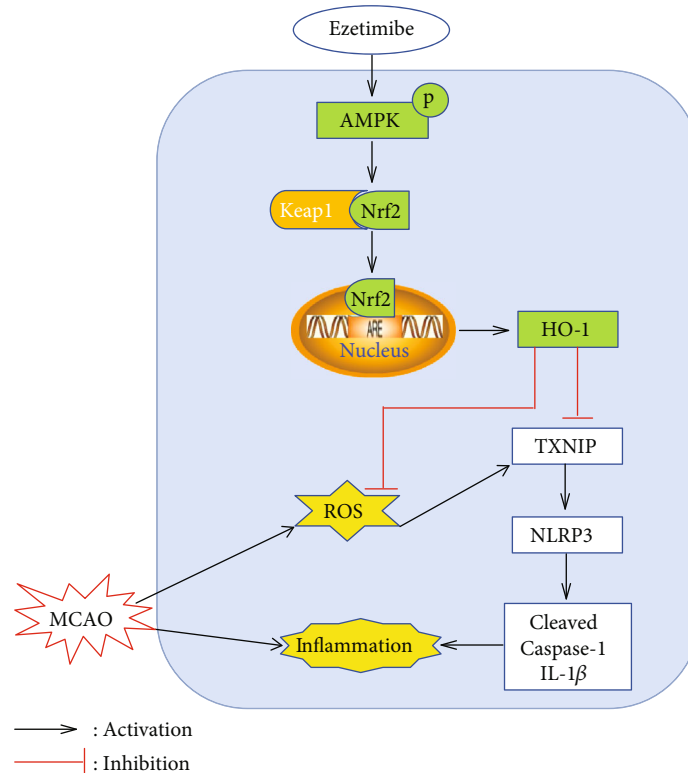


FIGURE 8: Proposed pathway for Eze and its downstream targets. Eze increases levels of phosphorylated AMPK and activates Nrf2, which translocates into the nucleus to increase the transcription of HO-1—a protein that inhibits ROS and inflammation.

when knocking down the endogenous Nrf2 with Nrf2 siRNA, the protective effects of Eze were reversed: the intervention increased infarction volumes and neurobehavioral deficits, reducing the activation of Nrf2 and HO-1, with an associated increase in the levels of TXNIP, NLRP3, Cleaved Caspase-1, and IL-1 $\beta$ . Taken together, we can conclude that Eze exerts antioxidative and anti-inflammatory effects via activation of the AMPK/Nrf2/TXNIP signaling pathway.

There were some limitations in our study. First, due to the limited nature of this pilot study, we only evaluated a one-time window target for Eze treatment after MCAO. Second, our results do not fully exclude the possibility of alternative pathways that modulate the inflammasome pathway; thus, further research will need to investigate the relationship between other inflammasome activators (e.g., NF- $\kappa$ B [52]) and the proposed pathway of Eze to fully exclude or incorporate alternative pathways. Finally, we have previously reported that Eze attenuates neuronal apoptosis via AMPK-induced autophagy [16]. In addition to these downstream targets, in the present study, Eze also decreased oxidative stress and subsequent neuroinflammation via activation of the AMPK/Nrf2/TXNIP pathway. Therefore, Eze may exert these effects by increasing the oxygen consumption rate, which then decreases the amount of ATP and phosphorylates AMPK, activating other downstream targets such as autophagy. However, since lowering cholesterol may also contribute to AMPK activation [16], NPC1L1 may have played a role in our proposed pathway. In sum, further

research is needed to better understand the pleiotropic effects of Eze.

## 5. Conclusion

In summary, our findings suggest that intranasal administration of Eze reduced brain infarction, oxidative stress, and neuroinflammation, while neurological outcomes were improved after transient MCAO in rats. Mechanistically, the neuroprotective effects of Eze were mediated through activation of the AMPK/Nrf2/TXNIP pathway. This research supports the continued investigation of Eze as a potential therapy for the treatment of patients with ischemic stroke.

## Data Availability

All data are available upon request.

## Conflicts of Interest

The authors declare that they have no conflict of interest.

## Authors' Contributions

Jing Yu and Wen-na Wang contributed equally to this manuscript.



## Acknowledgments

This study was supported by grants from the National Institutes of Health NS091042 and NS082184 to Dr. JH. Zhang.

## Supplementary Materials

Figure S1: the effects of dorsomorphin on the expression of p-AMPK. Representative western blot bands and quantitative analysis of p-AMPK. \* $p < 0.05$  vs. naive+DMSO, # $p < 0.05$  vs. naive+Eze+DMSO,  $n = 6$  per group. (Supplementary Materials)

## References

- [1] GBD 2016 Causes of Death Collaborators, "Global, regional, and national age-sex specific mortality for 264 causes of death, 1980-2016: a systematic analysis for the Global Burden of Disease Study 2016," *The Lancet*, vol. 390, no. 10100, pp. 1151–1210, 2017.
- [2] R. Moretti, J. Pansiot, D. Bettati et al., "Blood-brain barrier dysfunction in disorders of the developing brain," *Frontiers in Neuroscience*, vol. 9, p. 40, 2015.
- [3] A. Ozkul, A. Akyol, C. Yenisey, E. Arpacı, N. Kiylioglu, and C. Tataroglu, "Oxidative stress in acute ischemic stroke," *Journal of Clinical Neuroscience*, vol. 14, no. 11, pp. 1062–1066, 2007.
- [4] A. Chamorro, U. Dirnagl, X. Urra, and A. M. Planas, "Neuroprotection in acute stroke: targeting excitotoxicity, oxidative and nitrosative stress, and inflammation," *Lancet Neurology*, vol. 15, no. 8, pp. 869–881, 2016.
- [5] M. H. Shen, C. B. Zhang, J. H. Zhang, and P. F. Li, "Electroacupuncture attenuates cerebral ischemia and reperfusion injury in middle cerebral artery occlusion of rat via modulation of apoptosis, inflammation, oxidative stress, and excitotoxicity," *Evidence-based Complementary and Alternative Medicine*, vol. 2016, Article ID 9438650, 15 pages, 2016.
- [6] W. Cai, S. Liu, M. Hu et al., "Post-stroke DHA treatment protects against acute ischemic brain injury by skewing macrophage polarity toward the M2 phenotype," *Translational Stroke Research*, vol. 9, no. 6, pp. 669–680, 2018.
- [7] J. Tian, S. Guo, H. Chen et al., "Combination of emricasan with ponatinib synergistically reduces ischemia/reperfusion injury in rat brain through simultaneous prevention of apoptosis and necroptosis," *Translational Stroke Research*, vol. 9, no. 4, pp. 382–392, 2018.
- [8] G. Yu, Y. Liang, S. Zheng, and H. Zhang, "Inhibition of myeloperoxidase by N-acetyl lysyltyrosylcysteine amide reduces oxidative stress-mediated inflammation, neuronal damage, and neural stem cell injury in a murine model of stroke," *The Journal of Pharmacology and Experimental Therapeutics*, vol. 364, no. 2, pp. 311–322, 2018.
- [9] Y. J. Chen, H. M. Nguyen, I. Maezawa et al., "The potassium channel KCa3.1 constitutes a pharmacological target for neuroinflammation associated with ischemia/reperfusion stroke," *Journal of Cerebral Blood Flow and Metabolism*, vol. 36, no. 12, pp. 2146–2161, 2016.
- [10] V. L. Roger, A. S. Go, D. M. Lloyd-Jones et al., "Heart disease and stroke statistics—2012 update: a report from the American Heart Association," *Circulation*, vol. 125, no. 1, pp. e2–e220, 2012.
- [11] S. W. Altmann, H. R. Davis Jr., L. J. Zhu et al., "Niemann-Pick C1 like 1 protein is critical for intestinal cholesterol absorption," *Science*, vol. 303, no. 5661, pp. 1201–1204, 2004.
- [12] M. Garcia-Calvo, J. Lisnock, H. G. Bull et al., "The target of ezetimibe is Niemann-Pick C1-like 1 (NPC1L1)," *Proceedings of the National Academy of Sciences of the United States of America*, vol. 102, no. 23, pp. 8132–8137, 2005.
- [13] M. Trocha, A. Merwid-Lad, T. Sozański et al., "Influence of ezetimibe on ADMA-DDAH-NO pathway in rat liver subjected to partial ischemia followed by global reperfusion," *Pharmacological Reports*, vol. 65, no. 1, pp. 122–133, 2013.
- [14] M. Trocha, A. Merwid-Lad, E. Chlebda et al., "Influence of ezetimibe on selected parameters of oxidative stress in rat liver subjected to ischemia/reperfusion," *Archives of Medical Science*, vol. 10, no. 4, pp. 817–824, 2014.
- [15] L. Qin, Y. B. Yang, Y. X. Yang et al., "Inhibition of smooth muscle cell proliferation by ezetimibe via the cyclin D1-MAPK pathway," *Journal of Pharmacological Sciences*, vol. 125, no. 3, pp. 283–291, 2014.
- [16] J. Yu, X. Li, N. Matei et al., "Ezetimibe, a NPC1L1 inhibitor, attenuates neuronal apoptosis through AMPK dependent autophagy activation after MCAO in rats," *Experimental Neurology*, vol. 307, pp. 12–23, 2018.
- [17] Y. Dalla, N. Singh, A. S. Jaggi, D. Singh, and P. Ghulati, "Potential of ezetimibe in memory deficits associated with dementia of Alzheimer's type in mice," *Indian Journal of Pharmacology*, vol. 41, no. 6, pp. 262–267, 2009.
- [18] L. Yang, P. Zhao, J. Zhao, J. Wang, L. Shi, and X. Wang, "Effects of ezetimibe and anticoagulant combined therapy on progressing stroke: a randomized, placebo-controlled study," *Journal of Neurology*, vol. 263, no. 12, pp. 2438–2445, 2016.
- [19] S. H. Kim, G. Kim, D. H. Han et al., "Ezetimibe ameliorates steatohepatitis via AMP activated protein kinase-TFEB-mediated activation of autophagy and NLRP3 inflammasome inhibition," *Autophagy*, vol. 13, no. 10, pp. 1767–1781, 2017.
- [20] D. H. Lee, D. H. Han, K. T. Nam et al., "Ezetimibe, an NPC1L1 inhibitor, is a potent Nrf2 activator that protects mice from diet-induced nonalcoholic steatohepatitis," *Free Radical Biology & Medicine*, vol. 99, pp. 520–532, 2016.
- [21] S. Y. Park, M. L. Jin, M. J. Ko, G. Park, and Y. W. Choi, "Anti-neuroinflammatory effect of emodin in LPS-stimulated microglia: involvement of AMPK/Nrf2 activation," *Neurochemical Research*, vol. 41, no. 11, pp. 2981–2992, 2016.
- [22] W. Y. Wu, Y. D. Li, Y. K. Cui et al., "The natural flavone acacetin confers cardiomyocyte protection against hypoxia/reoxygenation injury via AMPK-mediated activation of Nrf2 signaling pathway," *Frontiers in Pharmacology*, vol. 9, p. 497, 2018.
- [23] R. Zhou, A. Tardivel, B. Thorens, I. Choi, and J. Tschopp, "Thioredoxin-interacting protein links oxidative stress to inflammasome activation," *Nature Immunology*, vol. 11, no. 2, pp. 136–140, 2010.
- [24] T. Ishrat, I. N. Mohamed, B. Pillai et al., "Thioredoxin-interacting protein: a novel target for neuroprotection in experimental thromboembolic stroke in mice," *Molecular Neurobiology*, vol. 51, no. 2, pp. 766–778, 2015.
- [25] Y. Li, J. Li, S. Li et al., "Curcumin attenuates glutamate neurotoxicity in the hippocampus by suppression of ER stress-associated TXNIP/NLRP3 inflammasome activation in a manner dependent on AMPK," *Toxicology and Applied Pharmacology*, vol. 286, no. 1, pp. 53–63, 2015.

- [26] Y. Hou, Y. Wang, Q. He et al., "Nrf2 inhibits NLRP3 inflammasome activation through regulating Trx1/TXNIP complex in cerebral ischemia reperfusion injury," *Behavioural Brain Research*, vol. 336, pp. 32–39, 2018.
- [27] C. Kilkenny, W. J. Browne, I. C. Cuthill, M. Emerson, and D. G. Altman, "Improving bioscience research reporting: the ARRIVE guidelines for reporting animal research," *PLoS Biology*, vol. 8, no. 6, article e1000412, 2010.
- [28] N. Matei, J. Camara, D. McBride et al., "Intranasal wnt3a attenuates neuronal apoptosis through Frz1/PIWIL1a/FOXO1 pathway in MCAO rats," *The Journal of Neuroscience*, vol. 38, no. 30, pp. 6787–6801, 2018.
- [29] G. Wu, D. W. McBride, and J. H. Zhang, "Axl activation attenuates neuroinflammation by inhibiting the TLR/TRAF/NF- $\kappa$ B pathway after MCAO in rats," *Neurobiology of Disease*, vol. 110, pp. 59–67, 2018.
- [30] J. Y. An, L. L. Zhou, P. Sun et al., "Role of the AMPK signaling pathway in early brain injury after subarachnoid hemorrhage in rats," *Acta Neurochirurgica*, vol. 157, no. 5, pp. 781–792, 2015.
- [31] K. Zhou, B. Enkhjargal, Z. Xie et al., "Dihydrolipoic acid inhibits lysosomal rupture and NLRP3 through lysosome-associated membrane protein-1/calcium/calmodulin-dependent protein kinase II/TAK1 pathways after subarachnoid hemorrhage in rat," *Stroke*, vol. 49, no. 1, pp. 175–183, 2018.
- [32] J. H. Garcia, S. Wagner, K. F. Liu, and X. J. Hu, "Neurological deficit and extent of neuronal necrosis attributable to middle cerebral artery occlusion in rats," *Stroke*, vol. 26, no. 4, pp. 627–635, 1995.
- [33] F. Wahl, M. Allix, M. Plotkine, and R. G. Boulu, "Neurological and behavioral outcomes of focal cerebral ischemia in rats," *Stroke*, vol. 23, no. 2, pp. 267–272, 1992.
- [34] A. F. Germano, C. E. Dixon, D. d'Avella, R. L. Hayes, and F. Tomasello, "Behavioral deficits following experimental subarachnoid hemorrhage in the rat," *Journal of Neurotrauma*, vol. 11, no. 3, pp. 345–353, 1994.
- [35] L. B. Goldstein and J. N. Davis, "Beam-walking in rats: studies towards developing an animal model of functional recovery after brain injury," *Journal of Neuroscience Methods*, vol. 31, no. 2, pp. 101–107, 1990.
- [36] E. V. Griemert, K. Recarte Pelz, K. Engelhard, M. K. Schäfer, and S. C. Thal, "PAI-1 but not PAI-2 gene deficiency attenuates ischemic brain injury after experimental stroke," *Translational Stroke Research*, vol. 10, no. 4, pp. 372–380, 2019.
- [37] D. W. McBride, J. Tang, and J. H. Zhang, "Development of an infarct volume algorithm to correct for brain swelling after ischemic stroke in rats," *Acta Neurochirurgica. Supplement*, vol. 121, pp. 103–109, 2016.
- [38] N. Xu, Y. Zhang, D. M. Doycheva et al., "Adiponectin attenuates neuronal apoptosis induced by hypoxia-ischemia via the activation of AdipoR1/APPL1/LKB1/AMPK pathway in neonatal rats," *Neuropharmacology*, vol. 133, pp. 415–428, 2018.
- [39] D. W. McBride, G. Wu, D. Nowrangi et al., "Delayed recanalization promotes functional recovery in rats following permanent middle cerebral artery occlusion," *Translational Stroke Research*, vol. 9, no. 2, pp. 185–198, 2018.
- [40] H. W. Wang, B. S. Huang, R. A. White, A. Chen, M. Ahmad, and F. H. Leenen, "Mineralocorticoid and angiotensin II type 1 receptors in the subfornical organ mediate angiotensin II - induced hypothalamic reactive oxygen species and hypertension," *Neuroscience*, vol. 329, pp. 112–121, 2016.
- [41] Z. Xie, B. Enkhjargal, L. Wu et al., "Exendin-4 attenuates neuronal death via GLP-1R/PI3K/Akt pathway in early brain injury after subarachnoid hemorrhage in rats," *Neuropharmacology*, vol. 128, pp. 142–151, 2018.
- [42] S. Chen, L. Zhao, P. Sherchan et al., "Activation of melanocortin receptor 4 with RO27-3225 attenuates neuroinflammation through AMPK/JNK/p38 MAPK pathway after intracerebral hemorrhage in mice," *Journal of Neuroinflammation*, vol. 15, no. 1, p. 106, 2018.
- [43] Y. M. Chung, J. S. Kim, and Y. D. Yoo, "A novel protein, Romo1, induces ROS production in the mitochondria," *Biochemical and Biophysical Research Communications*, vol. 347, no. 3, pp. 649–655, 2006.
- [44] S. Zhang, L. Jiang, F. Che, Y. Lu, Z. Xie, and H. Wang, "Arctigenin attenuates ischemic stroke via SIRT1-dependent inhibition of NLRP3 inflammasome," *Biochemical and Biophysical Research Communications*, vol. 493, no. 1, pp. 821–826, 2017.
- [45] J. Qiu, M. Wang, J. Zhang et al., "The neuroprotection of sinomenine against ischemic stroke in mice by suppressing NLRP3 inflammasome via AMPK signaling," *International Immunopharmacology*, vol. 40, pp. 492–500, 2016.
- [46] T. Nakamura, E. Sato, N. Fujiwara et al., "Ezetimibe decreases serum levels of asymmetric dimethylarginine (ADMA) and ameliorates renal injury in non-diabetic chronic kidney disease patients in a cholesterol-independent manner," *Pharmacological Research*, vol. 60, no. 6, pp. 525–528, 2009.
- [47] K. T. Lappégard, M. Pop-Purceleanu, W. van Heerde, J. Sexton, I. Tendolkar, and G. Pop, "Improved neurocognitive functions correlate with reduced inflammatory burden in atrial fibrillation patients treated with intensive cholesterol lowering therapy," *Journal of Neuroinflammation*, vol. 10, no. 1, p. 844, 2013.
- [48] A. Hernandez-Mijares, C. Banuls, S. Rovira-Llopis et al., "Effects of simvastatin, ezetimibe and simvastatin/ezetimibe on mitochondrial function and leukocyte/endothelial cell interactions in patients with hypercholesterolemia," *Atherosclerosis*, vol. 247, pp. 40–47, 2016.
- [49] S. V. Narayanan, K. R. Dave, and M. A. Perez-Pinzon, "Ischemic preconditioning protects astrocytes against oxygen glucose deprivation via the nuclear erythroid 2-related factor 2 pathway," *Translational Stroke Research*, vol. 9, no. 2, pp. 99–109, 2018.
- [50] M. McMahan, K. Itoh, M. Yamamoto, and J. D. Hayes, "Keap1-dependent proteasomal degradation of transcription factor Nrf2 contributes to the negative regulation of antioxidant response element-driven gene expression," *The Journal of Biological Chemistry*, vol. 278, no. 24, pp. 21592–21600, 2003.
- [51] P. J. Shaw, M. F. McDermott, and T. D. Kanneganti, "Inflammasomes and autoimmunity," *Trends in Molecular Medicine*, vol. 17, no. 2, pp. 57–64, 2011.
- [52] F. Bauernfeind, A. Ablasser, E. Bartok et al., "Inflammasomes: current understanding and open questions," *Cellular and Molecular Life Sciences*, vol. 68, no. 5, pp. 765–783, 2011.

## Research Article

# Apolipoprotein E Deficiency Aggravates Neuronal Injury by Enhancing Neuroinflammation via the JNK/c-Jun Pathway in the Early Phase of Experimental Subarachnoid Hemorrhage in Mice

Yue Wu,<sup>1</sup> Jinwei Pang,<sup>2</sup> Jianhua Peng,<sup>2</sup> Fang Cao,<sup>3</sup> Zongduo Guo ,<sup>1</sup> Li Jiang,<sup>1</sup> Zhipeng Teng,<sup>4</sup> Zhijian Huang,<sup>1</sup> Chongjie Cheng ,<sup>1</sup> Yong Jiang ,<sup>2</sup> and Xiaochuan Sun <sup>1</sup>

<sup>1</sup>Department of Neurosurgery, The First Affiliated Hospital of Chongqing Medical University, Chongqing, China

<sup>2</sup>Department of Neurosurgery, The Affiliated Hospital of Southwest Medical University, Luzhou, China

<sup>3</sup>Department of Cerebrovascular Disease, The Affiliated Hospital of Zunyi Medical College, Zunyi, China

<sup>4</sup>Department of Neurosurgery, Chongqing Traditional Chinese Medicine Hospital, Chongqing, China

Correspondence should be addressed to Yong Jiang; [jiangyong@swmu.edu.cn](mailto:jiangyong@swmu.edu.cn) and Xiaochuan Sun; [sunxch1445@qq.com](mailto:sunxch1445@qq.com)

Received 12 April 2019; Revised 6 July 2019; Accepted 24 September 2019; Published 26 December 2019

Guest Editor: Maurizio Forte

Copyright © 2019 Yue Wu et al. This is an open access article distributed under the Creative Commons Attribution License, which permits unrestricted use, distribution, and reproduction in any medium, provided the original work is properly cited.

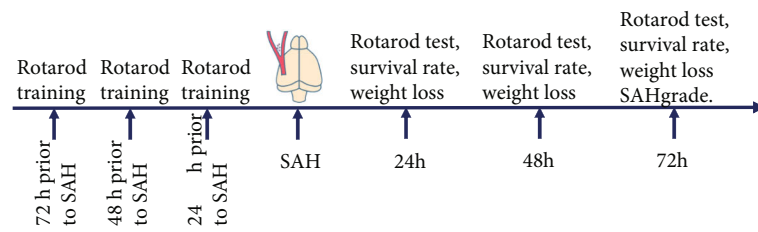
Neuronal injury is the primary cause of poor outcome after subarachnoid hemorrhage (SAH). The apolipoprotein E (APOE) gene has been suggested to be involved in the prognosis of SAH patients. However, the role of APOE in neuronal injury after SAH has not been well studied. In this study, SAH was induced in APOE-knockout (APOE<sup>-/-</sup>) and wild-type (WT) mice to investigate the impact of APOE deficiency on neuronal injury in the early phase of SAH. The experiments of this study were performed in murine SAH models *in vivo* and primary cultured microglia and neurons *in vitro*. The SAH model was induced by endovascular perforation in APOE<sup>-/-</sup> and APOE WT mice. The mortality rate, weight loss, and neurological deficits were recorded within 72 h after SAH. The neuronal injury was assessed by detecting the neuronal apoptosis and axonal injury. The activation of microglia was assessed by immunofluorescent staining of Iba-1, and clodronate liposomes were used for inhibiting microglial activation. The expression of JNK/c-Jun was evaluated by immunofluorescent staining or western blotting. The expression of TNF- $\alpha$ , IL-1 $\beta$ , and IL-6 was evaluated by ELISA. Primary cultured microglia were treated with hemoglobin (Hb) *in vitro* for simulating the pathological process of SAH. SP600125, a JNK inhibitor, was used for evaluating the role of JNK in neuroinflammation. Nitrite production was detected for microglial activation, and flow cytometry was performed to detect apoptosis *in vitro*. The results suggested that SAH induced early neuronal injury and neurological deficits in mice. APOE deficiency resulted in more severe neurological deficits after SAH in mice. The neurological deficits were associated with exacerbation of neuronal injury, including neuronal apoptosis and axonal injury. Moreover, APOE deficiency enhanced microglial activation and related inflammatory injury on neurons. Inhibition of microglia attenuated neuronal injury in mice, whereas inhibition of JNK inhibited microglia-mediated inflammatory response *in vitro*. Taken together, JNK/c-Jun was involved in the enhancement of microglia-mediated inflammatory injury in APOE<sup>-/-</sup> mice. APOE deficiency aggravates neuronal injury which may account for the poor neurological outcomes of APOE<sup>-/-</sup> mice. The possible protective role of APOE against EBI via the modulation of inflammatory response indicates its potential treatment for SAH.

## 1. Introduction

Subarachnoid hemorrhage (SAH) is a fatal neurovascular disease with an overall mortality of approximately 50%, and more than 30% of survivors remain severely disabled [1]. Over the past decade, more efforts have been made to eluci-

date the pathophysiological processes of early brain injury (EBI) which is widely accepted as one of the primary causes of poor outcome of SAH [2]. Acute neuronal injury is the core issue of EBI. Integrity of neurons is the basis of intact neurological functions. SAH induces complicated pathological processes including neuroinflammation, oxidative stress,

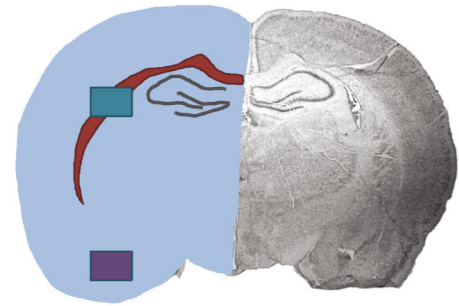
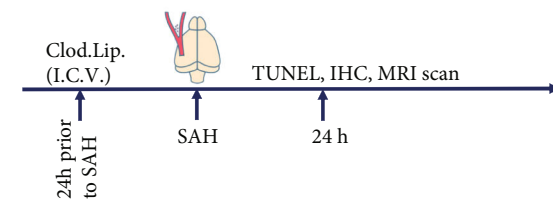
## Experiment 1. Effects of APOE deficiency on neurobehavior



## Experiment 2. Effects of APOE deficiency on pathological processes of SAH



## Experiment 3. Effects of microglia on pathological processes of SAH



- FA of MRI scan and  $\beta$ -APP
- Activation of microglia
- TUNEL and activation of microglia
- WB and ELISA

FIGURE 1: The schema of in vivo study design. SAH: subarachnoid hemorrhage; TUNEL: terminal-deoxynucleotidyl transferase-mediated nick end labeling; IHC: immunohistochemistry; WB: western blot; Clod. Lip.: clodronate liposome; I.C.V.: intracerebroventricularly.

and blood-brain barrier (BBB) interruption, which ultimately aggravate neuronal injury [2]. Therefore, these processes are potential targets for preservation of neuronal function.

Experimental and clinical studies suggest that inflammatory response is a major cause of brain injury after SAH [3–5]. Microglia are primary mediators of the immunological system in the central nervous system (CNS), which rapidly respond to injury and initiate an inflammatory effect [6, 7]. SAH induces activation of resident microglia [8], thereby exerting inflammatory responses in the brain. The roles of microglia in neurological diseases are complicated [9, 10], and whether this cell group is beneficial or harmful is still unclear in the early phase of SAH. Therefore, revealing the role of microglia following SAH provides evidence for targeting immunological cells and their consequent neuroinflammation as a potential treatment for neuronal injury after SAH.

Apolipoprotein E (APOE for gene, ApoE for protein), the major apolipoprotein in the CNS, is a multifunctional protein that is predominantly involved in the transportation of cholesterol and lipid. APOE has been suggested to influence the pathological process of SAH. We have previously found that APOE exerts neuroprotective effects via BBB preservation after SAH [11]. An exogenous ApoE peptide has been demonstrated to improve the neurological functions of SAH mice [12]. Furthermore, in a model of microglial activation, exogenous ApoE inhibited microglial activation and the release of proinflammatory chemicals [13]. Nevertheless, the role of APOE in the process of EBI has not yet been explored. Furthermore, the modulation of SAH-induced inflammatory responses by APOE remains unclear.

Based on the previous reports, we hypothesized that APOE protects against neuronal injury after SAH in an

anti-inflammatory manner. To investigate the hypothesis, the impacts of APOE on the neurological outcomes, neuronal damage, and inflammatory responses were assessed in a mouse model of SAH.

## 2. Materials and Methods

**2.1. Animals.** All experiments were conducted in strict accordance with the recommendations of the Guide for the Care and Use of Laboratory Animals of China. The protocol was approved by the committee on the Ethics of Animal Experiments of Chongqing Medical University. Adult (8–12 weeks) male wild-type (WT) C57BL/6J mice and APOE-knockout (APOE<sup>-/-</sup>) mice on a C57BL/6J background were obtained from the Laboratory Animal Center of Chongqing Medical University. The design of the in vivo study is revealed in Figure 1.

**2.2. Induction of SAH.** SAH induction was performed as previously described [14]. Briefly, animals were anesthetized with an intraperitoneal injection of pentobarbital sodium (50 mg/kg). The right common carotid artery (CCA), external carotid artery (ECA), and internal carotid artery (ICA) were exposed. A 5-0 Prolene filament (Ethicon, Somerville, USA) was advanced into the anterior cerebral artery (ACA) via the ECA and ICA. After a subtle resistance was encountered, the filament was advanced 2 mm further to perforate the ACA. Subsequently, the filament was immediately withdrawn. In the sham operation group, the same procedure was performed with the exception of the perforation of the ACA. The body temperature was maintained at  $37.5 \pm 0.5^\circ\text{C}$  during the operation. The SAH score is assessed

according to a previously reported grading system [15]. Since SAH induces a high mortality rate, mice that died within 72 h were excluded and relevant mice were supplemented.

**2.3. Rotarod Test and Weight Loss.** The rotarod test (TME, Chengdu, China) was used to evaluate the motor deficits of the SAH mice according to the method reported by Hamm et al. [16]. Briefly, all mice were trained at a speed of 16 rpm three times a day for three days prior to SAH induction. Before SAH induction, the baseline of rotarod latency of each mouse was examined with an accelerating speed (starting from 0 rpm, accelerated by 3 rpm every 10 seconds until the rotating speed reached 30 rpm). The accelerating test was repeated at 24 h after SAH induction. Every test was repeated three times. The test ended when mice fell from the rod, and the latencies were recorded. The weight of each mouse was recorded before the rotarod test, and the weight loss was calculated according to the original weight of animals.

**2.4. Clodronate Liposome Administration.** Clodronate liposomes (FormuMax Scientific, Inc., Palo Alto, CA, USA) were injected intracerebroventricularly 1 day prior to SAH induction. Briefly, after mice were anesthetized, a burr hole was drilled 0.22 mm posterior to the bregma, 1 mm lateral, and 2.25 mm in depth to enter the bilateral ventricle. PBS liposomes which do not contain clodronate were used as controls. The dose of clodronate liposomes was adjusted according to the instructions (0.2 ml/20 g).

**2.5. Cell Culture and Treatment Protocols.** Primary microglia were prepared from postnatal day 1 C57BL/6J mice as previously reported [13]. Primary neurons were prepared from a day 15 embryonic cortex obtained from the pregnant C57BL/6J mice as previously reported [17]. All experiments were carried out 24 h after cells were seeded. The cells were treated with hemoglobin (Hb) (Sigma, St. Louis, MO, USA) diluted in culture medium or combined with SP600125 (Abcam, Cambridge, USA) diluted in DMSO for 24 h. The vehicle was used as the control. The supernatants were removed and replaced with fresh DMEM for another 24 h. Then, microglia were collected for assays. The conditioned medium of microglia was collected and added to neurons which were cultured in DMEM/F12 supplemented with 10% FBS for 24 h. Then, the cells were harvested for experiments.

**2.6. Nitrite Quantification.** The production of NO was assessed as the accumulation of nitrite from the spontaneous oxidation of NO in conditioned media after 24 h. Accumulation of nitrite was quantified using a colorimetric reaction with the Griess reagent (Invitrogen, Waltham, MA, USA). Absorbance was measured at 570 nm by spectrophotometry.

**2.7. Enzyme-Linked Immunosorbent Assay.** Quantification of the protein levels of TNF- $\alpha$ , IL-1 $\beta$ , and IL-6 was performed by the enzyme-linked immunosorbent assay (ELISA). Homogenates of the brain of mice or cultured medium of microglia were prepared for detection according to the manufacturer's instructions of the ELISA kits (Boster, Wuhan, China). The protein content of each sample was detected

with a BCA kit (Beyotime, Haimen, China). The results were normalized to protein levels.

**2.8. Immunofluorescence Staining.** Brain samples were fixed with 4% paraformaldehyde for 4 h, followed by overnight immersion in phosphate buffer containing 30% sucrose. The brain samples then were embedded in OCT solution, and coronal frozen sections (10  $\mu$ m) were prepared. The sections were incubated with primary antibodies at 4°C overnight, including anti- $\beta$ -APP (1:100, Abcam, Cambridge, USA), anti-ApoE (1:100, Abcam, Cambridge, USA), anti-NeuN (Abcam, Cambridge, USA), anti-Iba-1 (1:200, Wako, Osaka, Japan), and anti-P-JNK (Abcam, Cambridge, USA). Sections were then incubated with DyLight 488-conjugated goat anti-rabbit and DyLight 549-conjugated goat anti-mouse secondary antibodies (Abbkine, Redlands, USA). DAPI was used for nuclear staining. The number of positive cells was counted with Image-Pro Plus 6.0 software (Media Cybernetics, Bethesda, USA).

**2.9. Apoptosis Assay.** Coronal frozen sections of around the layer of ICA bifurcation were prepared. A NeuN primary antibody (1:100, Abcam, Cambridge, USA) was incubated overnight using the sections prior to TUNEL. TUNEL staining was performed as per the instructions of an in situ cell death detection kit (Roche, Indianapolis, USA). DAPI was used for nuclear staining. TUNEL-NeuN-costained cells were identified as apoptotic neurons with a fluorescence microscope (Leica, Wetzlar, Germany).

**2.10. MRI Scan.** Magnetic resonance imaging (MRI) was performed on a 7.0 T animal scanner (Bruker Biospin, Germany). Mice were anesthetized with 1.5% isoflurane in a mixture of 30% O<sub>2</sub> and 70% N<sub>2</sub>O and fixed on a holder. Diffusion tensor imaging (DTI) images were acquired using RARE (repetition time = 3000 ms, echo time = 25 ms, field of view = 2.5 cm, and slice thickness = 0.5 mm). A voxel-weighted fractional anisotropy (FA) measure was calculated for the region of the corpus callosum. All images were calculated with Bruker ParaVision 6.0 software (Bruker Biospin, Germany).

**2.11. Western Blots.** Brain hemispheres of mice were homogenized with RIPA (Beyotime, Haimen, Jiangsu, China) plus protease inhibitor cocktail (Roche, Indianapolis, IN, USA) and phosphatase inhibitors (Boster, Wuhan, Hubei, China). Prepared protein extracts were subjected to sodium dodecyl sulfate-polyacrylamide gel electrophoresis and transferred to polyvinylidene difluoride membranes. The membranes were probed overnight at 4°C with the following primary antibodies: anti-ApoE (1:500, Abcam, Cambridge, USA), anti-Iba-1 (1:500, Wako, Osaka, Japan), anti-P-JNK (1:1000, CST, Danvers, MA, USA), anti-JNK (1:500, Santa Cruz, Dallas, TX, USA), anti-P-c-Jun (1:1000, CST, Danvers, MA, USA), and anti-c-Jun (1:1000, CST, Danvers, MA, USA) followed by incubation with secondary antibodies conjugated with horseradish peroxidase. The bands were revealed using an ECL western blotting kit (Thermo Scientific, Pittsburgh, PA, USA) and photographed with a chemiluminescence imaging system (Bio-Rad, Hercules, CA, USA). The amount

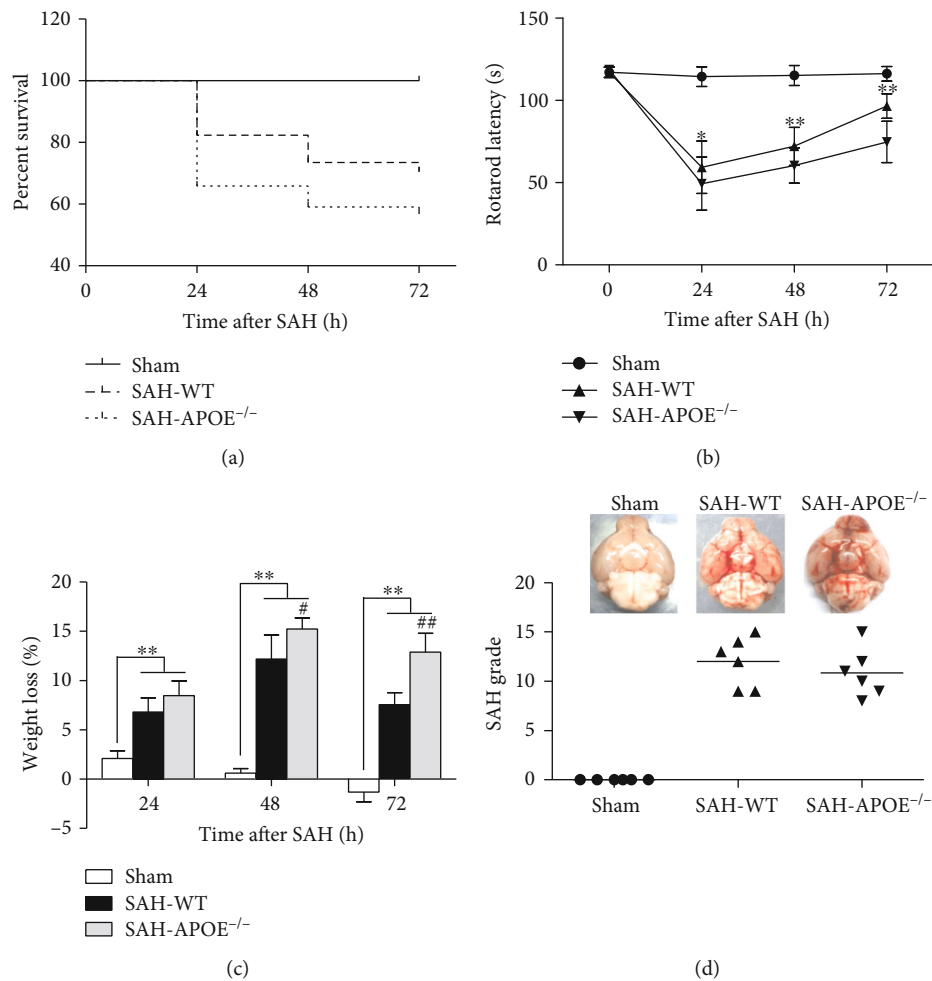


FIGURE 2: APOE deficiency aggravated neurological deficit within 72 h after SAH. (a) APOE<sup>-/-</sup> SAH mice exhibited a lower tendency of survival percentage than WT mice. However, the difference was nonsignificant. (b) APOE<sup>-/-</sup> mice exhibited a more severe motor deficit than WT mice at both time points (\* $P < 0.05$ , \*\* $P < 0.01$ ;  $n = 6$  for each group). (c) SAH induced weight loss of all mice (\*\* $P < 0.01$ , compared to sham). Weight loss of APOE<sup>-/-</sup> mice exceeded that of WT mice at 48 h and 72 h after SAH (# $P < 0.05$ , ## $P < 0.01$ ;  $n = 6$  for each group). (d) No difference was observed between APOE<sup>-/-</sup> and WT mice in the SAH grade.

of protein in each band was quantified using Image Lab Software (Bio-Rad, Hercules, CA, USA).

**2.12. Flow Cytometry.** For apoptotic detection, cultured neurons were harvested after treatment. Neurons were prepared according to the introduction of an apoptosis detection kit (BD, San Jose, CA, USA). Briefly, cells were incubated with 5  $\mu$ l of Annexin V-FITC dye solution for 15 min at 4°C and 10  $\mu$ l of PI dye solution for 5 min at room temperature. Then, the cells were subjected to flow cytometry. Annexin V-FITC<sup>+</sup>PI<sup>+</sup> and Annexin V-FITC<sup>+</sup>PI<sup>-</sup> cells were deemed apoptotic cells.

**2.13. Statistical Analysis.** Parametric values were expressed as the mean  $\pm$  standard deviation (SD). Two-tailed Student's *t*-test was used for comparison between two groups, and one-way analysis of variance (ANOVA) was applied for multiple comparisons. Bonferroni's *post hoc* method was applied for comparison among groups. The Fisher exact test was used in two-group comparisons for mortality analy-

sis. All statistic values were calculated using SPSS 19.0 (SPSS, Inc., Chicago, USA). Significance was assumed at  $P < 0.05$ .

### 3. Results

**3.1. APOE Deficiency Aggravated Neurological Deficits in the Early Phase of SAH.** In order to investigate the impact of APOE deficiency on early neurological dysfunction after SAH, the mortality rates, rotarod test, and weight loss were assessed in APOE<sup>-/-</sup> and WT mice. No animal died in the sham-operated group. The overall mortality rate of the WT group within 72 h after SAH was 29.4% (10 of 34), whereas 43.2% of the APOE<sup>-/-</sup> mice (19 of 44) died within 72 h after SAH (Figure 2(a)). However, the mortality exhibited no significant difference between WT and APOE<sup>-/-</sup> mice after SAH.

The rotarod latencies of both the APOE<sup>-/-</sup> and WT mice decreased drastically 24 h after SAH relative to the sham-operated mice, and the neurological functions recovered gradually at 48 h and 72 h after SAH. Meanwhile, APOE<sup>-/-</sup> mice exhibited worse motor function as indicated by shorter

rotarod latencies, relative to WT mice at 24 h, 48 h, and 72 h after SAH (Figure 2(b)). SAH induced weight loss of all mice. Weight loss of APOE<sup>-/-</sup> mice exceeded that of WT mice at 48 h and 72 h after SAH (Figure 2(c)). No difference was observed between APOE<sup>-/-</sup> and WT mice in the SAH grade score (Figure 2(d)).

These results revealed that APOE deficiency aggravates neurological deficits in the early phase of SAH. Hence, lacking APOE may cause more severe neuronal damage. To investigate the hypothesis, we further test the neuronal damage in APOE<sup>-/-</sup> and WT mice after SAH.

**3.2. APOE Deficiency Aggravated Neuronal Apoptosis and White Matter Injury in the Early Phase of SAH.** To reveal the mechanism underlying the varying degrees of neurological deficits between APOE<sup>-/-</sup> and WT mice, the neuronal damage was investigated. As the neuronal function relies on the integrity of neuronal cell bodies and axons, we further tested neuronal apoptosis and white matter injury in APOE<sup>-/-</sup> and WT mice at 24 h after SAH. SAH induced evident neuronal apoptosis (Figure 3(a)), while the apoptotic neurons of APOE<sup>-/-</sup> mice outnumbered those of WT mice (Figure 3(d)). Accumulation of  $\beta$ -APP is usually deemed a mark of axonal injury [18]. SAH induced axonal injury in the early phase of SAH, while APOE<sup>-/-</sup> mice exhibited more severe damage than WT mice after insult (Figure 3(b)). These results provide pathological evidence that APOE<sup>-/-</sup> mice are more vulnerable in SAH-induced axonal injury. To confirm the pathological findings, the FA in the injured white matter regions was determined with 7.0 T MRI at 24 h after SAH. SAH caused FA decrease in white matter regions (Figure 3(c)), while APOE<sup>-/-</sup> mice exhibited a greater degree of FA decrease than WT mice (Figure 3(e)).

These results suggested that APOE deficiency exacerbates neuronal damage, including injuries of neuronal cell bodies and axons, which may explain the worse neurological function of APOE<sup>-/-</sup> mice in the early phase of SAH. We further investigated the mechanisms behind the different degrees of neuronal injury between APOE<sup>-/-</sup> and WT mice. Based on a previous report, APOE is associated with mediation of microglial activation [13]. Thus, the number of microglia was detected after SAH.

**3.3. APOE Deficiency Aggravated Microglial Activation.** Microglia-mediated neuroinflammation is associated with neuronal damage in neurological diseases. A previous report suggests that ApoE inhibits microglial activation in vitro [13]. Our results showed a significant increase in microglia in both the cortex and white matter after SAH. APOE deficiency promoted microglial activation manifesting as more Iba-1-positive cells detected in cortex and white matter SAH (Figure 4(a)). Western blotting confirmed a more active microglial response after SAH (Figure 4(b)).

These results indicated that APOE deficiency aggravated microglial activation, which may exacerbate inflammatory damage of neurons. To verify whether microglial activation is associated with neuronal injury, we further applied clodronate liposome to deplete microglia and detected the neuronal damage after SAH.

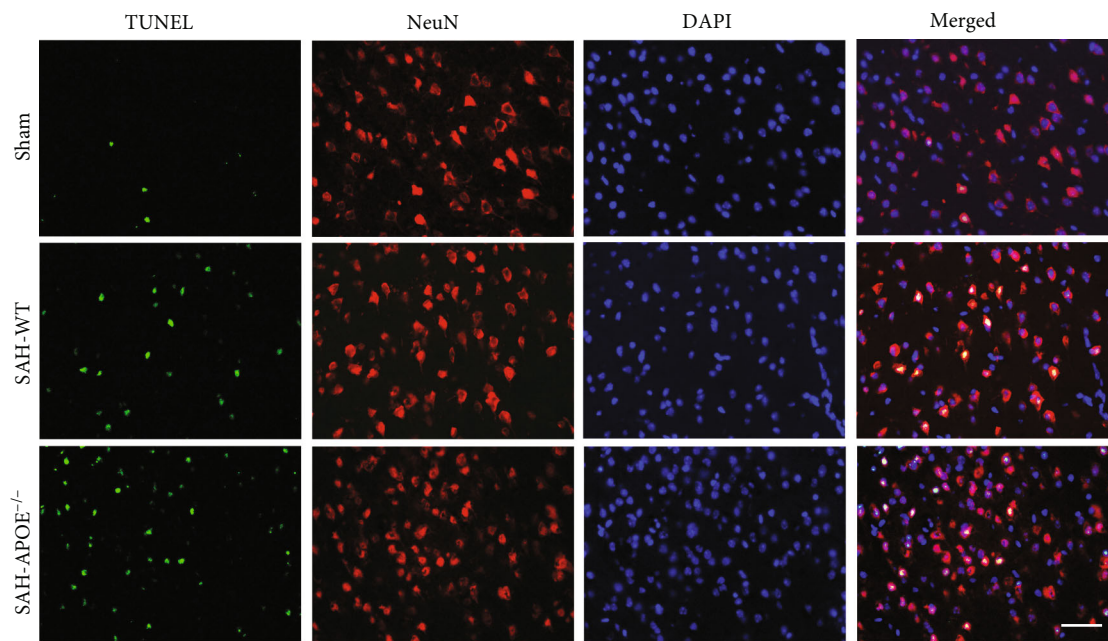
**3.4. Microglial Depletion Alleviated Neuronal Damage.** Clodronate liposome is widely used to deplete microglia and macrophages [9, 19]. A SAH model was applied in WT mice to test the influence of clodronate liposome on neuronal damage. Systemic administration of clodronate liposome reduced the number of microglia in the brain (Figure 5(a)). Clodronate liposome inhibited neuronal apoptosis after SAH (Figures 5(b) and 5(d)). Additionally, clodronate liposome ameliorated  $\beta$ -APP accumulation in the white matter after SAH (Figure 5(e)). A DTI image exhibited that clodronate liposome reserved FA (Figures 5(c) and 5(f)), indicating the protection for the white matter by clodronate liposome.

These results showed that microglial depletion alleviates neuronal injury after SAH, which indicates that microglia may mediate inflammatory injury of neurons. To investigate the influence of APOE on microglial inflammatory response, we further detected the expression of inflammation-relative molecules, JNK/c-Jun, and proinflammatory cytokines.

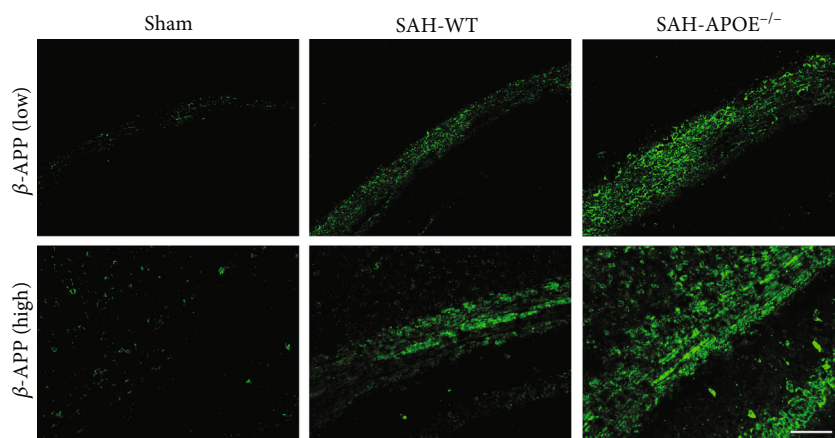
**3.5. APOE Deficiency Promoted JNK-Mediated Neuroinflammation.** The findings above indicate that APOE deficiency may aggravate neuronal injury via overactivation of microglia after SAH. The previous report suggests that APOE inhibits microglial activation in vitro via inhibiting the JNK pathway through binding to LRP1, a receptor of ApoE on microglia [20]. Therefore, we evaluated the JNK/c-Jun pathway in SAH mice. SAH promoted JNK and c-Jun phosphorylation, and the phosphorylation levels of JNK and c-Jun in APOE<sup>-/-</sup> mice were higher than those in WT mice (Figures 6(a) and 6(b)). Costaining was applied to confirm the expression of JNK/c-Jun in microglia. The microglia in sham mice barely expressed P-JNK. SAH promoted JNK phosphorylation in microglia, while APOE deficiency stimulated JNK phosphorylation in microglia after SAH (Figure 6(c)). The expression of downstream proinflammatory cytokines of JNK/c-Jun, TNF- $\alpha$ , IL-1 $\beta$ , and IL-6, exhibited that APOE deficiency promoted proinflammatory cytokine expression after SAH (Figures 6(d)–6(f)).

These results showed that APOE deficiency promotes JNK/c-Jun activation in microglia and its expression of proinflammatory cytokines after SAH, indicating that APOE may inhibit microglia-induced inflammatory injury on neurons via JNK/c-Jun. To test this hypothesis, we further investigated the role of JNK/c-Jun in inflammatory neuronal injury in vitro.

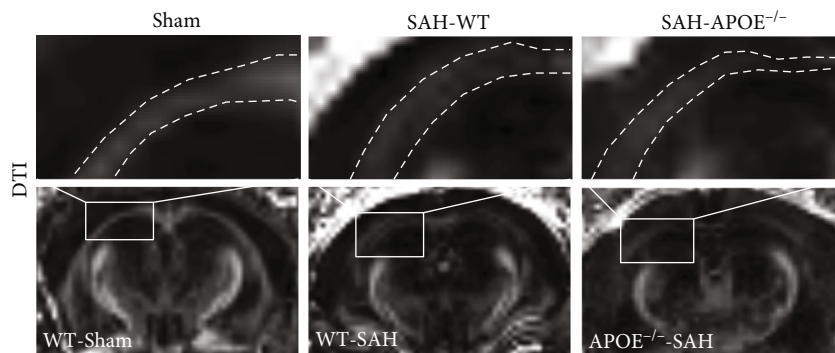
**3.6. Microglia Exerted Neuronal Injury via JNK/c-Jun In Vitro.** Hb is one of the major proinflammatory gradients released in the subarachnoid space after SAH [21]. To test the neuronal injury by activated microglia, cultured microglia were treated with Hb or vehicle for 24 h. The supernatants were removed and replaced with fresh DMEM for another 24 h, and then, the cultured medium was collected, respectively, to treat cultured neurons for 24 h (Figure 7(a)). Hb treatment induced microglial activation manifested by the release of the proinflammatory reagent nitrite (Figure 7(b)). Hb treatment stimulated JNK/c-Jun



(a)



(b)



(c)

FIGURE 3: Continued.



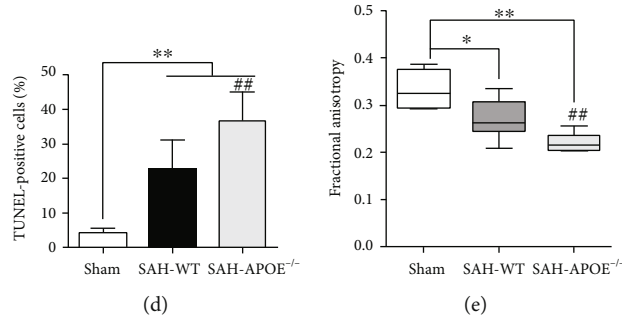
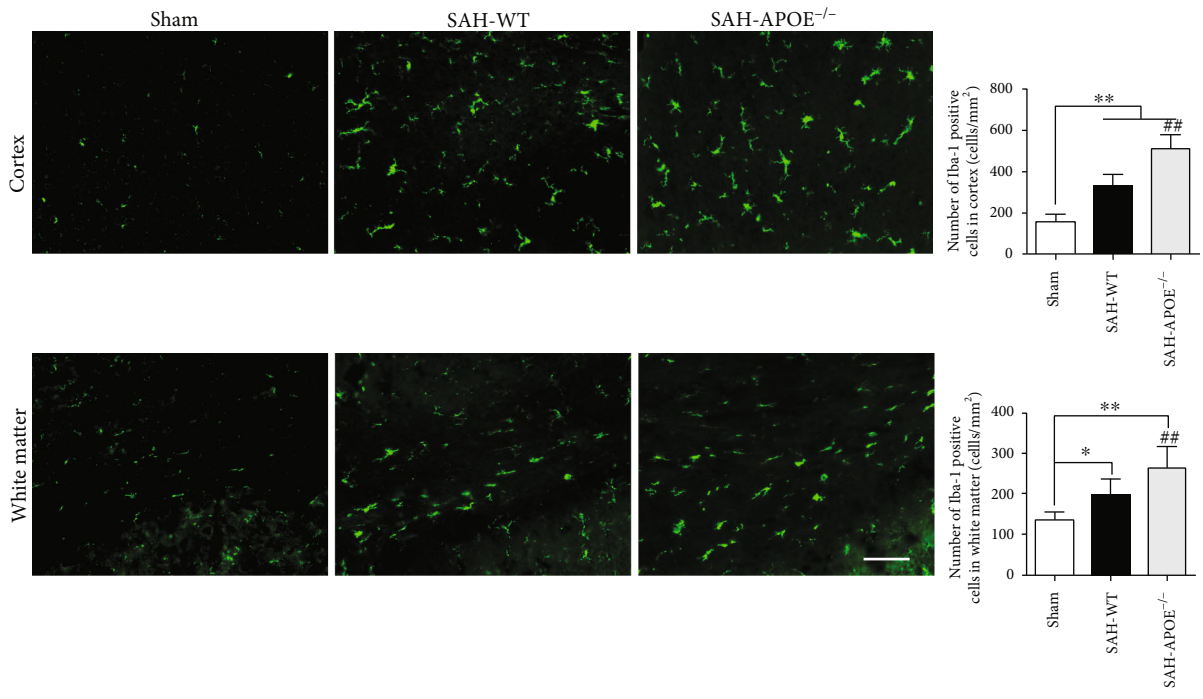
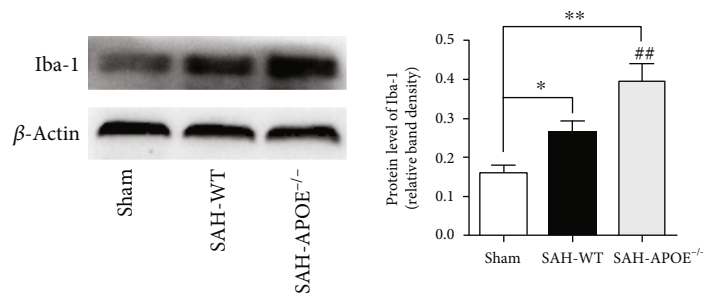


FIGURE 3: APOE deficiency aggravated neuronal damage in the early phase of SAH. (a) Costaining of TUNEL and NeuN showing apoptotic neurons. (d) SAH induced neuronal apoptosis in the cortex (\*\* $P < 0.01$ , compared to sham,  $n = 5$ ), while the number of apoptotic neurons of APOE<sup>-/-</sup> mice was more than that of WT mice (\*\* $P < 0.01$ ). (b) APOE deficiency aggravated  $\beta$ -APP accumulation in the white matter after SAH ( $n = 5$ ). Low magnification (200x), high magnification (400x). (c) DTI showing FA decrease after SAH. (e) SAH induced FA decrease (\* $P < 0.05$ , \*\* $P < 0.01$ , compared to sham,  $n = 4$ ), while the FA of APOE<sup>-/-</sup> mice in the white matter was lower than that of WT mice (\*\* $P < 0.01$ ). Bar = 50  $\mu$ M.



(a)



(b)

FIGURE 4: APOE deficiency aggravated microglial activation. (a) SAH increased the number of microglia in the cortex and white matter (\* $P < 0.05$ , \*\* $P < 0.01$ , compared to sham,  $n = 5$ ), while more microglia increased in APOE<sup>-/-</sup> mice than in WT mice (\*\* $P < 0.01$ ). (b) Western blotting showing overexpression of Iba-1 after SAH (\* $P < 0.05$ , \*\* $P < 0.01$ , compared to sham,  $n = 5$ ). APOE<sup>-/-</sup> mice exhibited higher Iba-1 level than WT mice (\*\* $P < 0.01$ ). Bar = 50  $\mu$ M.

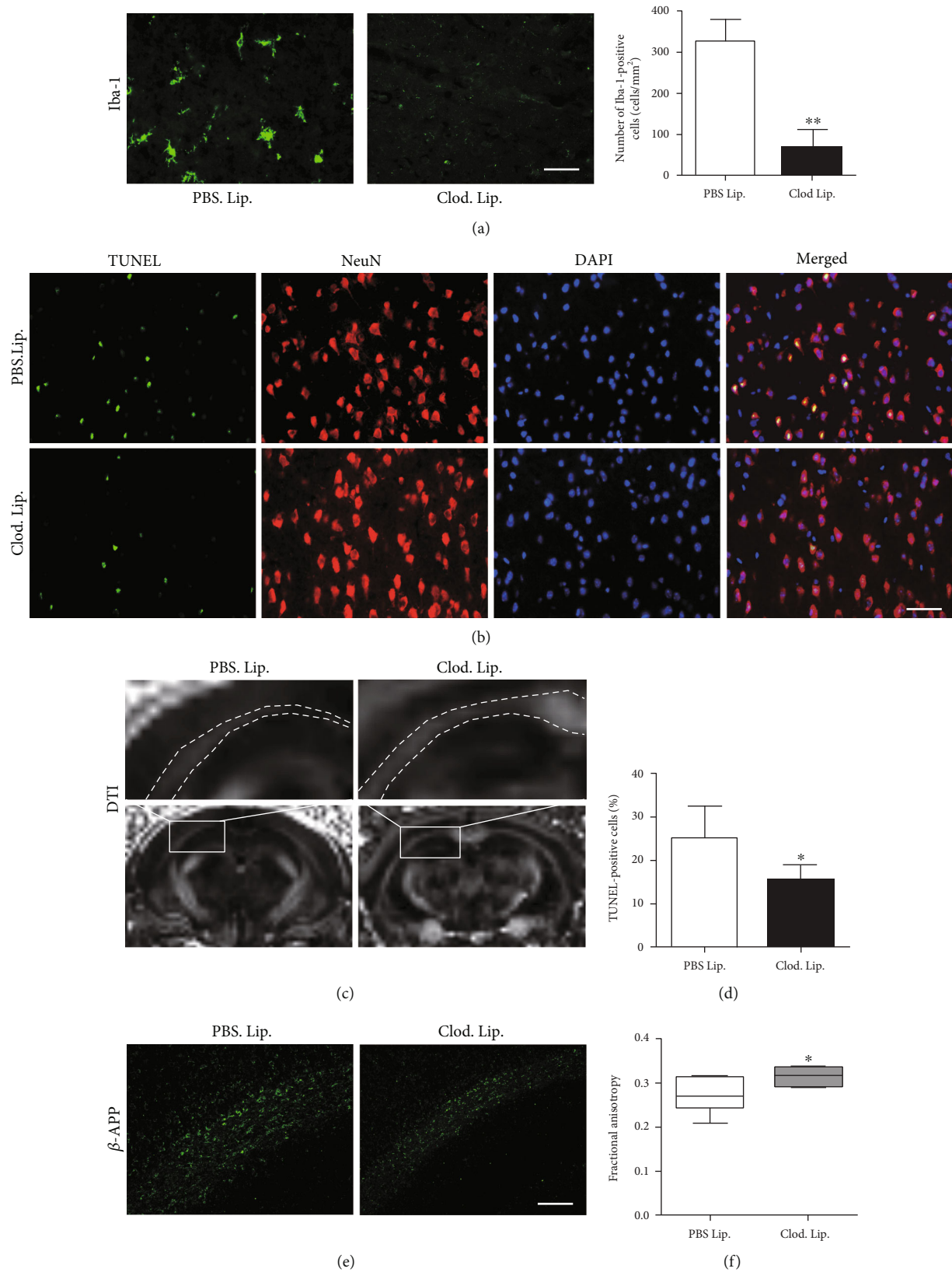


FIGURE 5: Microglial depletion alleviated neuronal damage. (a) Clod. Lip. reduced Iba-1-positive cells after SAH (\*\* $P < 0.01$ ,  $n = 5$ ). (b, d) Clod. Lip. reduced apoptotic neurons in the cortex after SAH (\* $P < 0.05$ ,  $n = 5$ ). (e) Clod. Lip. inhibited  $\beta$ -APP accumulation in the white matter after SAH. (c, f) DTI showing that Clod. Lip. reserved FA in the white matter after SAH (\* $P < 0.05$ ,  $n = 4$ ). Bar = 50  $\mu$ M.

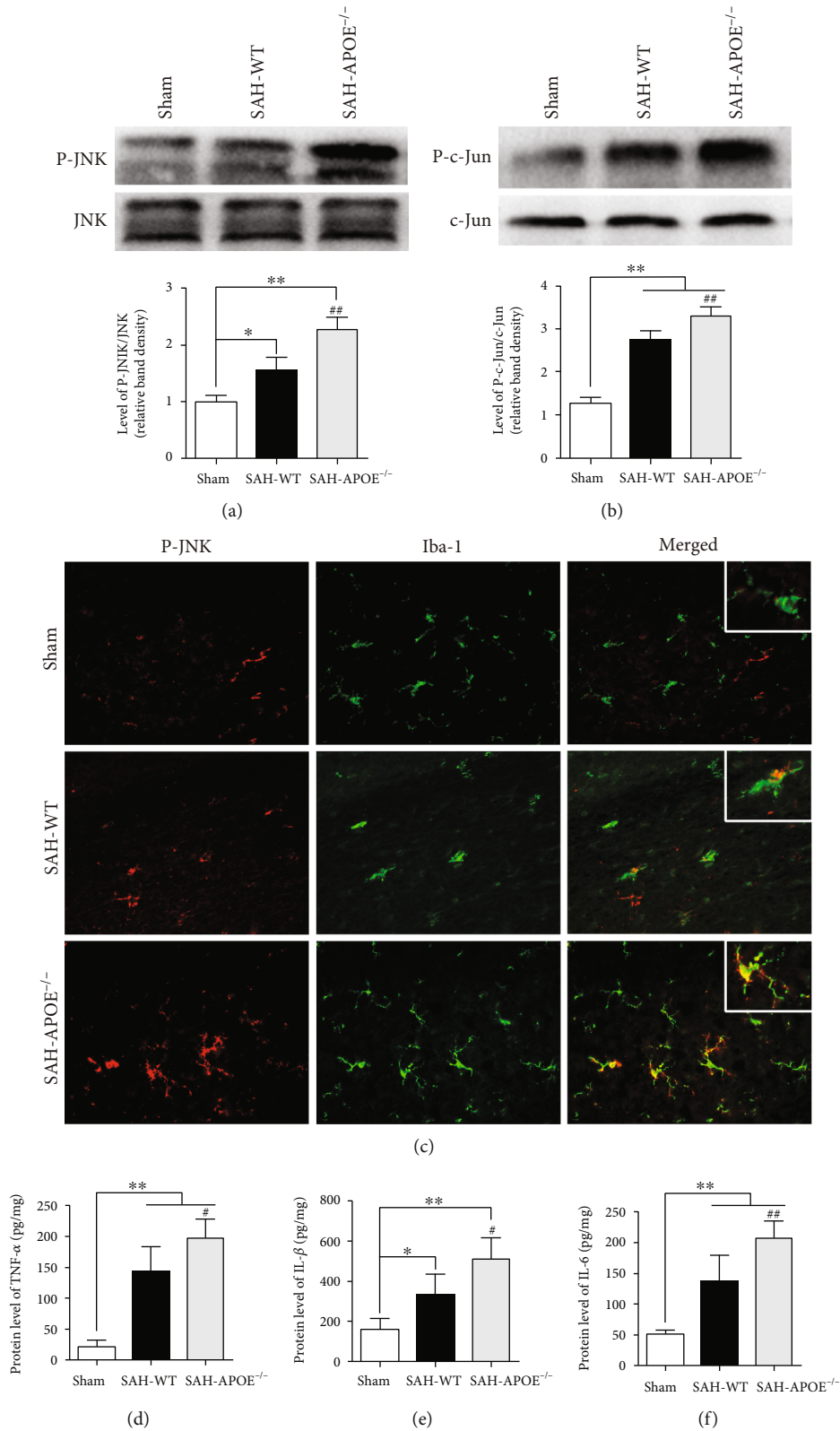
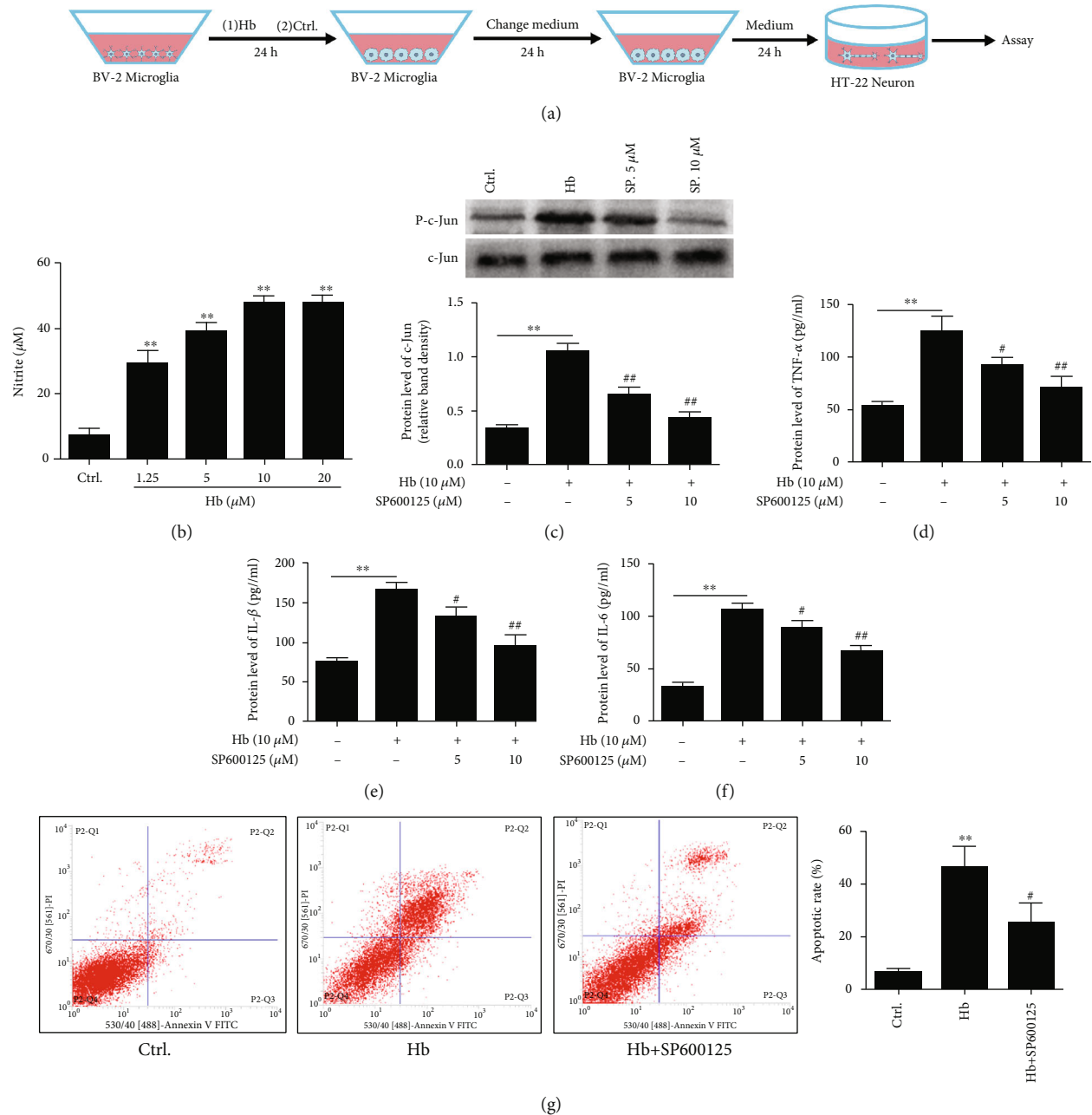


FIGURE 6: APOE deficiency enhanced JNK-mediated neuroinflammation. (a) SAH promoted JNK phosphorylation ( $*P < 0.05$ ,  $**P < 0.01$ , compared to sham,  $n = 5$ ), while P-JNK level was higher in APOE<sup>-/-</sup> mice than in WT mice ( $^{##}P < 0.01$ ). (b) SAH promoted c-JUN phosphorylation ( $**P < 0.01$ , compared to sham,  $n = 5$ ), while P-c-Jun level was higher in APOE<sup>-/-</sup> mice than in WT mice ( $^{##}P < 0.01$ ). (c) Immunofluorescence showing higher level of JNK phosphorylation in microglia in APOE<sup>-/-</sup> mice than in WT mice. (d-f) ELISA showing that SAH promoted cytokine expression including TNF- $\alpha$ , IL-1 $\beta$ , and IL-6 ( $*P < 0.05$ , compared to sham,  $n = 5$ ), while the levels of these cytokines were higher in APOE<sup>-/-</sup> mice than in WT mice ( $^{#}P < 0.05$ ,  $^{##}P < 0.01$ ). Bar = 50  $\mu$ M.



**FIGURE 7: Involvement of JNK in microglial inflammation and neuronal injury.** (a) In vitro experiment using cultured microglia incubated with Hb or vehicle control for 24 h. The conditioned medium was applied for incubation of neurons for 24 h. (b) Hb stimulated nitrite expression in microglia. As the doses of Hb increased, the nitrite expression elevated in microglia (\*\* $P < 0.01$ ,  $n = 3$ ). (c) Hb induced phosphorylation of c-Jun in microglia (\*\* $P < 0.01$ ,  $n = 3$ ). SP600125 attenuated c-Jun phosphorylation after Hb incubation (\*\* $P < 0.01$ ,  $n = 3$ ). (d–f) Hb induced cytokine expression including TNF- $\alpha$ , IL-1 $\beta$ , and IL-6 in microglia (\*\* $P < 0.01$ , compared to ctrl.), while SP600125 inhibited cytokine expression stimulated by Hb (\* $P < 0.05$ , \*\* $P < 0.01$ ,  $n = 3$ ). (g) Conditioned medium of Hb-treated microglia induced neuronal apoptosis (\*\* $P < 0.01$ ,  $n = 3$ ), while conditioned medium from SP600125-treated microglia attenuated neuronal apoptosis (\* $P < 0.05$ ). Bar = 50  $\mu\text{M}$ .

activation, while SP600125, a JNK inhibitor, inhibited the effect of Hb (Figure 7(c)). Additionally, Hb promoted the release of downstream cytokines, TNF- $\alpha$  and IL-1 $\beta$ , in the medium, while SP600125 reduced cytokine release by microglia (Figures 7(d)–7(f)). These results suggest that microglia-mediated inflammatory response depends on the activation of JNK/c-Jun.

We further investigated the effect of microglia-mediated inflammatory response on neurons by treating them with conditioned medium. Conditioned medium from Hb- (10  $\mu\text{M}$ ) treated microglia induced neuronal apoptosis. In contrast, conditioned medium from microglia treated with Hb (10  $\mu\text{M}$ ) and SP600125 (10  $\mu\text{M}$ ) combination ameliorated neuronal apoptosis (Figure 7(g)). These results showed that

JNK/c-Jun was involved in microglia-mediated inflammation which subsequently exerted neuronal injury.

**3.7. Potential Implication of APOE in Brain Injury in the Early Phase of SAH.** To examine the expression features of ApoE protein after SAH, we further tested the time course of ApoE expression within 72 h after SAH. The results showed an elevation of ApoE expression and peaked at 24 h after SAH, while APOE<sup>-/-</sup> mice did not express ApoE protein (Figure 8(a)). Costaining of cell markers and ApoE exhibited that ApoE was expressed dominantly in astrocytes and partly in neurons after SAH (Figure 8(b)). Although microglia were not the major source of endogenous ApoE, abundant LRP1, a major receptor of ApoE mediating a JNK/c-Jun signal, was observed in microglia (Figure 8(c)).

Combined with the findings above, APOE deficiency may enhance the JNK/c-Jun activation after SAH, which promotes the microglial inflammatory response. The enhanced neuroinflammation then aggravates neuronal injury and subsequently deteriorates the neurological deficits of APOE<sup>-/-</sup> mice. In contrast, APOE may exert protection in WT mice after SAH (Figure 8(d)).

#### 4. Discussion

In summary, SAH induced neuronal injury and neurological deficits in mice in the early phase. APOE deficiency resulted in more severe neurological deficits after SAH in mice. These deficits were associated with exacerbation of neuronal injury, including neuronal apoptosis and axonal injury. Moreover, APOE deficiency enhanced microglial activation and related inflammatory injury. JNK/c-Jun was involved in the enhancement of inflammatory injury in APOE<sup>-/-</sup> mice. These results indicate that APOE may exert a protective role against neuronal injury via the suppression of the inflammatory response.

The impact of APOE on the neurological outcomes of SAH animals has been observed in a previous report [22]. The evidence suggests that APOE is involved in the brain injury after SAH. For better understanding of this question, the role of APOE (e.g., protective or damaging) in SAH needs proving. Our results showed that APOE deficiency depleted the endogenous ApoE and its subsequent signaling modulation, which eventually resulted in the aggravation of brain injury. Reversely, we previously found that exogenous ApoE exerts protective effects in SAH mice [12]. These findings suggest that the downstream signaling effect of APOE is protective after SAH. Moreover, it is reported that the different impacts of APOE subtypes on the outcomes of SAH may be due to their diverse affinity to the functional receptors [23, 24]. From this perspective, we speculate that the influence of APOE polymorphisms on the outcomes of SAH may depend on the degrees of neuroprotective effects of different APOE alleles. Combined with the present work, APOE mediates beneficial effects in the early phase of SAH.

SAH has long been discovered to induce neuroinflammatory response [2]. We observed that APOE deficiency increased the microglial count in the brain early after SAH.

Microglia play important roles in immunological surveillance and homeostasis maintenance in CNS. Resting microglia that are stimulated by blood cells and lysate transform into an activated phenotype, thereby exerting immunological responses after SAH [8]. It remains unclear whether the microglia in the early phase of SAH are beneficial or harmful. The role of microglia varies in different phases of neurological diseases, which may be due to the complex activating features of these cells [25]. Microglia are observed to transform into different phenotypes which possess totally different biological nature, referred to as microglial polarization. Modulation of microglial polarization is reported to protect against neuronal injury [26]. However, queries suggest that microglia demonstrate a dynamic phenotype determined by the local environment [27]. A black box model may avoid the controversy and assess the comprehensive effect of microglia directly. Hanafy [9] reported that depleting resident microglia by clodronate liposome in mice attenuates neural apoptosis after SAH. In the present study, neuronal injury including apoptosis and white matter injury was attenuated by microglial depletion, indicating that microglia exert a comprehensive harmful effect on neurons in the early phase of SAH.

Elevated levels of inflammatory cytokines are associated with poor outcome of SAH patients in the early phase of SAH [1], suggesting the damaging role of inflammation in SAH. The present findings were consistent with the clinical observation that neuroinflammation contributes to brain injury after SAH. The suppression of the inflammatory response is considered an important aspect of the neuroprotective effects of APOE [28]. For instance, exogenous ApoE attenuates microglial activation and its subsequent inflammatory response in vitro [13]. Additionally, our previous study demonstrated that ApoE inhibits microglial activation and alleviates neuronal damage in EBI [12]. It was observed that the major cellular source of ApoE in the brain is astrocytes, and neurons partly express ApoE. Although microglia barely express ApoE, they are abundant in ApoE receptors. ApoE binds to the functional receptors expressed on the cellular membrane of microglia [29], which may explain the modulation of microglial function by APOE. Besides inflammatory response, oxidative stress may also contribute to the neuronal injury after SAH. Tu et al. [30] reported that ApoE-derived peptide reduces oxidative stress and improves outcome in an ischemic stroke mouse model, indicating that APOE may also regulate oxidative stress in the acute brain pathological process. Chen et al. [31] reported that oxidative stress is related to ROS/JNK signaling pathway acute stress-induced kidney injury. Our study revealed a regulation of the JNK pathway by APOE, which indicates that APOE may modulate oxidative stress via the JNK signaling pathway. The role of oxidative stress in SAH and the possible influence of APOE on oxidative stress need further exploration.

Previous reports have shown that JNK/c-Jun contributes to EBI after SAH [32]. JNK is activated early after SAH, and the inhibition of JNK attenuates apoptosis and BBB interruption. APOE has been demonstrated to suppress microglial activation by inhibiting the JNK pathway in vitro [13]. In the present study, the activation of JNK/c-Jun in microglia

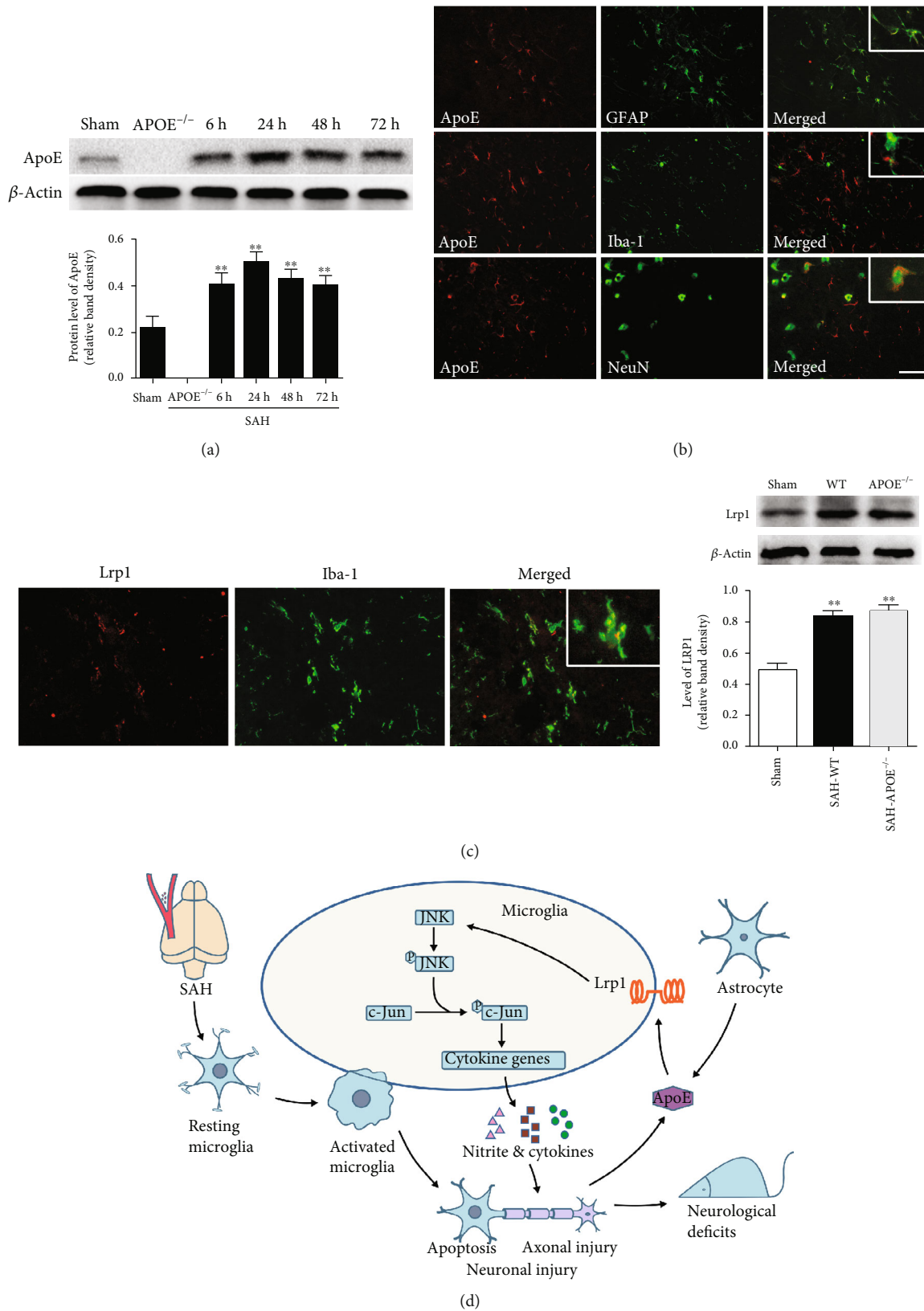


FIGURE 8: Potential implication of APOE in brain injury in the early phase of SAH. (a) Time course of ApoE expression in the early phase of SAH. The ApoE level elevated after SAH and peaked at 24 h after SAH (\*\* $P < 0.01$ , compared to sham,  $n = 5$ ). (b) Cellular location of ApoE after SAH. ApoE expressed mainly in astrocytes and partly in neurons. (c) Microglia expressed LRP1. The expression of LRP1 elevated in both APOE<sup>-/-</sup> and WT mice at 24 h after SAH. (d) Potential mechanisms for involvement of ApoE in brain injury in the early phase of SAH. Bar = 50  $\mu$ M.

was enhanced by APOE deficiency *in vivo*, while inhibition of JNK phosphorylation alleviated neuronal injury, thereby indicating that APOE attenuates microglia-mediated inflammation, at least in part, via the suppression of the JNK pathway after SAH. Pociavsek et al. [20] reported that the modulation of microglial inflammation via JNK/c-Jun and the effect are predominantly mediated by LRP1. Moreover, Zhu et al. [33] revealed that ApoE binding to cell surface receptors and the consequential inhibition of JNK/c-Jun activation are required for IL-6, IL-1 $\beta$ , and TNF- $\alpha$  secretion in macrophages. Higher levels of cytokine production were observed in APOE<sup>-/-</sup> mice. These cytokines exert inflammatory brain injury in the early phase of SAH. TNF- $\alpha$  has been demonstrated to initiate apoptosis by triggering the caspase cascade [27] and mediate myelin and neuronal damage [34]. Microglia are the major source of IL-1 following SAH [35]. IL-1 $\beta$  is reported to participate in EBI via activating JNK and MMP-9 [36]. Combined with this evidence, JNK/c-Jun is a key signal in APOE-mediated microglial inflammation after SAH.

Neuronal injury is the major cause of neurological deficits in SAH mice. Axons in the white matter consist in the integrity of neuronal function. White matter injury has recently been reported in SAH mice [37, 38]. Nevertheless, information on how these changes occur is lacking. Mechanical insult from sudden arterial rupture is thought to play a pivotal role in SAH-induced white matter injury, especially in the region distant from the rupture point [38]. More recently, Egashira et al. [39] reported that MMP-9-induced BBB disruption contributes to white matter injury after SAH. Consistent with the study, we found that endogenous ApoE increased as early as 6 h after SAH, and APOE deficiency induced a greater production of IL-1 $\beta$  which was previously shown to activate MMP-9 and cause BBB disruption [36]. In the present study, we observed that microglia exert a damaging effect on neurons after Hb treatment, which suggests that inflammation may be responsible for white matter injury after SAH. Wang et al. [10] reported that microglia mediate axonal damage after experimental TBI, which indicates that microglia play important roles in white matter injury. Moreover, we previously observed that microglial response is associated with white matter injury after SAH [40]. Besides the fact that microglia secreting nitrite and cytokines to induce neuronal injury were observed in the present study, it is suggested that microglia may exert direct injury on axons by physical cell-cell interactions [41]. Therefore, we favor the hypothesis that neuroinflammation also contributes to white matter injury, which may be a novel explanation for the vulnerability of APOE<sup>-/-</sup> mice in SAH, and indicate the prospect of treatment targeting white matter injury.

There are several limitations to the current study. The influence of APOE on brain injury was only tested in the acute-phase post-SAH. APOE may also be involved in the later course of the condition. Therefore, long-term observations should be applied in the future. The semiquantitative nature of the *in vivo* measurement of microglia is a further limitation. Future *in vivo* stereological quantifications should be considered. White matter injury was observed in the present study. The mechanisms by which these insults result in

EBI and their influences on neurological functions require further exploration.

In conclusion, APOE deficiency aggravates neurological deficits of SAH mice, which may be due to the exacerbation of neuronal apoptosis and white matter injury in the early phase. The aggravated neuronal damage is associated with enhanced microglial activation, which is mediated by APOE via the JNK/c-Jun signal. These results demonstrate the protective role of the APOE gene against neuronal injury and provide evidence for the exploration of APOE-based treatments for SAH.

## Data Availability

All data used to support the findings of this study are available from the corresponding authors upon request.

## Ethical Approval

All experiments were conducted in strict accordance with the recommendations of the Guide for the Care and Use of Laboratory Animals of China. The protocol was approved by the committee on the Ethics of Animal Experiments of Chongqing Medical University.

## Disclosure

Yue Wu and Jinwei Pang are considered the co-first authors.

## Conflicts of Interest

The authors have no conflicts of interest to declare.

## Authors' Contributions

YJ and XCS conceived and designed the experiments. YW, JWP, JHP, ZDG, LJ, and FC performed the experiments. ZPT, ZJH, and CJC analyzed the data. YW interpreted the data and drafted the manuscript. YJ and XCS reviewed and revised the manuscript. Yue Wu and Jinwei Pang contributed equally to this work.

## Acknowledgments

This work was supported by the National Natural Science Foundation of China (81771278, 81971132, 81801176, 81571159, 81901210, and 81960229), the Sichuan Science and Technology Program (2018RZ0090, 2019JDTD0004, and 2019JDR0062), the Science and Technology Program of Luzhou (2016LZXNYD-J12, 2016LZXNYD-Z02), the Fostering Fund of the First Affiliated Hospital of Chongqing Medical University (PYJJ2017-21), and the Doctoral Boot of Affiliated Hospital of Zunyi Medical College (201505).

## References

- [1] Y. Z. Al-Tamimi, N. M. Orsi, A. C. Quinn, S. Homer-Vanniasinkam, and S. A. Ross, "A review of delayed ischemic neurologic deficit following aneurysmal subarachnoid hemorrhage: historical overview, current treatment,

- and pathophysiology," *World Neurosurgery*, vol. 73, no. 6, pp. 654–667, 2010.
- [2] S. Chen, H. Feng, P. Sherchan et al., "Controversies and evolving new mechanisms in subarachnoid hemorrhage," *Progress in Neurobiology*, vol. 115, pp. 64–91, 2014.
  - [3] C. Muroi, M. Hugelshofer, M. Seule, and E. Keller, "The impact of nonsteroidal anti-inflammatory drugs on inflammatory response after aneurysmal subarachnoid hemorrhage," *Neurocritical care*, vol. 20, no. 2, pp. 240–246, 2014.
  - [4] S. J. Hopkins, C. J. McMahon, N. Singh et al., "Cerebrospinal fluid and plasma cytokines after subarachnoid haemorrhage: Csf interleukin-6 may be an early marker of infection," *Journal of Neuroinflammation*, vol. 9, no. 1, p. 255, 2012.
  - [5] K. Murakami, M. Koide, T. M. Dumont, S. R. Russell, B. I. Tranmer, and G. C. Wellman, "Subarachnoid hemorrhage induces gliosis and increased expression of the pro-inflammatory cytokine high mobility group box 1 protein," *Translational stroke research*, vol. 2, no. 1, pp. 72–79, 2011.
  - [6] S. Amor, F. Puentes, D. Baker, and P. van der Valk, "Inflammation in neurodegenerative diseases," *Immunology*, vol. 129, no. 2, pp. 154–169, 2010.
  - [7] X. Jin, H. Ishii, Z. Bai, T. Itokazu, and T. Yamashita, "Temporal changes in cell marker expression and cellular infiltration in a controlled cortical impact model in adult male c57bl/6 mice," *PLoS one*, vol. 7, no. 7, article e41892, 2012.
  - [8] S. Smithason, S. K. Moore, and J. J. Provencio, "Systemic administration of lps worsens delayed deterioration associated with vasospasm after subarachnoid hemorrhage through a myeloid cell-dependent mechanism," *Neurocritical care*, vol. 16, no. 2, pp. 327–334, 2012.
  - [9] K. A. Hanafy, "The role of microglia and the TLR 4 pathway in neuronal apoptosis and vasospasm after subarachnoid hemorrhage," *Journal of Neuroinflammation*, vol. 10, no. 1, p. 83, 2013.
  - [10] G. Wang, J. Zhang, X. Hu et al., "Microglia/macrophage polarization dynamics in white matter after traumatic brain injury," *Journal of cerebral blood flow and metabolism*, vol. 33, no. 12, pp. 1864–1874, 2013.
  - [11] J. Pang, Y. Wu, J. Peng et al., "Potential implications of apolipoprotein E in early brain injury after experimental subarachnoid hemorrhage: involvement in the modulation of blood-brain barrier integrity," *Oncotarget*, vol. 7, no. 35, pp. 56030–56044, 2016.
  - [12] Y. Wu, J. Pang, J. Peng et al., "An apoE-derived mimic peptide, COG1410, alleviates early brain injury via reducing apoptosis and neuroinflammation in a mouse model of subarachnoid hemorrhage," *Neuroscience Letters*, vol. 627, pp. 92–99, 2016.
  - [13] A. Pocivavsek, M. P. Burns, and G. W. Rebeck, "Low-density lipoprotein receptors regulate microglial inflammation through c-Jun n-terminal kinase," *Glia*, vol. 57, no. 4, pp. 444–453, 2009.
  - [14] S. Feiler, B. Friedrich, K. Scholler, S. C. Thal, and N. Plesnila, "Standardized induction of subarachnoid hemorrhage in mice by intracranial pressure monitoring," *Journal of neuroscience methods*, vol. 190, no. 2, pp. 164–170, 2010.
  - [15] T. Sugawara, R. Ayer, V. Jadhav, and J. H. Zhang, "A new grading system evaluating bleeding scale in filament perforation subarachnoid hemorrhage rat model," *Journal of neuroscience methods*, vol. 167, no. 2, pp. 327–334, 2008.
  - [16] R. J. Hamm, B. R. Pike, D. M. O'Dell, B. G. Lyeth, and L. W. Jenkins, "The rotarod test: an evaluation of its effectiveness in assessing motor deficits following traumatic brain injury," *Journal of Neurotrauma*, vol. 11, no. 2, pp. 187–196, 1994.
  - [17] Z. Yu, N. Liu, Y. Li, J. Xu, and X. Wang, "Neuroglobin overexpression inhibits oxygen-glucose deprivation-induced mitochondrial permeability transition pore opening in primary cultured mouse cortical neurons," *Neurobiology of Disease*, vol. 56, pp. 95–103, 2013.
  - [18] R. Coltmann, A. Spain, Y. Tsenkina et al., "Selective white matter pathology induces a specific impairment in spatial working memory," *Neurobiology of aging*, vol. 32, no. 12, pp. 2324.e7–2324.e12, 2011.
  - [19] Y. Ma, Y. Li, L. Jiang et al., "Macrophage depletion reduced brain injury following middle cerebral artery occlusion in mice," *Journal of Neuroinflammation*, vol. 13, no. 1, p. 38, 2016.
  - [20] A. Pocivavsek, I. Mikhailenko, D. K. Strickland, and G. W. Rebeck, "Microglial low-density lipoprotein receptor-related protein 1 modulates c-Jun n-terminal kinase activation," *Journal of Neuroimmunology*, vol. 214, no. 1-2, pp. 25–32, 2009.
  - [21] M. S. Kwon, S. K. Woo, D. B. Kurland et al., "Methemoglobin is an endogenous toll-like receptor 4 ligand-relevance to subarachnoid hemorrhage," *International journal of molecular sciences*, vol. 16, no. 3, pp. 5028–5046, 2015.
  - [22] J. Gao, H. Wang, H. Sheng et al., "A novel apoE-derived therapeutic reduces vasospasm and improves outcome in a murine model of subarachnoid hemorrhage," *Neurocritical care*, vol. 4, no. 1, pp. 25–31, 2006.
  - [23] R. D. Bell, E. A. Winkler, I. Singh et al., "Apolipoprotein E controls cerebrovascular integrity via cyclophilin A," *Nature*, vol. 485, no. 7399, pp. 512–516, 2012.
  - [24] R. W. Mahley, K. H. Weisgraber, and Y. Huang, "Apolipoprotein E: structure determines function, from atherosclerosis to Alzheimer's disease to aids," *Journal of lipid research*, vol. 50, Supplement, pp. S183–S188, 2009.
  - [25] J. D. Cherry, J. A. Olschowka, and M. K. O'Banion, "Neuroinflammation and M2 microglia: the good, the bad, and the inflamed," *Journal of Neuroinflammation*, vol. 11, no. 1, p. 98, 2014.
  - [26] H. Zhang, Y. Li, J. Yu et al., "Rho kinase inhibitor fasudil regulates microglia polarization and function," *Neuroimmunomodulation*, vol. 20, no. 6, pp. 313–322, 2013.
  - [27] R. M. Ransohoff, "A polarizing question: do M1 and M2 microglia exist?," *Nature neuroscience*, vol. 19, no. 8, pp. 987–991, 2016.
  - [28] J. R. Lynch, D. Morgan, J. Mance, W. D. Matthew, and D. T. Laskowitz, "Apolipoprotein e modulates glial activation and the endogenous central nervous system inflammatory response," *Journal of Neuroimmunology*, vol. 114, no. 1-2, pp. 107–113, 2001.
  - [29] Q. W. Fan, I. Iosbe, H. Asou, K. Yanagisawa, and M. Michikawa, "Expression and regulation of apolipoprotein E receptors in the cells of the central nervous system in culture: a review," *Journal of the American Aging Association*, vol. 24, no. 1, pp. 1–10, 2001.
  - [30] T. M. Tu, B. J. Kolls, E. J. Soderblom et al., "Apolipoprotein E mimetic peptide, CN-105, improves outcomes in ischemic stroke," *Annals of clinical and translational neurology*, vol. 4, no. 4, pp. 246–265, 2017.
  - [31] Y. Chen, X. Feng, X. Hu et al., "Dexmedetomidine ameliorates acute stress-induced kidney injury by attenuating oxidative stress and apoptosis through inhibition of the ROS/JNK



- signaling pathway,” *Oxidative medicine and cellular longevity*, vol. 2018, Article ID 4035310, 12 pages, 2018.
- [32] H. Yatsushige, R. P. Ostrowski, T. Tsubokawa, A. Colohan, and J. H. Zhang, “Role of c-Jun n-terminal kinase in early brain injury after subarachnoid hemorrhage,” *Journal of Neuroscience Research*, vol. 85, no. 7, pp. 1436–1448, 2007.
- [33] Y. Zhu, A. Kodvawala, and D. Y. Hui, “Apolipoprotein E inhibits toll-like receptor (TLR)-3- and TLR-4-mediated macrophage activation through distinct mechanisms,” *The Biochemical journal*, vol. 428, no. 1, pp. 47–54, 2010.
- [34] R. Sercombe, Y. R. Dinh, and P. Gomis, “Cerebrovascular inflammation following subarachnoid hemorrhage,” *Japanese journal of pharmacology*, vol. 88, no. 3, pp. 227–249, 2002.
- [35] A. D. Greenhalgh, D. Brough, E. M. Robinson, S. Girard, N. J. Rothwell, and S. M. Allan, “Interleukin-1 receptor antagonist is beneficial after subarachnoid haemorrhage in rat by blocking haem-driven inflammatory pathology,” *Disease models & mechanisms*, vol. 5, no. 6, pp. 823–833, 2012.
- [36] T. Sozen, R. Tsuchiyama, Y. Hasegawa et al., “Role of interleukin-1 $\beta$  in early brain injury after subarachnoid hemorrhage in mice,” *Stroke*, vol. 40, no. 7, pp. 2519–2525, 2009.
- [37] Y. Egashira, Y. Hua, R. F. Keep, and G. Xi, “Acute white matter injury after experimental subarachnoid hemorrhage: potential role of lipocalin 2,” *Stroke*, vol. 45, no. 7, pp. 2141–2143, 2014.
- [38] T. T. Kummer, S. Magnoni, C. L. Mac Donald et al., “Experimental subarachnoid haemorrhage results in multifocal axonal injury,” *Brain*, vol. 138, no. 9, pp. 2608–2618, 2015.
- [39] Y. Egashira, H. Zhao, Y. Hua, R. F. Keep, and G. Xi, “White matter injury after subarachnoid Hemorrhage,” *Stroke*, vol. 46, no. 10, pp. 2909–2915, 2015.
- [40] Y. Wu, J. Peng, J. Pang, X. Sun, and Y. Jiang, “Potential mechanisms of white matter injury in the acute phase of experimental subarachnoid haemorrhage,” *Brain*, vol. 140, no. 6, article e36, 2017.
- [41] K. P. Horn, S. A. Busch, A. L. Hawthorne, N. van Rooijen, and J. Silver, “Another barrier to regeneration in the CNS: activated macrophages induce extensive retraction of dystrophic axons through direct physical interactions,” *The Journal of neuroscience*, vol. 28, no. 38, pp. 9330–9341, 2008.

## Research Article

# miR-185 and SEPT5 Genes May Contribute to Parkinson's Disease Pathophysiology

Arman Rahimmi <sup>1,2</sup>, Ilaria Peluso <sup>3</sup>, Aref Rajabi <sup>4</sup>, and Kambiz Hassanzadeh <sup>2,5</sup>

<sup>1</sup>Student Research Committee, Kurdistan University of Medical Sciences, Sanandaj, Iran

<sup>2</sup>Cellular and Molecular Research Center, Research Institute for Health Development, Kurdistan University of Medical Sciences, Sanandaj, Iran

<sup>3</sup>Council for Agricultural Research and Economics, Research Centre for Food and Nutrition (CREA-AN), Via Ardeatina 546, 00178 Rome, Italy

<sup>4</sup>Department of Neurology, Kurdistan University of Medical Sciences, Sanandaj, Iran

<sup>5</sup>Department of Physiology and Pharmacology, Kurdistan University of Medical Sciences, Sanandaj, Iran

Correspondence should be addressed to Arman Rahimmi; [a.rahimmi@yahoo.com](mailto:a.rahimmi@yahoo.com)  
and Kambiz Hassanzadeh; [kambizhassanzadeh@gmail.com](mailto:kambizhassanzadeh@gmail.com)

Received 23 May 2019; Revised 2 September 2019; Accepted 12 October 2019; Published 14 November 2019

Guest Editor: Maurizio Forte

Copyright © 2019 Arman Rahimmi et al. This is an open access article distributed under the Creative Commons Attribution License, which permits unrestricted use, distribution, and reproduction in any medium, provided the original work is properly cited.

There are still unknown mechanisms involved in the development of Parkinson's disease (PD), which elucidating them can assist in developing efficient therapies. Recently, studies showed that genes located on the human chromosomal location 22q11.2 might be involved in the development of PD. Therefore, the present study was designed to evaluate the role of two genes located on the chromosomal location (miR-185 and SEPT5), which were the most probable candidates based on our bibliography. *In vivo* and *in vitro* models of PD were developed using male Wistar rats and SHSY-5Y cell line, respectively. The expression levels of miR-185, SEPT5, LRRK2, and PARK2 genes were measured at a mRNA level in dopaminergic areas of rats' brains and SHSY-5Y cells using the SYBR Green Real-Time PCR Method. Additionally, the effect of inhibition on the genes or their products on cell viability and gene expression pattern in SHSY-5Y cells was investigated. The level of miR-185 gene expression was significantly decreased in the substantia nigra (SN) and striatum (ST) of the rotenone-treated group (control group) compared to the healthy normal group ( $P < 0.05$ ). In addition, there was a significant difference in the expression of SEPT5 gene ( $P < 0.05$ ) in the substantia nigra between two studied groups. The results of an *in vitro* study showed no significant change in the expression of the genes; however, the inhibition on miR-185 gene expression led to the increase in LRRK2 gene expression in SHSY-5Y cells. The inhibition on LRRK2 protein also decreased the cellular toxicity effect of rotenone on SHSY-5Y cells. The results suggested the protective role of miR-185 gene in preventing the development of PD.

## 1. Introduction

Parkinson's disease (PD) is a prevalent central nervous system (CNS) disorder, which develops due to the loss of nigrostriatal dopaminergic neurons in the midbrain [1]. Whereupon, movement (resting tremor, muscular rigidity, bradykinesia, gait impairment, etc.) and behavioral (cognitive impairment and dementia) disorders appeared [2]. The prevalence of PD is about 1-2% in people older than 65 years old, 4% in people older than 85 years old, and 0.3% in total

population [3]. About one million people suffer from PD in United States of America and 50,000 to 60,000 new cases are diagnosed every year. The prevalence of PD is estimated to increase two folds until 2030 [4]. The economic burden of PD is estimated to be 10.8 billion dollars annually only in the United States; out of which, 58% is directly related to the medical care services [4]. Furthermore, PD is a chronic and progressive disease, lasting for years and decreasing life quality of the patients intensely [5]. Thus, finding factors causing PD has a great importance, since it can help

uncovering the nature of the disease and developing more efficient therapies.

Researchers have determined many factors for the development of PD, including environmental toxins (e.g., pesticides and herbicides), genetic background (mutations in particular genes such as SNCA, PINK1, Parkin, LRRK2, and DJ-1), certain viruses and/or a combination of all [6, 7]. Importantly, most of the recent studies show that no matter what the cause is, oxidative stress and inflammation always play a key role in the death of the dopaminergic cells of substantia nigra (SN) [8, 9]. Oxidative stress is caused by many external and internal sources, such as certain toxins and pathogens, dopamine metabolism, mitochondrial impairment, and reactive iron stored in neuromelanin [10]. Numerous studies frequently reported the increase in the inflammatory factors, such as TNF- $\alpha$ , NF- $\kappa$ B, IL-6, and IL-2 in the SN of PD patients and PD animal models [11, 12]. Indubitably, PD is a multifactorial disease, which many factors can contribute in its development, either alone or accompanied with other factors, although neither all causing factors are discovered yet nor complete molecular mechanism of the disease is known.

Recently, researchers discovered a locus on human chromosome 22 (22q11.1), which its congenital absence due to the microdeletion (DiGeorge syndrome) could lead to the early onset of PD [13]. The locus is consisted of about 30 genes; none of them are among the genes known to be involved in the development of PD [13, 14]. Interestingly, it appears that some of the genes in 22q11.2 locus are probable candidates involving in the molecular mechanisms of the development and progression of PD. miR-185 is one of those genes predicted to target LRRK2 [15, 16]. SEPT5 is another gene located on 22q11.2 locus, which its protein product interacts with the products of certain genes such as PARK2 and catechol-O-methyltransferase (COMT) [14]. LRRK2 is a kinase present in cytoplasm and outer membrane of mitochondria. Mutations or overexpressions of LRRK2 gene are strongly associated with development of Parkinson's disease [17]. PARK2 is a ligase which assist proteasome complexes to degrade misfolded proteins. Mutations or overexpressions of PARK2 gene are also strongly associated with development of Parkinson's disease [18].

On the other hand, some researchers believe that disorders such as epilepsy, schizophrenia, and failure of certain internal secretory glands (thyroid, parathyroid, and thymus) are more straightforward consequences of 22q11.2 microdeletion. They suggest that PD is caused as a result of the psychological drugs, consumed by the patients with DiGeorge syndrome [19]. However, more recent studies challenge this belief, since it is observed that the patients with DiGeorge syndrome show movement disorders even in their childhood. Additionally, PD develops in those adult patients with DiGeorge syndrome, who are not under the treatment with psychological drug regimens [13, 20]. Therefore, PD can be considered to be an independent aspect of 22q11.2 microdeletion, not a result of psychological drug consumption.

Despite the potential role of those two genes (miR-185 and SEPT5), only a few studies showed the possible role of the genes in the development of PD. Therefore, evaluation

regarding the expression of these genes can provide a new and important insight into the pathogenesis of PD.

In order to investigate the possible role of miR-185 and SEPT5 genes in the pathogenesis of PD, their transcript expression level was assessed in SHSY-5Y cell line (a human cell line) treated by rotenone (*in vitro* model of PD) and brain tissues (substantia nigra and striatum) of male Wistar rat as the *in vivo* model of PD (induced by rotenone). The expression of two molecular targets of miR-185 and SEPT5 (i.e., LRRK2 and PARK2) was assessed to determine whether there is a presumptive relation among the two genes (miR-185 and SEPT5) and the known genes causing PD.

## 2. Materials and Methods

**2.1. Chemicals.** Rotenone, sunflower oil and DMSO were purchased from Sigma-Aldrich Company (St. Louis, MO, USA). HG-10-102-01 (LRRK2 inhibitor) was purchased from Cayman Chemical Company (New York, NY, USA). miRZip-185 was purchased from Sanbio Company (Uden, Netherlands).

**2.2. Animals.** Sixteen male Wistar rats (Pasteur Institute of Iran) weighing  $300 \pm 25$  g and aged 5 months were selected randomly. Animals were housed in polycarbonate cages (2 rats per cage) under controlled conditions, including 12 h light/dark cycles, the environment temperature of  $23 \pm 2^\circ\text{C}$ , and the environment humidity of  $60 \pm 5\%$ . Standard food and water were accessible for the animals ad libitum. All experiments were performed, while considering the Guide for the Care and Use of Laboratory Animals (National Institutes of Health Publication No. 85-23, revised 1985). The research ethics committee of Kurdistan University of Medical Sciences also approved all experiments in this study.

**2.3. Experimental Groups.** Animals were randomly divided into two groups ( $n = 8$ ), which are as follows:

- (i) The control group consisting of the rats received rotenone (1.5 mg/kg/24 h, SC)
- (ii) The healthy normal group consisting of the rats received rotenone vehicle (1 ml/kg/24 h, SC)

The sample size was calculated by G power software.

**2.4. Method Used for Induction of Parkinson's Disease in Animals.** Rotenone solution was freshly prepared before injections. So that, it was dissolved in dimethyl sulfoxide. Then, sunflower oil was added to the solution to dilute it and reach a final concentration of 1.5 mg/ml of rotenone. The ratio of dimethyl sulfoxide to sunflower oil in the final solution was equal to 2:98. In order to induce Parkinson's disease, animals received rotenone at a concentration of 1.5 mg/kg each for 24 h. The injections continued until motor dysfunction was declared on all behavioral tests (rotarod test, bar test, and rearing test) in the control group. Animals were tested every 5 days, before daily injection of rotenone. The day in which the significant decrease was observed in all behavioral tests was considered as the day of model

TABLE 1: The primer pairs used for the gene amplifications.

Primers	Sequence (5' → 3')	GC%	$T_m$ (°C)	PCR product length (n)
SEPT5 (forward)	GCTGAGGAACGCATCAAC	55.6%	56.5°C	167
SEPT5 (reverse)	AACTGCTGGTCTACATAGTC	45.0%	55.2°C	
LRRK2 (forward)	CCTGGATTGCTGGAGATTG	52.6%	57.3°C	175
LRRK2 (reverse)	GAATGGTGAGCCTTGTTG	52.6%	56.5°C	
PARK2 (forward)	GACGCTCAACTGGCTACTC	55.0%	57.1°C	131
PARK2 (reverse)	CACTCCTCGGCACCATAC	61.0%	57.6°C	
$\beta$ -act (forward)	CGTGCGTGACATTAAGAGAAG	45.5%	58.5°C	134
$\beta$ -act (reverse)	CATTGCCGATAGTGATGACC	50.0%	57.6°C	
miR-185 (forward)	Exclusively designed by Bon Yakhteh Company, Tehran, Iran	—	—	—
miR-185 (reverse)	Exclusively designed by Bon Yakhteh Company, Tehran, Iran	—	—	
U67 (forward)	Exclusively designed by Bon Yakhteh Company, Tehran, Iran	—	—	—
U67 (reverse)	Exclusively designed by Bon Yakhteh Company, Tehran, Iran	—	—	

development of Parkinson's disease (46<sup>th</sup> day since the first injection). On the last day, all the behavioral tests were repeated 10 min after injection of apomorphine (1 mg/kg, SC), to confirm whether the motor dysfunctions were dopamine-dependent and not a result of the unspecific consequences of rotenone treatment on peripheral organs. This protocol was a modified protocol based on our previous studies and was conducted several times as pilot, in order to be optimized in our lab [21]. The methods used for performing behavioral tests are presented in details in one of our previous studies [22].

**2.5. Body Weight Measurement.** Animals were weighted every 48 h before the injections, and it was done to be an index for monitoring the health condition and possible peripheral toxicity induced by rotenone. Indeed, a significant decrease in the body weight shows the unspecific effects of rotenone treatment [23].

**2.6. Tissue Collection.** At the end of the motor and behavioral assessments (46<sup>th</sup> day), the animals were sacrificed by decapitation under deep anesthesia using ketamine/xylazine cocktail. The substantia nigra and striatum were removed, cleaned, and frozen in liquid nitrogen and then were stored at  $-80^\circ\text{C}$  until use.

**2.7. Extraction of Total RNA, cDNA Synthesis, and Real-Time PCR.** Total RNA was extracted from the frozen tissues of animals or isolated cells obtained from cell cultures within 2 weeks after collecting samples, using the total RNA extraction kit (Favorgen, Thailand). Briefly, approximately 50 mg of frozen brain tissue was homogenized by an ultrasound homogenizer on ice in a cold anti-RNase-containing buffer, and extraction processing was carried out according to the manufacturer's instructions. RNA concentration and purity was determined by the absorbance at 230, 260, and 280 nm.

Reverse transcription was conducted by the cDNA synthesis kit (Favorgen, Thailand). Briefly, 1  $\mu\text{g}$  of RNA, 1  $\mu\text{l}$  of random hexamer primer, and appropriate amount of DEPC-treated water up to 13.5  $\mu\text{l}$  were mixed in a 0.2 ml microtube. Then, the mixture was incubated at  $70^\circ\text{C}$  for

5 min and was chilled on ice. Next, 4  $\mu\text{l}$  of 5x first-strand buffer, 1  $\mu\text{l}$  of dNTPs (10 mM each), 0.5  $\mu\text{l}$  of RNasin (40 U/ $\mu\text{l}$ ), and 1  $\mu\text{l}$  of M-MLV enzyme were added, and reverse transcription was performed at  $37^\circ\text{C}$  for 60 min. Finally, the reaction was terminated at  $70^\circ\text{C}$  for 5 min.

Real-Time PCR was done using the Corbett Rotor Gene 6000 Real-Time PCR system (Corbett Research, Australia) and SYBR Green Real-Time PCR super master mix (Favorgen, Thailand). The total volume was equal to 20  $\mu\text{l}$  containing 2  $\mu\text{l}$  of cDNA, 10  $\mu\text{M}$  of forward primer (1  $\mu\text{l}$ ), 10  $\mu\text{M}$  of reverse primer (1  $\mu\text{l}$ ), 10  $\mu\text{l}$  of 2x SYBR Green PCR super master mix, and 5.8  $\mu\text{l}$  of dH<sub>2</sub>O. Conditions for PCR included denaturation at  $95^\circ\text{C}$  for 3 min, 40 cycles of 10 sec at  $95^\circ\text{C}$ , 10 sec at  $55\text{--}59^\circ\text{C}$  (depending on the primer type), 20 sec at  $72^\circ\text{C}$ , and final extension at  $72^\circ\text{C}$  for 5 min. The housekeeping gene  $\beta$ -actin was used as internal control for protein-coding genes. U67 gene was used as internal control for miR-185 gene. The gene expression ratio was obtained by LinRegPCR software version 2017.0, based on the  $\Delta\Delta\text{CT}$  method. In order to avoid nonspecific products and primer-dimer products, all PCR products were evaluated by melting curve analysis of the rotor gene. The primer sequences are shown in Table 1.

**2.8. Cell Culture and Development of PD for the In Vitro Model.** SHSY-5Y cells obtained from the Institute Pasteur of Iran (IPI) were cultured in DMEM/F12 medium (Invitrogen), supplied with 10% of fetal bovine serum (Invitrogen) and 1% of GlutaMax (Invitrogen), in a humidified atmosphere containing 5% of CO<sub>2</sub> at  $37^\circ\text{C}$ . Rotenone was dissolved in dimethyl sulfoxide (DMSO, final concentration of DMSO was equal to 0.01%). Rotenone (500 nM) was used for 24 h to induce cell damage [24]. In this stage, we wanted to evaluate the changes in the expression level of miR-185, SEPT5, PARK2, and LRRK2 genes in response to rotenone treatment. We also wanted to know if inhibiting each one of the above genes or their products could affect their predicted molecular targets or cellular viability. To address these questions, we designed an experiment on SHSY-5Y

cells with eight different treatments. Each experiment was repeated three times.

- (1) Control positive group (SHSY-5Y cells treated with rotenone for 24 h)
- (2) Control negative group (SHSY-5Y cells with no treatment)
- (3) Vehicle group (SHSY-5Y cells treated with rotenone vehicle for 24 h)
- (4) LRRK2 inhibitor+rotenone group (SHSY-5Y cells pretreated with HG-10-102-01 (50 nM) for 1 h followed by treatment with rotenone for 24 h)
- (5) LRRK2 inhibitor group (treated with HG-10-102-01 (50 nM))
- (6) miR-185 inhibitor group (SHSY-5Y cells transfected with a plasmid containing siRNA sequence for inhibiting miR-185 transcript)
- (7) SEPT5 inhibitor group (SHSY-5Y cells transfected with a plasmid containing siRNA sequence for inhibiting SEPT5 gene transcript)
- (8) SEPT5 inhibitor+rotenone group (transfected with a plasmid containing siRNA sequence for inhibiting SEPT5 gene transcript, followed by treatment with rotenone for 24 h)

**2.9. Transfection of SHSY-5Y Cells.** Cells at the logarithmic growth phase were plated into 96-well microtiter plates 24 h before transfection, in order to reach 60-80% of confluency. Plasmid DNA (containing SEPT-5 siRNA or miR-185 siRNA) was transiently transfected using FuGENE® reagent (Promega, Madison, WI, USA), according to the manufacturer's protocol. Briefly, 0.1  $\mu$ l of the FuGENE® 6 Transfection Reagent was mixed into 10  $\mu$ l of serum-free medium (Opti-MEM® I reduced serum medium) and was incubated for 5 minutes at room temperature. Then, 10  $\mu$ l of the FuGENE® 6/Opti-MEM® I mixture was added to each well of cells to be transfected and was incubated at 37°C for 48 hours. There was no need to remove serum or change culture conditions or remove the transfection complex. Cells were collected and used in further experiments, 48 hours after transfection.

**2.10. MTT Assay.** Cell viability was measured by the 3-(4,5-dimethylthiazol-2-yl)-2,5-diphenyltetrazolium bromide (MTT) method [27, 28]. As a colorimetric assay, MTT assay can measure the activity of NAD(P)H-dependent cellular oxidoreductase enzyme, so that the enzyme reduces the tetrazolium dye, MTT, into insoluble formazan crystals which has a purple color. Briefly, SHSY-5Y cells were plated at a density of  $1 \times 10^4$  cells per well in 96-well plates. After exposure to the treatments, 20  $\mu$ l of MTT (5 mg/ml, Sigma-Aldrich) was added into each well and the cell culture plates were incubated in a humidified incubator at 37°C for 4 hours to allow the formation of purple formazan crystal. Next, 100  $\mu$ l of the solubilization reagent (0.1 N HCl in anhydrous isopropa-

nol, Sigma-Aldrich) was added into each well, and cell lysates were assessed by spectrophotometric assays, so that the optical density was read at  $\lambda$  570 nm and background was subtracted at 690 nm. Cell viability was shown as a percentage of the value in untreated control cells [24]. All samples were run in triplicate.

**2.11. Data Analysis.** Data were presented by the mean  $\pm$  SEM of eight rats per group. The dependent *t*-test and one-way ANOVA followed by Tukey's test were used to analyze the statistical significance in two and multiple comparisons, respectively. SPSS software version 23 was used to conduct statistical analyses. *P* values at <0.05 were considered to be significant in all analyses.

### 3. Results

**3.1. Behavioral Assessment of the Rotenone Model of Parkinson's Disease.** The results of three behavioral tests (Rotarod, rearing, and bar tests) showed significant decreases in the muscle strength and balance in the control group compared to both baseline and healthy normal groups ( $P < 0.001$ ) (see Figure 1). Additionally, treatment with apomorphine could reverse the decrease in motor performance on three behavioral tests (rotenone-treated vs. rotenone-treated+apomorphine; ( $P < 0.001$ ) see Figure 1). Furthermore, the body weight analysis showed a moderate weight loss in rotenone-treated groups. Weight difference was statistically significant in the control group compared to baseline and healthy normal groups ( $P < 0.001$ ). However, the decrease in body weight was observed to be only 8.2% compared to the baseline group and 13.2% compared to the healthy normal group.

**3.2. Gene Expression Analysis of Brain Tissues.** Figure 2(a) shows the results of the gene expression analysis in the transcription level demonstrating that miR-185 ( $P < 0.01$ ) and PARK2 ( $P < 0.05$ ) gene expression significantly decreased in the SN of the control group, compared to the healthy normal group. Furthermore, mRNA of SEPT5 and LRRK2 genes significantly increased in the SN of the control group, compared to the healthy normal group ( $P < 0.05$ ).

In addition, the analysis of the genes' transcripts in the ST of the control group showed a significant decrease in the gene expression of miR-185 ( $P < 0.05$ ) and LRRK2 ( $P < 0.05$ ), compared to the healthy normal group. However, there was no significant difference in the expression of SEPT5 and PARK2 genes between two groups (Figure 2(b)).

**3.3. Analysis of Gene Expression of SHSY-5Y Cells and Their Viability.** The results of MTT assay showed that the cell viability rate significantly decreased in SHSY-5Y cells treated by rotenone (control group), compared to the control negative (vehicle) group ( $P < 0.001$ ) (see Figure 3). However, there was no significant difference in the expression of miR-185, LRRK2, SEPT5, and PARK2 genes in rotenone (control group) compared to the control negative (vehicle) group (see Figure 3). The cell viability rate significantly increased due to the inhibition on LRRK2 protein in cells treated by HG-10-102-01 (50 nM) compared to the control group

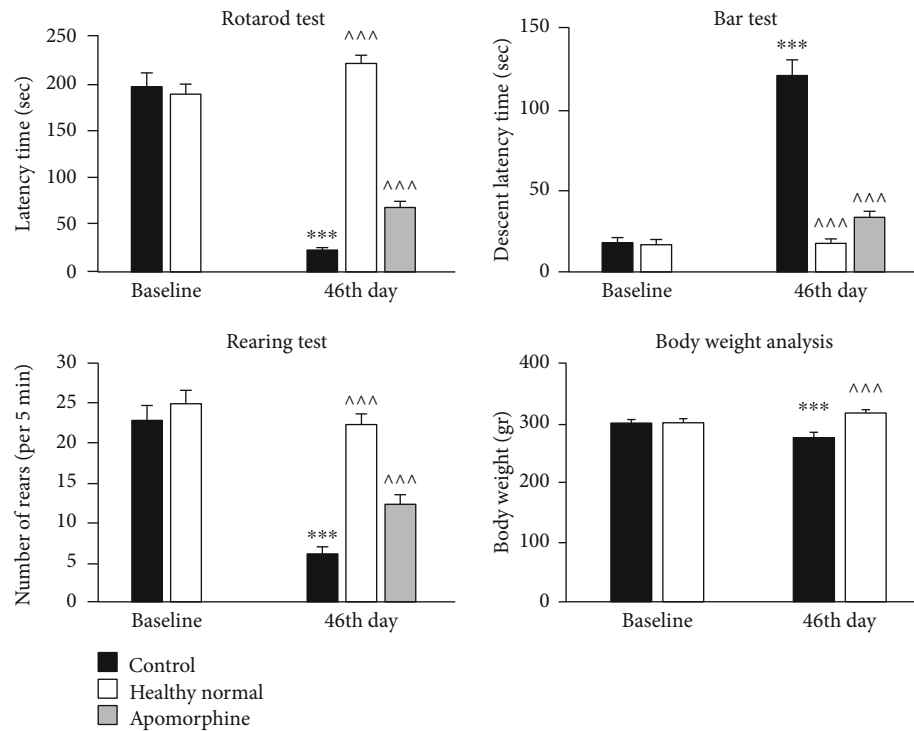


FIGURE 1: Comparison of the behavioral performance in different experimental groups. The results of the behavioral tests on baseline day and 46th day are shown. Data are presented as mean  $\pm$  standard error of the mean.  $P$  value at  $<0.05$  was considered as the significance level. \*\*\* $P$  value at  $<0.001$  represents a significant difference compared to the baseline on first day of the experiments. ^^^ $P$  value at  $<0.001$  represents a significant difference in test results of the healthy normal group or the apomorphine-treated group compared to the control group.

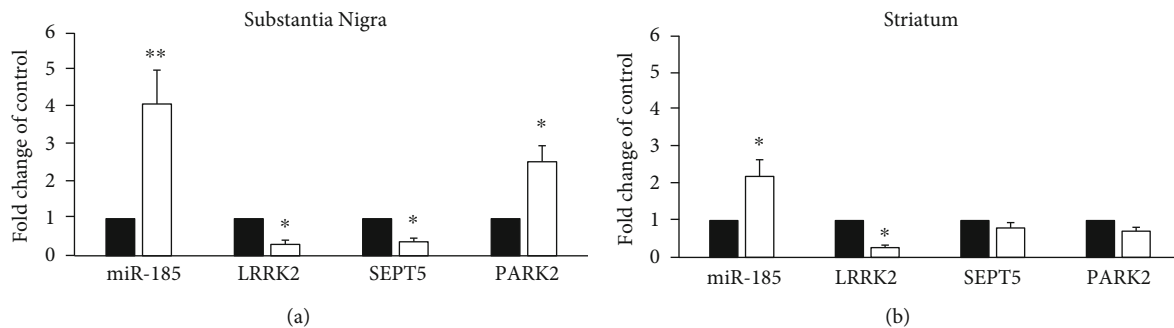


FIGURE 2: Comparison of the gene expression in the substantia nigra (a) and striatum (b) of the experimental groups. The bands were normalized to beta-actin, and data were expressed as fold change of the control group. Data are presented as mean  $\pm$  standard error of the mean.  $P$  values of less than 0.05 were considered as significant. \* $P$  values at  $<0.05$  and \*\* $P$  values at  $<0.01$  represent a significant difference between the healthy normal group and the control group.

( $P < 0.001$ ) (see Figure 3). Additionally, the expression of miR-185 gene ( $P < 0.001$ ) decreased and the expression of LRRK2 ( $P < 0.001$ ) gene increased, simultaneously due to the inhibition on miR-185 transcript by its exclusive siRNA (see Figure 4). However, inhibition on SEPT5 transcript by its exclusive siRNA decreased the SEPT5 mRNA level, while could not affect the levels of PARK2, LRRK2, or miR-185 transcripts significantly (see Figure 4).

#### 4. Discussion

Results of the movement assessments showed a significant decrease in the performance of the control group indicating

that the animal model of PD has been well developed regarding the previous studies [22]. Additionally, apomorphine injection could relieve the signs of the behavioral impairments significantly. Thus, treatment with rotenone could specifically induce dopaminergic cell death in the SN of rats' brain, with the least peripheral effects.

The results of this study showed that the level of miR-185 and PARK2 transcripts significantly decreased in the SN of the control group, while mRNA of SEPT5 and LRRK2 genes significantly increased in the SN of the group, compared to the healthy normal group. Furthermore, the analysis of the genes' transcripts in the ST of the control group showed significant decreases in miR-185 and LRRK2 expressions,

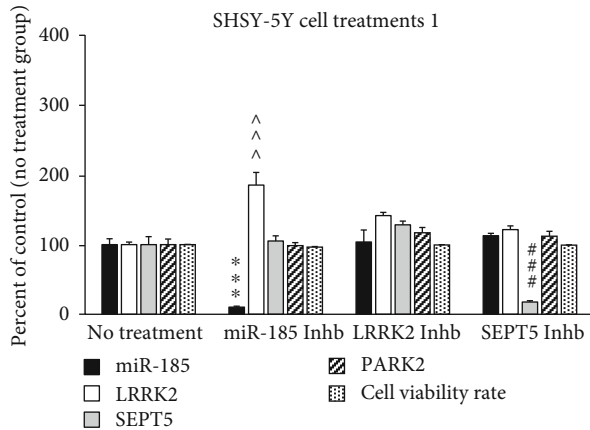


FIGURE 3: Comparison of the gene expression in SHSY-5Y cell treated by different treatments. The bands were normalized to beta-actin, and data were presented as percentage of the control group. Data are presented as mean  $\pm$  standard error of the mean.  $P$  values of less than 0.05 were considered as significant. \*\*\* $P$  values at  $<0.001$ , ^^ $P$  values at  $<0.001$ , and ### $P < 0.001$  represent a significant difference in miR-185, LRRK2, and SEPT5 gene expressions, respectively, between the healthy “no treatment” group and other groups. Abbreviations are as follows: Inhb represents inhibitor; Veh represents vehicle.

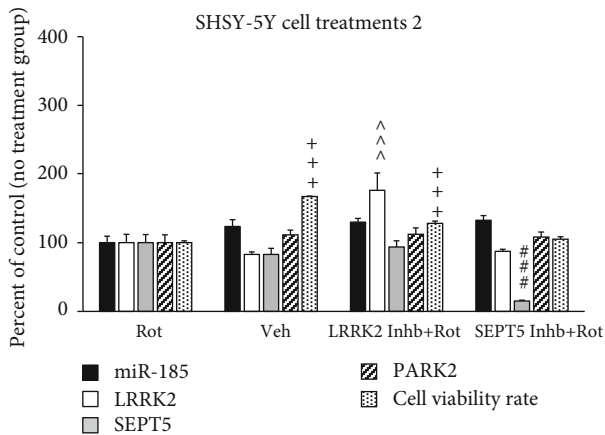


FIGURE 4: Comparison of the gene expression in SHSY-5Y cell treated by different treatments. The bands were normalized to beta-actin, and data were presented as percentage of the control group. Data are expressed as mean  $\pm$  standard error of the mean.  $P$  values of less than 0.05 were considered as significant. \*\*\* $P$  values at  $<0.001$ , ^^ $P$  values at  $<0.001$ , and ### $P < 0.001$  represent a significant difference in miR-185, LRRK2, and SEPT5 gene expressions, respectively, between the Rot (control) group and other groups. +++ $P$  value at  $<0.001$  represents a significant difference in the cell viability rate between the Rot (Control) group and other groups. Abbreviations are as follows: Rot represents rotenone; Veh represents vehicle; Inhb represents inhibitor.

compared to the healthy normal group. However, there was no significant difference in the expression of SEPT5 and PARK2 genes in the ST between two groups. These results show the possible role of all the four genes in the development of the PD model and dopaminergic cell death in the

SN. However, there was no significant difference in the PARK2 and SEPT5 transcript level in the ST between two groups, which is probably due to the less density of dopaminergic neurons. Additionally, it appears that miR-185 and PARK2 genes play a neuroprotective role in the SN, which lack of them can contribute in dopaminergic cell death and the development of PD. In this regard, Wen et al. reported that the overexpression of miR-185 gene can lead to the inhibition on apoptosis of dopaminergic neurons through regulating the mTOR-dependent autophagy pathway [25]. Furthermore, Elmazoglu et al. reported a decrease in the PARK2 gene expression level in an *in vitro* model of PD induced by rotenone [26]. The increase in the PARK2 gene expression level was also observed in clinical cases of PD or PD models occurred through certain epigenetic processes. For example, certain mutation or decrease in the expression in midnolin (MIDN) gene, observed in almost 10.5% of so-called sporadic PD, can lead to the decrease in PARK2 mRNA [27].

Additionally, previous studies show that the increase in SEPT5 gene expression can lead in dopaminergic cell death through the formation of the Lewy bodies [28, 29]. In current study, the expression of normal LRRK2 increased, while most of other studies only show the increase in the kinase activity of LRRK2 due to the certain mutations [30]. Indeed, those studies neither confirm nor deny the increase in the LRRK2 gene expression level. However, some studies showed the increase in the LRRK2 gene expression level in the microglia present at the SN of the brain in patients with PD occurred due to the inflammation which is an inevitable phenomenon inside the brains of the patients with PD [31, 32]. This reason may be the cause of what was observed about the LRRK2 gene expression level in the current study.

Assessments on SHSY-5Y cells showed no significant difference in all of the four genes between the control group (rotenone-treated group) and the vehicle-treated group. However, the cell viability rate significantly decreased in the control group. These results were not surprising, since we do not expect a perfect similarity in gene expression pattern between *in vitro* and *in vivo* models. The results also showed that inhibition on miR-185 caused by specific siRNA led to the significant increase in the expression level of LRRK2 gene. However, the analysis of gene expression in the SN of rats' brains also showed that there was an inverse relation between miR-185 and LRRK2, but we could not interpret it as a real reliable relation, since we performed no intervention and genetic manipulation on animals. More reliable straightforward results were obtained by assessment of the gene expression level in genetically manipulated SHSY-5Y cells indicating that miR-185 could target LRRK2 mRNA and reduce its expression level. Dweep et al. previously predicted that miR-185 targets LRRK2 mRNA; however, there was no experimental study to confirm the results of their *in silico* study [33]. Current study for the first time showed that LRRK2 could probably be a target for miR-185 transcript. Additionally, the results of this study revealed that inhibition on LRRK2 protein by its specific inhibitor (HG-10-102-01) could prevent rotenone toxicity and lead to the increase in the cell viability rate. In this regard, previous studies showed

that the increase in the kinase activity of LRRK2 protein occurred due to the certain mutations (e.g., G2019S) or simply the increase in LRRK2 gene expression can influence its molecular target at least through three pathways: (1) implying the synaptic dysfunction due to the phosphorylation of endothelin A (EndoA), which is a direct target of LRRK2 [34], (2) uncontrolled translation and consequently a bulk increase in protein synthesis through phosphorylation of eukaryotic initiation factor 4E- (eIF4E-) binding protein (4E-BP) and ribosomal protein S15 (RPS15), which induce the formation of the Lewy bodies [35], and (3) deregulation of autophagy processes through influencing Rab7-dependent perinuclear lysosome clustering and lysosomal degradation [36, 37]. Therefore, it appears that the present study found a missing link located in the upstream of the LRRK2-related pathophysiological process. Accordingly, miR-185 gene is likely a noteworthy molecular target, which would be considered in designing upcoming preclinical and clinical therapeutic approaches. It is noteworthy that the increase in LRRK2 gene expression due to the inhibition on miR-185 gene expression could not lead to the decrease in the cell viability rate. However, it is difficult to interpret this finding and further experiments are needed to elaborate this finding, but probably it results from the multifactorial nature of PD, so that only the increase in LRRK2 expression cannot imply enough pressure to induce SHSY-5Y cell death.

The results of the current study showed that inhibition on the expression of SEPT5 gene could neither influence the expression of the other three genes nor prevent the toxicity of rotenone on SHSY-5Y cells. However, it was predictable that SEPT5 gene cannot influence the expression of miR-185, LRRK2, or PARK2, since there was no accordant report or prediction in this regard. Indeed, SEPT5 protein is a molecular target of PARK2, so that a decrease in the expression level of PARK2 can lead to the high cellular amount of SEPT5, contributing in the formation of the Lewy bodies [38]. Thus, we did not manipulate the expression level of PARK2 to evaluate the changes in the expression of SEPT5 gene, since it was predictable based on the previous studies.

## 5. Conclusion

The findings of the study recommended the protective role of miR-185 gene in preventing the development of the PD model, although further preclinical and clinical studies are needed to confirm the findings and to develop novel therapeutic approaches for the treatment of PD based on this finding. SEPT5 gene is also probably involved in the pathophysiological mechanisms of PD. In addition, further studies are recommended to evaluate the probable associations between oxidative stress pathways and miR-185 and SEPT5.

## Data Availability

The data used to support the findings of this study are available from the corresponding author upon request.

## Ethical Approval

All applicable international, national, and/or institutional guidelines for the care and use of animals were followed.

## Conflicts of Interest

On behalf of all the authors, the corresponding author states that there is no conflict of interest.

## Acknowledgments

We also thank the Vice Chancellor's office for Research Affairs of Kurdistan University of Medical Sciences for financial support.

## References

- [1] C. A. Davie, "A review of Parkinson's disease," *British Medical Bulletin*, vol. 86, no. 1, pp. 109–127, 2008.
- [2] S. Sveinbjornsdottir, "The clinical symptoms of Parkinson's disease," *Journal of Neurochemistry*, vol. 139, Suppl 1, pp. 318–324, 2016.
- [3] M. C. de Rijk, L. J. Launer, K. Berger et al., "Prevalence of Parkinson's disease in Europe: a collaborative study of population-based cohorts. Neurologic diseases in the elderly research group," *Neurology*, vol. 54, 11 Suppl 5, pp. S21–S23, 2000.
- [4] E. R. Dorsey, R. Constantinescu, J. P. Thompson et al., "Projected number of people with Parkinson disease in the most populous nations, 2005 through 2030," *Neurology*, vol. 68, no. 5, pp. 384–386, 2007.
- [5] B. Thomas and M. F. Beal, "Molecular insights into Parkinson's disease," *F1000 Medicine Reports*, vol. 3, p. 7, 2011.
- [6] L. Wang, Q. Zhang, H. Li, and H. Zhang, "SPECT Molecular Imaging in Parkinson's Disease," *Journal of Biomedicine & Biotechnology*, vol. 2012, Article ID 412486, 11 pages, 2012.
- [7] J. C. Rochet, B. A. Hay, and M. Guo, "Molecular insights into Parkinson's disease," *Progress in Molecular Biology and Translational Science*, vol. 107, pp. 125–188, 2012.
- [8] J. Blesa, I. Trigo-Damas, A. Quiroga-Varela, and V. R. Jackson-Lewis, "Oxidative stress and Parkinson's disease," *Frontiers in Neuroanatomy*, vol. 9, p. 91, 2015.
- [9] S. R. Subramaniam and M.-F. Chesselet, "Mitochondrial dysfunction and oxidative stress in Parkinson's disease," *Progress in Neurobiology*, vol. 106–107, pp. 17–32, 2013.
- [10] K. Hassanzadeh and A. Rahimmi, "Oxidative stress and neuroinflammation in the story of Parkinson's disease: could targeting these pathways write a good ending?," *Journal of Cellular Physiology*, vol. 234, no. 1, pp. 23–32, 2019.
- [11] K. Hassanzadeh, A. Rahimmi, and K. Hassanzadeh, "Effect of N-acetylcysteine on TNF- $\alpha$  level of substantia nigra and striatum in rat model of Parkinson's disease," *Journal of Mazandaran University of Medical Sciences*, vol. 24, no. 118, pp. 40–48, 2014.
- [12] P. Whitton, "Inflammation as a causative factor in the aetiology of Parkinson's disease," *British Journal of Pharmacology*, vol. 150, no. 8, pp. 963–976, 2007.
- [13] E. Boot, N. J. Butcher, T. van Amelsvoort et al., "Movement disorders and other motor abnormalities in adults with



- 22q11.2 deletion syndrome,” *American Journal of Medical Genetics Part A*, vol. 167a, no. 3, pp. 639–645, 2015.
- [14] N. J. Butcher, T. R. Kiehl, L. N. Hazrati et al., “Association between early-onset Parkinson disease and 22q11.2 deletion syndrome: identification of a novel genetic form of Parkinson disease and its clinical implications,” *JAMA Neurology*, vol. 70, no. 11, pp. 1359–1366, 2013.
- [15] M. Oki, S. Hori, S. Asayama, R. Wate, S. Kaneko, and H. Kusaka, “Early-onset Parkinson’s disease associated with chromosome 22q11.2 deletion syndrome,” *Internal Medicine*, vol. 55, no. 3, pp. 303–305, 2016.
- [16] K. L. Stark, B. Xu, A. Bagchi et al., “Altered brain microRNA biogenesis contributes to phenotypic deficits in a 22q11-deletion mouse model,” *Nature Genetics*, vol. 40, no. 6, pp. 751–760, 2008.
- [17] D. R. Alessi and E. Sammler, “LRRK2 kinase in Parkinson’s disease,” *Science*, vol. 360, no. 6384, pp. 36–37, 2018.
- [18] T. M. Dawson and V. L. Dawson, “The role of parkin in familial and sporadic Parkinson’s disease,” *Movement disorders : official journal of the Movement Disorder Society*, vol. 25, no. S1, pp. S32–S39, 2010.
- [19] P. M. Haddad and S. M. Dursun, “Neurological complications of psychiatric drugs: clinical features and management,” *Human Psychopharmacology: Clinical and Experimental*, vol. 23, no. S1, pp. S15–S26, 2008.
- [20] C. Zaleski, A. S. Bassett, K. Tam, A. L. Shugar, E. W. C. Chow, and E. McPherson, “The co-occurrence of early onset Parkinson disease and 22q11.2 deletion syndrome,” *American Journal of Medical Genetics*, vol. 149A, no. 3, pp. 525–528, 2009.
- [21] A. R. M. A. N. Rahimmi, F. A. R. N. O. O. S. H. Khosrobakhsh, E. S. M. A. I. L. Izadpanah, and K. A. M. B. I. Z. Hassanzadeh, “Induction of Parkinson’s disease model in rat by rotenone,” *Journal of Isfahan Medical School*, vol. 32, no. 296, pp. 1250–1258, 2014.
- [22] A. Rahimmi, F. Khosrobakhsh, E. Izadpanah, M. R. Moloudi, and K. Hassanzadeh, “N-Acetylcysteine prevents rotenone-induced Parkinson’s disease in rat: an investigation into the interaction of parkin and Drp1 proteins,” *Brain Research Bulletin*, vol. 113, pp. 34–40, 2015.
- [23] N. Xiong, J. Xiong, G. Khare et al., “Edaravone guards dopamine neurons in a rotenone model for Parkinson’s disease,” *PLoS One*, vol. 6, no. 6, article e20677, 2011.
- [24] Y.-N. Deng, J. Shi, J. Liu, and Q. M. Qu, “Celastrrol protects human neuroblastoma SH-SY5Y cells from rotenone-induced injury through induction of autophagy,” *Neurochemistry International*, vol. 63, no. 1, pp. 1–9, 2013.
- [25] Z. Wen, J. Zhang, P. Tang, N. Tu, K. Wang, and G. Wu, “Overexpression of miR-185 inhibits autophagy and apoptosis of dopaminergic neurons by regulating the AMPK/mTOR signaling pathway in Parkinson’s disease,” *Molecular Medicine Reports*, vol. 17, no. 1, pp. 131–137, 2018.
- [26] Z. Elmazoglu, A. S. Yar Saglam, C. Sonmez, and C. Karasu, “Luteolin protects microglia against rotenone-induced toxicity in a hormetic manner through targeting oxidative stress response, genes associated with Parkinson’s disease and inflammatory pathways,” *Drug and Chemical Toxicology*, pp. 1–8, 2018.
- [27] Y. Obara and K. Ishii, “Transcriptome analysis reveals that midnolin regulates mRNA expression levels of multiple Parkinson’s disease causative genes,” *Biological and Pharmaceutical Bulletin*, vol. 41, no. 1, pp. 20–23, 2018.
- [28] J. H. Son, H. Kawamata, M. S. Yoo et al., “Neurotoxicity and behavioral deficits associated with septin 5 accumulation in dopaminergic neurons,” *Journal of Neurochemistry*, vol. 94, no. 4, pp. 1040–1053, 2005.
- [29] E. Sopova, O. Korenkova, and O. Shupliakov, “Malfunctions in synaptic membrane trafficking in early pathology of Parkinson’s disease: new molecular clues,” *Biological Communications*, vol. 62, no. 4, pp. 272–277, 2017.
- [30] I. Martin, J. W. Kim, V. L. Dawson, and T. M. Dawson, “LRRK2 pathobiology in Parkinson’s disease,” *Journal of Neurochemistry*, vol. 131, no. 5, pp. 554–565, 2014.
- [31] M. S. Moehle, P. J. Webber, T. Tse et al., “LRRK2 inhibition attenuates microglial inflammatory responses,” *Journal of Neuroscience*, vol. 32, no. 5, pp. 1602–1611, 2012.
- [32] I. Russo, L. Bubacco, and E. Greggio, “LRRK2 and neuroinflammation: partners in crime in Parkinson’s disease?,” *Journal of Neuroinflammation*, vol. 11, no. 1, p. 52, 2014.
- [33] H. Dweep, C. Sticht, P. Pandey, and N. Gretz, “miRWalk - database: prediction of possible miRNA binding sites by “walking” the genes of three genomes,” *Journal of Biomedical Informatics*, vol. 44, no. 5, pp. 839–847, 2011.
- [34] S. Matta, K. van Kolen, R. da Cunha et al., “LRRK2 controls an EndoA phosphorylation cycle in synaptic endocytosis,” *Neuron*, vol. 75, no. 6, pp. 1008–1021, 2012.
- [35] I. Martin, J. W. Kim, B. D. Lee et al., “Ribosomal protein s15 phosphorylation mediates LRRK2 neurodegeneration in Parkinson’s disease,” *Cell*, vol. 157, no. 2, pp. 472–485, 2014.
- [36] M. W. Dodson, T. Zhang, C. Jiang, S. Chen, and M. Guo, “Roles of the Drosophila LRRK2 homolog in Rab7-dependent lysosomal positioning,” *Human Molecular Genetics*, vol. 21, no. 6, pp. 1350–1363, 2012.
- [37] A. Sánchez-Danés, Y. Richaud-Patin, I. Carballo-Carbajal et al., “Disease-specific phenotypes in dopamine neurons from human iPS-based models of genetic and sporadic Parkinson’s disease,” *EMBO Molecular Medicine*, vol. 4, no. 5, pp. 380–395, 2012.
- [38] N. Ageta-Ishihara, H. Yamakado, T. Morita et al., “Chronic overload of SEPT4, a parkin substrate that aggregates in Parkinson’s disease, causes behavioral alterations but not neurodegeneration in mice,” *Molecular Brain*, vol. 6, no. 1, p. 35, 2013.